Reconstruction of Paleoclimate Time-Series in the Peace-Athabasca Delta, Northern Alberta, from Stable Isotopes in Tree-Rings

by

Joscelyn Nesto-Leigh Bailey

A thesis
presented to the University of Waterloo
in fulfilment of the
thesis requirement for the degree of
Master of Science
in
Earth Sciences

Waterloo, Ontario, Canada, 2008

Authors Declaration

I hereby declare that I am the sole author of this thesis. This is a true copy of the thesis, including any required final revisions, as accepted by my examiners. I understand that my thesis may be made electronically available to the public.

Abstract

The isotopic labelling of carbon in tree-rings varies as a function of growth season temperature and relative humidity. The isotopic labelling of oxygen in tree-rings varies as a function of source-water isotopic composition and humidity-dependent evaporative enrichment of leaf water during the growth season. The season of carbon-isotope labelling was identified statistically as late-spring to early-fall (April to October) for temperatures and relative humidity with a three-year weighted (50-30-20) carry-over due mainly to stored photosynthates. The season of oxygen-isotope labelling was identified statistically as a combination of a winter (pDecember to March) source-water signal (temperature-dependent precipitation isotope composition) with a late-spring to early-fall (April to October) humidity signal (evaporative enrichment of leaf water). A two-year carry-over was attributed to the residence time of soil water, but no notable photosynthate carry-over was identified. Carbon- and oxygen- (mechanistic) isotope response surface models were then compared and contrasted to regression-based bivariate and univariate models. It was found that in most cases the isotope response surface models were the best means of predicting isotopic labelling when environmental data are known. The carbon-isotope response surface was used to reconstruct 50-years (AD 1900-1954) of relative humidity data by introducing measured carbon isotope values and instrumental growth season temperature. During the analysis of the oxygen-isotope response surface we found an isotope-temperature relation that appears to reflect circulation-dependent damping. To verify this we introduced scaled values of the North Pacific index as a proxy for this suppression. The coupling of the isotope response surfaces generated a humidity reconstruction that is also thought to be driven by atmospheric circulation. Our reconstruction shows that the fluctuations in temperature range have not exceeded the natural variability in the instrumental record of the 20th century; however, the atmospheric moisture (humidity) reconstruction predicts a directional drying trend in the Peace-Athabasca Delta that appears to reflect increasingly zonal circulation in western Canada over this period.

"Out of theories we create a world; not the real world, but our own nets in which we try to catch the real world."

Karl Popper, Unending Quest

Acknowledgements

Table of Contents

List of Tables

List of Figures

I   Background and Rational

Synopsis

Chapter I provides a general introduction stating the rationale, objectives and preliminary findings regarding the carbon-, oxygen- and coupled-isotope response-surface approaches. This chapter gives a review of the formation, evolution and geological setting of the Peace-Athabasca Delta and then breaks down the five sampling locations into three sub-categories based on previously defined physiographic setting - upland, lowland or island. This chapter also contains a literature review which focuses on: known factors controlling the distribution of Picea glauca, the isotopic labelling of carbon- and oxygen-isotopes (including Péclet Effect, Rayleigh distillation and temperature-dependent alterations of the isotopic composition of precipitation). We also discuss recent dendrochronology studies in the Peace-Athabasca Delta to highlight progress from one study to the next.

I.1   Introduction

The primary objective of this thesis is to develop proxy climate records for the Peace-Athabasca Delta (PAD) that extend beyond the available instrumental climate records in the region; limited to ~100 years for temperature and precipitation and ~ 50 years for relative humidity. Improved documentation of pre-instrumental climate variability is essential to provide context for recent and ongoing paleo-environmental studies in the PAD. The new proxy records developed here are based on carbon- and oxygen-isotope data from annual tree-ring α-cellulose obtained from living white spruce (*Picea glauca*). Sampling was conducted at two lowland sites and two upland sites within the delta in 2003. An additional fifth site, Bustard Island, was added in 2005. Isotopic data are available at all five sites over the most recent ~150 years and a ~300 year time-series is available for the lowland sites. The reconstructions are based on testing, calibration and application of the coupled-isotope response-surface approach, which resolves temperature- and moisture- dependent signals in the carbon- and oxygen-isotope labelling of tree-ring α-cellulose to produce estimates of the oxygen-isotope composition of source-water and relative humidity during the growth season.

I.2 Study Site

I.2.1 The Review of the Peace-Athabasca Delta

The PAD (58°42'N, 111°08'W) (Figure I-1) is a 4,000 km^2 inland freshwater delta complex that was internationally recognized in 1982 under the Ramsar Convention as a wetland of significance for its importance to migratory waterfowl (RAMSAR, 1971; RAMSAR, 2003). Approximately 80% of the delta lies within Wood Buffalo National Park (44,807 km^2) which was a recognized in 1983 as a United Nations Educational, Scientific and Cultural Organization World heritage site.

The PAD began to form approximately 10,000 years ago in Glacial Lake McConnell, which was ponded against the retreating Laurentide Ice Sheet. The PAD is predominantly underlain by Athabasca sandstone (Proterozoic) and Archean igneous and metamorphic rocks (PADPG, 1973). The bedrock is overlain by fluvial, lacustrine and deltaic sediments (BAYROCK and ROOT, 1973; BEDNARSKI, 1999).

The PAD can be separated into three deltas, the Peace (1,680 km^2), Athabasca (1,970 km^2) and Birch (170 km^2). The Peace Delta is relatively inactive except during periods of ice-jam flooding and large flows of the Peace River (PETERS, 2003). There are five large lakes in the central area; Lake Athabasca, Claire, Baril, Mamawi and Richardson. Throughout the region there are numerous small ponds and wetlands (WOLFE et al., 2007).

Drainage of the PAD is north via the Slave River, however, during high flows which can occur during spring break-up, the Peace River may flow south into the Chenal des Quatre Fourches if the central lakes are comparatively low. Notable hydrological

connections between the large lakes in the PAD include Lake Athabasca to Lake Mamawi via the Prairie River and Lake Claire via the Chenal des Quatre Fourches. Lakes Mamawi and Claire then empty into the Peace River via the Revillon Coupé, Rivière des Rochers and Chenal des Quatre Fourches.

I.2.2   Modern Climate

Instrumental data for Fort Chipewyan include temperature and precipitation, Figure I-2. There are no long-term records for relative humidity available and thus data were obtained for Fort McMurray, Alberta, via the Adjusted Historical Canadian Climate Data (AHCCD) (GOODISON and LOUIE, 1986; MEKIS and HOGG, 1997; MEKIS and HOGG, 1999; METCALFE et al., 1997; VINCENT and GULLETT, 1999).

The monthly temperature in the PAD ranges from -35.8°C in January to 25.1°C in July with a mean value of -2.60°C (AD 1895-2000). The greatest variability in temperature occurs during the winter months, while the summer months are relatively stable. The temperature in the PAD has been increasing overall at rates of 0.019 K/year (AD 1895-2000) and 0.049 K/year (AD 1955-2000).

The monthly mean relative humidity is 69.92% (AD 1955-2005) and ranges between 59.72% (May) and 79.03% (November). The long-term annual mean humidity record shows high variability throughout the 45-year record. There are sharp inflections in the trend of relative humidity occurring at 1975; 1975-2000 (68.10% average) and 1953-1975 (72.36%), respectively.

On average 419 mm of precipitation fall in the PAD annually (AD 1955-2005). The majority of precipitation (64.74%) falls between May and October. Snowfall

averages 15.97 mm/month over the winter months of November, December and January and diminishes with increasing temperature.

I.2.3   Sampling Locations

At least 35 radii were collected at chest height (1.5 metres) from 15 to 25 living *P. glauca* trees per site (Figure I-1 and Table I-1) using a hand-held increment borer in 2003 and 2005. Glen McDonald, Dave Porinchu, Thomas Edwards and Natalie St. Amour sampled 96 trees in 2003 at two upland sites (Greenstar Lake [GSL], Quatre Fourches Upland [QFU]) beyond the influence of river flooding and two lowland sites (Peace-Rochers Confluence [PRC] and Quatre Fourches River [QFR]). These four sites were selected to reflect upland and lowland hydrologic and climatic conditions. Additional sampling was conducted on Bustard Island (BITC) in 2005 by Suzanne Jarvis, Thomas Edwards, Yi Yi and John Johnston. Ring-width measurements and cross-dating were conducted at the University of California at Los Angeles by David Porinchu and Glen McDonald using standard dendrochronology methods (PORINCHU, 2004; STOKES and SMILEY, 1968).

I.2.3.1 Upland Sites

Greenstar Lake (GSL, 58°90'N, 111°36'W; ± 238 metres above sea level [masl]) is a perched lake in a bedrock basin in the Peace Delta. This site lies approximately 1.2 km northeast and 5.2 km southwest of the Revillon Coupé and the Rivière des Rochers, respectively. This site is well above the reach of typical ice-jam flooding in the delta. Forty-seven radii from 23 trees were initially collected around the northern bedrock outcrop and the basin surrounding the lake's edge and span 175 years (AD

1828-2002).

Quatre Fourches Upland (QFU, 58°68'N, 111°36'W; ± 244 masl) is a tree stand on a rock outcrop, east of the Chenal des Quatre Fourches and is topographically isolated from the flood plain. Fifty-two radii from 23 trees produced a 182-year (AD 1821-2002) chronology.

I.2.3.2 Lowland Sites

Peace-Rochers Confluence (PRC, 59°00'N, W'111°42; ± 207 masl) lies at the confluence of the Peace River and the Rivière des Rochers. PRC is topographically low and flat. The site is thought to be sensitive to flooding during episodes of elevated discharge in the summer and during spring ice-jam floods. Thirty-five radii from 18 trees produced a 313-year (AD 1690 - 2002) chronology.

Quatre Fourches River (QFR, 58°71'N, 111°41'W; ± 210 masl) represents trees sampled along several kilometres of the banks of the Chenal des Quatre Fourches. Thirty-nine radii from 14 trees produced a 253-year (AD 1750 - 2002) chronology.

I.2.3.3 Island Site

Bustard Island (BITC, 58°80'N, 110°72'W; ± 216 masl) is an island in the western end of Lake Athabasca, within Fidler-Greywillow Wildland Provincial Park. The lake is 7,850 km^2 in area and relatively deep at 120 m. BITC has a maximum elevation of roughly 8 m above Lake Athabasca and is characterized by unconsolidated glacio-lacustrine, glacio-fluvial and aeolian sediments underlain by Precambrian bedrock (Bednarski, 1999; English et al., 1991). The samples were collected on barriers that isolate small inland ponds from Lake Athabasca.

6

I.3   Literature Review

I.3.1   *Picea glauca* **[Moench] Voss (white spruce)**

Picea glauca [Moench] Voss (white spruce) is a coniferous evergreen with bluish-green needles that is widespread across northwestern Canada. *P. glauca* has shallow roots, generally ranging from 90 to 120 cm in depth. The species is generally confined to well-drained uplands, river terraces and floodplains (HOSIE, 1969). On northern sites such as the PAD, large roots typically concentrate within 15 cm of the soil interface (NIENSTAEDT and ZASADA, 1990). The climate distribution of *P. glauca* is defined by mean June temperature ranging from 8°C to 21°C and total precipitation of 20 to 200 mm in July (ANDERSON et al., 1991; BARBER et al., 2004; THOMPSON et al., 2000). In western Canada, the northern extent of white spruce growth is controlled by moisture availability (BROOKS et al., 1998). *Picea glauca* is often used for dendroclimatological investigations. Tree-ring chronologies are highly valued as they are absolutely dated and variations in width, density, and isotopic composition are in response to external environmental factors (FRITTS, 1976; GRAY, 1981; SCHWEINGRUBER, 1988).

Previous studies on *P. glauca* from the PAD showed that the trees were not limited by moisture as the ring-width and carbon-isotope chronologies did not show sensitivity to precipitation (COUILLARD, 2004). The isotope chronologies did show sensitivity to relative humidity and temperature (BAILEY, 2005), with respect to both carbon and oxygen isotopes in α-cellulose.

I.3.2   Isotope Labelling

Isotope values are expressed as deviation from a given standard in delta notation (δ). The standard for carbon $\left(^{13}C/^{12}C\right)$ is fossil belemnite of the Pee Dee formation (V-PDB) and the standard for oxygen $\left(^{18}O/^{16}O\right)$ is Vienna-Standard Mean Ocean Water (V-SMOW):

$$\delta = \left(\frac{R_{SA}}{R_{ST}} - 1\right) \times 10^3 ‰ \quad (1)$$

where R is the carbon or oxygen isotope ratio in the sample (SA) and standard (ST) (FRITZ and FONTES, 1986; HOEFS, 1997)

I.3.3 $\delta^{13}C$ - Isotope Labelling in C$_3$ Plants

Stomatal conductance is believed to be the primary control on the isotopic labelling of carbon in cellulose as it minimizes water loss against the gain of carbon (λ). In equation (2), E is the transpiration rate, A is molar flux or the rate of CO$_2$ assimilation, g_s is the stomatal conductance of the boundary layer and the stomatal pores to the diffusion of CO_2 (COWAN, 1977). Figure I-3 illustrates the mechanisms outlined above and below.

$$\frac{\partial E/\partial g_s}{\partial A/\partial g_s} = \lambda \quad (2)$$

Farquhar el al. (1982) later refined this model and its processes in equations (3) and (4). As atmospheric CO_{2ATM} moves into the intercellular space of the leaf, via the

stomatal aperture, it undergoes a diffusional fractionation (ε_a) of -4.4‰. The aperture, surrounded by guard cells, moderates the ratio of the partial pressures (c_i / c_a) of CO_2 in the intercellular space (i) and the ambient atmosphere (a). When the CO_2 in the intercellular space dissolves, it is available to produce sugars and will undergo a second constant biochemical fractionation of $\varepsilon_b \cong -27‰$ by the rubulose-1,5-biphosphate (RuBP) enzyme.

$$\delta^{13}C_{PLANT} = \delta^{13}C_{ATM} - \varepsilon_a - (\varepsilon_b - \varepsilon_a)(c_i / c_a) \quad (3)$$

and

$$c_i = c_a - A \cdot P / g \quad (4)$$

Here $\delta^{13}C_{PLANT}$ is the isotopic composition of the plant tissue and P is atmospheric pressure. The moderator c_i / c_a is the main labeller of $\delta^{13}C_{PLANT}$. When the stomatal conductance is greater than the rate of photosynthesis, c_i is higher than c_a, RuBP will strongly discriminate against ^{13}C. If the rate of photosynthesis is higher than the stomatal conductance, c_i is less than c_a, which results in reduced ^{13}C discrimination. Thus, the environmental factors which control the rate of conductance and photosynthesis are the key labellers of $\delta^{13}C_{Cell}$ and varies in response to changing temperature (T), relative humidity (h) and soil moisture status (S_{ms}).

I.3.4 $\delta^{18}O$ - Isotope Labelling in C$_3$ Plants

Water (^2H and ^{18}O) isotopes in tree-rings originate from source-water (soil moisture), which is not fractionated during root uptake (WERSHAW et al., 1966). One

of the first models to approximate oxygen isotope labelling in tree-rings was presented by Dongmann et al. (1974)and was later modified by Farquhar and Lloyd (1992). The model, equations (5) to (7), accounts for evaporative enrichment of leaf water, $\delta^{18}O_{lw}$. When carbonyl oxygen exchange with free water is included, biochemical fractionation $\varepsilon_b \cong 27 \pm 3\%o$, the isotopic labelling of terrestrial cellulose can be modelled, $\delta^{18}O_{Cell}$. Both models are moderated by the ratio of the atmospheric (e_a) and intercellular air space (e_i) vapour pressure and describe it as a function of the isotopic composition of water vapour $(\delta^{18}O_{vap})$ relative to source-water $(\delta^{18}O_{sw})$, kinetic fractionation $(\varepsilon_k \cong 28\%o)$ of $H_2{}^{18}O$ through the stomata which is dependent on airflow dynamics at the leaf boundary layer (BUHAY et al., 1996; FARQUHAR et al., 1998; WANG et al., 1998) and ε^* (MAJOUBE, 1971), which is the proportional depression of equilibrium vapour pressure by heavier $H_2{}^{18}O$ which varies with temperature (DONGMANN and NURNBERG, 1974; HORITA and WESOLOWSKI, 1994).

$$\delta^{18}O_{lw} = \delta^{18}O_{sw} + \varepsilon_k + \varepsilon^* + \left(\delta^{18}O_{vap} - \delta^{18}O_{sw} - \varepsilon_k\right)\left(e_a / e_i\right) \quad (5)$$

or

$$\delta^{18}O_{lw} = \delta^{18}O_{sw} + \varepsilon_k + \varepsilon^* + \left(\delta^{18}O_{vap} - \delta^{18}O_{sw} - \varepsilon_k\right)\left(e_a / e_i\right) + \varepsilon_b \quad (6)$$

and

$$\varepsilon_k = \frac{32r_s + 21r}{r_s + r} \times 10^{-3} \quad (7)$$

Here $T(K)$ is temperature and r_s and r_b[1] are stomatal and boundary layer resistance

---

[1] May also be written as conductance (g) with the same subscripts.

to water flux, respectively. The fractionation factors were determined to be 32‰ (CAPPA et al., 2003) and 21‰ (CERNUSAK et al., 2003; KAY, 1966) for air diffusing through the stomata and the boundary layer, respectively. Because ε^* varies marginally under the range of temperatures observed during the growth season, leaf water enrichment depends predominantly on the difference between the isotopic composition of the source-water and ambient moisture vapour and on the ratio of vapour pressures, which is controlled by humidity deficit (MCCARROLL and LOADER, 2004). Figure I-4 illustrates the labelling defined above.

Equations (5) and (6) can be expressed more rigorously in alpha notation, equations (8), (9) (EDWARDS and FRITZ, 1986; YAPP and EPSTEIN, 1982) and (10) (GAT, 1996):

$$\delta^{18}O_{lw} = \alpha_e \left[\alpha_k (1-h)(10^3 + \delta^{18}O_{sw}) + (h)(10^3 + \delta^{18}O_{vap}) \right] - 10^3 \qquad (8)$$

and

$$\delta^{18}O_{cel} = \alpha_b \cdot \alpha_e \left[\alpha_k (1-h)(10^3 + \delta^{18}O_{sw}) + (h)(10^3 + \delta^{18}O_{vap}) \right] - 10^3 \quad (9)$$

where

$$\varepsilon = (\alpha - 1) \times 10^3 \qquad (10)$$

I.3.5 Damping of the Evaporative Enrichment Signal: Péclet Effect

Although the enrichment of leaf-water is empirically understood, additional exchanges such as the Péclet effect remain a topic of interest. The Péclet effect describes the discrepancy between the isotopic composition of measured and calculated leaf water $\left(\delta^{18}O_{lw} \right)$ and thus, cellulose $\left(\delta^{18}O_{Cell} \right)$. This discrepancy occurs because the backward diffusion of $H_2{}^{18}O$ from the site of evaporation is opposed by

11

the convection of water to the site of evaporation (Equations [11] and [12]) (BARBOUR and FARQUHAR, 2000; DENIRO and COOPER, 1989; MCCARROLL and LOADER, 2004; STERNBERG et al., 1986):

$$\Delta^{18}O_d = \Delta^{18}O_e \cdot e^{-vl/D} \quad (11)$$

and

$$v = Ek/C \qquad (12)$$

Here D is the diffusivity of $H_2^{18}O$ in water and v is the velocity of water movement, which is related to the evaporation rate, E, by a scaling factor k^2 and C is the concentration of water in $mol \cdot m^{-3}$. Another means of expressing the deviation is by using the dimensionless Péclet number, $\wp$, which scales $\Delta^{18}O_d \left(\Delta^{18}O_L\right)$ over the effective length of transfer, $L = k \times actual\,length$ (BARBOUR and FARQUHAR, 2000; FARQUHAR and LLOYD, 1992):

$$\Delta^{18}O_L = \frac{\Delta^{18}O_e \left(1 - e^{-\wp}\right)}{\wp} \qquad (13)$$

and

$$\wp = EL/(CD) \quad (14)$$

Authors Saurer et al. (1997) and Roden et al. (2000) have expressed the Péclet effect as a damping factor, f_o:

$$\delta^{18}O_{cel} = f_o \cdot \left(\alpha_b \delta^{18}O_{sw} + \varepsilon_b\right) + \left(1 - f_o\right) \cdot \left(\alpha_b \delta^{18}O_{lw} + \varepsilon_b\right) \qquad (15)$$

Additional exchanges may take place after the sucrose is transported from the leaves

---

[2] varies between 10^2 and 10^3

to the sink tissue (meristemic regions) in the phloem. One of these exchanges occurs as sucrose is cleaved to form hexose phosphate and up to 20% of the free oxygen can be replaced by oxygen in water. A portion of the hexose phosphate can also continue through the futile cycle, if not used immediately to form cellulose and can result in an additional 60% exchange of oxygen (BARBOUR and FARQUHAR, 2000; MCCARROLL and LOADER, 2004). Estimates have placed the proportion of exchangeable oxygen in cellulose to range from 0.38-0.47 (STERNBERG et al., 1986; YAKIR and DENIRO, 1990). Although there are more rigorous calculations (BARBOUR and FARQUHAR, 2000; BARBOUR et al., 2002), a f_o factor of 40% proposed by Roden et al. (2000) was applied and tested in Chapter IV. An example calculation is present in section 0 on page 161.

I.3.6   Precipitation

Precipitation originates from evaporated ocean water and follows a predictable enrichment pattern during evaporation and rainout due to the differences in vapour pressure between $H_2^{16}O$, HDO and $H_2^{18}O$. As the depleted air mass migrates poleward and precipitation events occur, the resulting precipitate and residual air mass follow along a predictable line in $\delta^2 H$ and $\delta^{18}O$ space called the Global Meteoric Water Line (GMWL) equation (16) and Figure I-6 *A*, (CRAIG and GORDON, 1965; DANSGAARD, 1964; ROZANSKI et al., 1993). This line however fluctuates as a result of local geographic and environmental factors and is defined as the Local Meteoric Water Line (LMWL) equation (17) and Figure I-6 *A*, Fort Chipewyan (WOLFE et al., 2005).

$$\delta^2 H = 8.17 \cdot \delta^{18}O + 10.35(‰) \qquad (16)$$

$$\delta^2 H = 6.7 \cdot \delta^{18}O - 19.2(‰) \qquad (17)$$

The factors include latitude, altitude, distance from the coast, amount of precipitation and surface air temperature (DANSGAARD, 1964). For this thesis two of these factors are especially important and will be discussed specifically. The first is the observed link between surface air temperature and the isotopic composition of precipitation; this relationship may propagate in tree-rings as a paleoclimate indicator. The second is the amount of precipitation and is generally a result of deep cooling of an air mass which results in increased rainfall, e.g. orographic rain events in the Rocky Mountains (HOEFS, 1997).

For simplification, it is assumed that when precipitation condenses from an air mass it occurs under equilibrium conditions (h =100%), thus, no kinetic exchange or evaporation effects have taken place during formation or rainout.

I.3.7   Variation in the Relation between Precipitation and Isotopic Composition

I.3.7.1 Circulation Regime

Over the last millennium the climate variability in the Northern Hemisphere has been strongly linked to variations in the pattern and strength of atmospheric circulation (FOLLAND et al., 2001; KREUTZ et al., 1997; LAMB, 1977). These variations in regime strength can systemically vary the pattern of migration of atmospheric moisture and thus, affect the amount and isotopic composition of precipitation, $\delta^{18}O_{\mathrm{Pr}ec}$, e.g. Tibetan Plateau, Rocky Mountains and Sierra Nevada Mountains (FOLLAND et al., 2001).

Four atmospheric circulation indices were selected for their potential to vary the isotopic composition of precipitation in the PAD due to orographic precipitation events or their ability to vary the pattern of moisture transport across the North American continent; Northern Hemisphere Annular Mode (NAM) or Arctic Oscillation (AO), North Atlantic Oscillation (NAO), Pacific/North American (PNA) pattern and the North Pacific index (NP). These patterns are indices of pressure and temperature at specific locations and are sometimes used as interchangeable terms due to teleconnection[3] (WALLACE and GUTZLER, 1981).

A negative NAM/AO is characterized by a pressure drop over the pole and a rise in high latitudes ~55ºN. This results in a strengthening of the westerly zonal flow along

---

[3] The concept of *teleconnection* was introduced by Wallace and Gutzler in 1981 and refers to a recurring and persistent large-scale pattern of pressure and circulation anomalies.

~55ºN and 35ºN from Russia towards western Canada. This is also accompanied by the displacement of atmospheric mass between the Arctic basin and the mid-latitudes (THOMPSON and WALLACE, 2001; TRENBERTH and HURRELL, 1994). The Southern Hemisphere Annular Mode (SAM) is an analogous pattern that occurs in the Southern Hemisphere (VISBECK et al., 2001).

NAO describes the fluctuation in atmospheric mass between the North Atlantic regions of the subpolar low pressure system near Iceland and the subtropical anticyclone near the Azores/Portugal (HURRELL, 1995a; TRENBERTH and HURRELL, 1994). It has been suggested that the NAM incorporates the smaller scale NAO which would make the NAO a regional manifestation of a larger signal (THOMPSON and WALLACE, 2001).The PNA index describes the synoptic pattern of the mid-tropospheric geopotential height field from eastern North America to the mid-Pacific (WALLACE and GUTZLER, 1981). Negative indices are associated with above-normal geopotential heights along the west coast of North America accompanied by strong negative geopotential heights in the mid-Pacific near ~45ºN and over the southeastern United States (WALLACE and GUTZLER, 1981). The alternative would be a west-to-east oriented mid-tropospheric flow pattern.

The NP index is a measure of circulation over the north Pacific and is characterized by the area-weighted mean sea surface pressure at 30 to 60ºN, 160ºE to 140ºW. This index is also a strong indicator of changes in the intensity of the winter Aleutian low (D'ARRIGO et al., 2005; TRENBERTH and HURRELL, 1994).

Theoretically a positive NAM/NAO or negative NP/PNA translates into westerly circulation which forces air masses over the Rocky Mountains causing depletion of

16

the heavy isotopes due to adiabatic cooling and precipitation amount effects. These forced rain events extend the rain shadow beyond the Rocky Mountains and result in depleted PAD precipitation during winter months. A negative NAM/NAO or positive NP/PNA results in meridional circulation which allows for moisture to be redirected around the northern flank of the Rocky Mountains. The redirection results in limited orographic precipitation events, a shorter rain shadow behind the Rockies and enriched precipitation during the winter months, Figure I-5.

I.3.7.2 Amount Effect

The amount effect relates the amount of precipitation to the progressive isotopic depletion of the residual air mass $\delta^{18}O(\text{‰})$, equation (18) and Figure I-6 *C*. This effect is pronounced in tropical regions near the equator. In regards to the PAD, the amount effect which is of interest does not occur directly over the region, but instead, occurs on the windward side of the Canadian Cordillera. As circulation drives an air mass up over the mountains, the volume of precipitation from adiabatic cooling results in the progressive and predictable depletion of the air mass (LAWRENCE and WHITE, 1991).

$$\delta^{18}O = -0.80883 \text{ x } P + 59.40(\text{‰}) \qquad (18)$$

Research indicates that the 20th century circulation regime is the most zonally driven over the last millennium (HURRELL, 1995a; HURRELL, 1995b; THOMPSON and WALLACE, 2001; TRENBERTH and HURRELL, 1994; VISBECK et al., 2001; WALLACE and GUTZLER, 1981). If measurements and reconstructions hold true, the isotopic composition of the air mass which reaches the PAD in the rain shadow on the

leeward side of the Cordillera is thus directly a function of the strength of the dominant circulation regime and the resulting trajectory of the air mass (tested and discussed in-depth in Chapter IV).

I.3.7.3 Temperature

A constant $\delta^{18}O - T$ relation, equation (19) and Figure I-6 *B*, is used in this thesis to represent the temporal isotope enrichment per degree Kelvin at ground surface (EDWARDS and FRITZ, 1986). If the earth was flat and all variables remained constant then the isotopic composition of precipitation with respect to temperature should have the same temporal slope through time (JOUZEL et al., 1997). The assumption that the modern $\delta^{18}O - T$ relation is constant is valid but the observed slope is variable due to variations in precipitation origin, microphysical processes, cloud/surface temperature ratio, seasonality of precipitation and atmospheric processes.

$$\Delta\delta^{18}O = 0.65\text{‰/K} \qquad (19)$$

The lack of a constant observed $\delta^{18}O - T$ was observed when ice-core $\delta^{18}O - T$ was compare to ice-core borehole paleo-thermometry (BOYLE, 1997; CUFFEY et al., 1995). During the study, the borehole thermometry indicated a 15-20°C temperature difference between the Last Glacial Maximum and the Holocene, double that of previous estimates. The borehole data were also reinforced by firn thickness analysis (BOYLE, 1997). Similar $\delta^{18}O - T$ variability has also been observed by Plummer et al. (1993), Lipp et al. (1996) Hammarlund et al. (2002)and Edwards et al. (2008; EDWARDS et al.) and have been attributed to circulation-dependent effects. Birks

(2003) also demonstrated that the isotopic composition of precipitation with respect to temperature at Wynyard, Saskatchewan, and Gimli and The Pas, Manitoba, varied directly with the PNA index. With an average PNA of +0.49 the average slope was 0.28 ‰/K, while with an average PNA of -0.49 the average slope was 0.48 ‰/K at Gimli, for example, during two different years.

I.4   Previous Tree-Ring Work in Peace-Athabasca Delta

I.4.1   Preliminary Dendrochronological and Dendroclimatological Assessment of New Tree-Ring Collections from the Peace-Rochers Confluence, Quatre Fourches River, Quatre Fourches Upland, Greenstar Lake and Bustard Island sites, Alberta, By Glen M. MacDonald, David F. Porinchu and Thomas W. D. Edwards. University of California at Los Angeles, June 2005 Interim Report to BC Hydro

MacDonald (2005) conducted this exercise to provide cross-dated tree-cores for isotopic analysis, an assessment of the further usefulness of tree-ring records to provide climate reconstructions for the PAD region and to characterize the climate-growth relations in tree-rings so that the isotopic records can be better interpreted.

After the tree-ring radii were cross-dated and verified using COFECHA (HOLMES, 2000) the individual dendrochronological statistics for all five sites (Described in above section I.2.3) were derived using ARSTAN (HOLMES, 2000).

MacDonald (2005) found that a common signal is present between the tree-ring records from each site. This common signal provides support for the application of dendrochronologies as a valid chronological tool in the PAD. His analysis also indicates that the trees are sensitive to regional precipitation variation over multiple years, up to five. MacDonald found that the trees were most sensitive (significantly positive) to annual precipitation (January to December). MacDonald also concluded that due to the multiple year climate sensitivity of tree-rings, annually resolved

comparisons with climate data may be misleading or unrealistic (2005). Finally, MacDonald found that multiple regression modelling using tree-ring chronologies has the potential to reconstruct dendroclimatologies when the chronologies used are carefully selected to reflect the PAD.

I.4.2 $\delta^{13}C$ and Ring Width Analysis: How Well Do they Correlate among themselves and with varying Environmental Factors? By Guillaume Couillard, University of Waterloo, Waterloo, Ontario, Canada, 2004. Bachelors Thesis.

The objective of Couillard's thesis (2004) was to identify the statistical relationships that exist between ring-widths and carbon chronologies from individual cores/trees from GSL and PRC and growth season environmental temperature and precipitation data from the Canadian homogenized historical gridded data (CANGRID, 2000; MCKENNEY et al., 2007).

Couillard completed this by identifying marker years in the ring-width chronology; e.g. maxima 1919, 1935, 1978 and minima 1921, 1961 and 1981. Couillard then concluded that the intra-tree and intra-site ring-width variation between cores was significant, r = 0.87 and 0.52 (average) respectively.

When comparing intra-tree and intra-site variability his analysis indicated stronger common environmental controls on isotopic labelling, r = 0.87 and 0.71 (average) respectively. Couillard then concluded that carbon isotopic labelling is more dependent on environmental conditions than ring-width.

When ring-width was compared against growth season precipitation and temperature

data, temperature correlated significantly while precipitation did not. This led Couillard to conclude that growth season precipitation is not a significant source of variability in ring width. Although, temperature correlated significantly with ring-width, it did not have significant consistent (long- or short-intervals) correlations and led Couillard to hypothesize that temperature was not a consistent or primary factor of tree-growth at Greenstar Lake. When comparing $\Delta\delta^{13}C(‰)$ with precipitation there were no significant correlations. Temperature showed strong positive correlations with $\Delta\delta^{13}C(‰)$ and was identified as a primary labeller.

Couillard (2004) also concluded that temperature labelling was not enough to account for the annual variability in $\Delta\delta^{13}C(‰)$ and thus, another parameter such as relative humidity should also be a factor in labelling.

I.4.3 Isotope Dendroclimatology Studies in the Peace-Athabasca Delta, Alberta by Joscelyn Nesto-Leigh Bailey, University of Waterloo, Waterloo, Ontario, Canada, 2005. Bachelors Thesis.

Bailey's (2005)objective was to separate climate and hydrology in the Peace sector of the PAD by comparing $\delta^{13}C$ and $\delta^{18}O$ and ring-width chronologies at GSL and PRC. Using these data, Bailey (2005) also modelled a number of proxies for flood frequency and intensity and compared his reconstructions by comparing them to instrumental data and independent proxy-based reconstructions (TIMONEY et al., 1997).

Bailey hypothesised that the variability between PRC's ring-width chronologies increased with sampling distance from the river. This hypothesis was strengthened

after comparing PRC's chronologies to those of GSL, which have less variable irrigation due to its separation from the majors rivers in the delta. PRC's chronology variability is thought to reflect the tree micro-environment as a function of topography and distance from the confluence of the Rivière des Rochers and the Peace River.

The above hypothesis was supported when the $\delta^{13}C$ chronologies from PRC and GSL were used to reconstruct flood frequency, r = 0.54. The oxygen chronology showed little or no significant correlation to mean annual temperature or precipitation, average r = -0.17.

Bailey applied the coupled-isotope response surface approach, using coefficients defined by Edwards et al. (2004a; 2004b), to 50- and 300-year chronologies of $\delta^{13}C$ and $\delta^{18}O$ to reconstruct summer atmospheric moisture and mean annual air temperature. These reconstructions predicted shifts in mean annual temperature and growth season relative humidity at the end of the Little Ice Age, AD 1890s. Edwards et al. (2008; 2004a; 2004b) also found these shifts and hypothesised them to be the result of an environment shift due to more zonal circulation regime.

I.4.4   Comparison of Early- and Latewood $\delta^{13}C$ and $\delta^{18}O$ Signals in White Spruce (Picea glauca) from Northern Alberta, By Jeffrey James Melchin, University of Waterloo, Waterloo, Ontario, Canada, 2007. Bachelors Thesis.

The objective of Melchin's Bachelors thesis (2007) was to identify seasonal isotopic labelling of $\delta^{13}C$ and $\delta^{18}O$ in earlywood, latewood and wholewood with respect to

23

temperature, relative humidity and precipitation.

Earlywood, latewood and wholewood chronologies where developed from a ~70-year old tree on BITC. Although this tree showed 30- to 35-year of juvenile effects (discussed in detail below in Chapter II), it was selected for its large and well-defined earlywood and latewood sections. Each of the three chronologies were compared to two mature (120 and 190 year old) trees from BITC.

Melchin observed that earlywood $\delta^{13}C$ was ~ 1.0 to 2.5‰ more enriched in ^{12}C than latewood during the juvenile interval. His initial hypothesis was that the enrichment is due to the initiation of spring growth due to warming temperatures and the availability of moisture from melting snow. Melchin then noted a convergence of the chronologies after the cessation of the juvenile effects and hypothesized that this trend was due to decreasing ring-width growth with increasing tree age, effectively the earlywood decreased in size with age while the latewood remained approximately the same. Melchin then assumed that the isotopic signals should converge.

When Melchin compared the wholewood $\Delta\delta^{13}C$ to the earlywood and latewood chronologies he found correlations of 0.67 and 0.64 (r, P < 0.001), respectively. Between the early- and latewood chronologies Melchin found correlation of 0.72 (r, P < 0.001). There were no significant correlations between unrelated wholewood and the earlywood and latewood chronologies, highest r = 0.34. When Melchin compared the $\Delta\delta^{18}O$ values from the earlywood and latewood samples he again found a significant relationship, r = 0.73 (P < 0.001). $\Delta\delta^{18}O$ wholewood chronologies from early- and latewood were not available but the unrelated chronologies showed no significance correlations.

Melchin also examined a carry-over effect in $\Delta\delta^{13}C$ and $\Delta\delta^{18}O$ with regards to the early- and latewood. Melchin proposed that the earlywood $\Delta\delta^{13}C$ of the present year were produced from photosynthates of the previous year. When the analysis was repeated with $\Delta\delta^{18}O$ chronologies, Melchin found no evidence to suggest that there was any substantial carry-over effect.
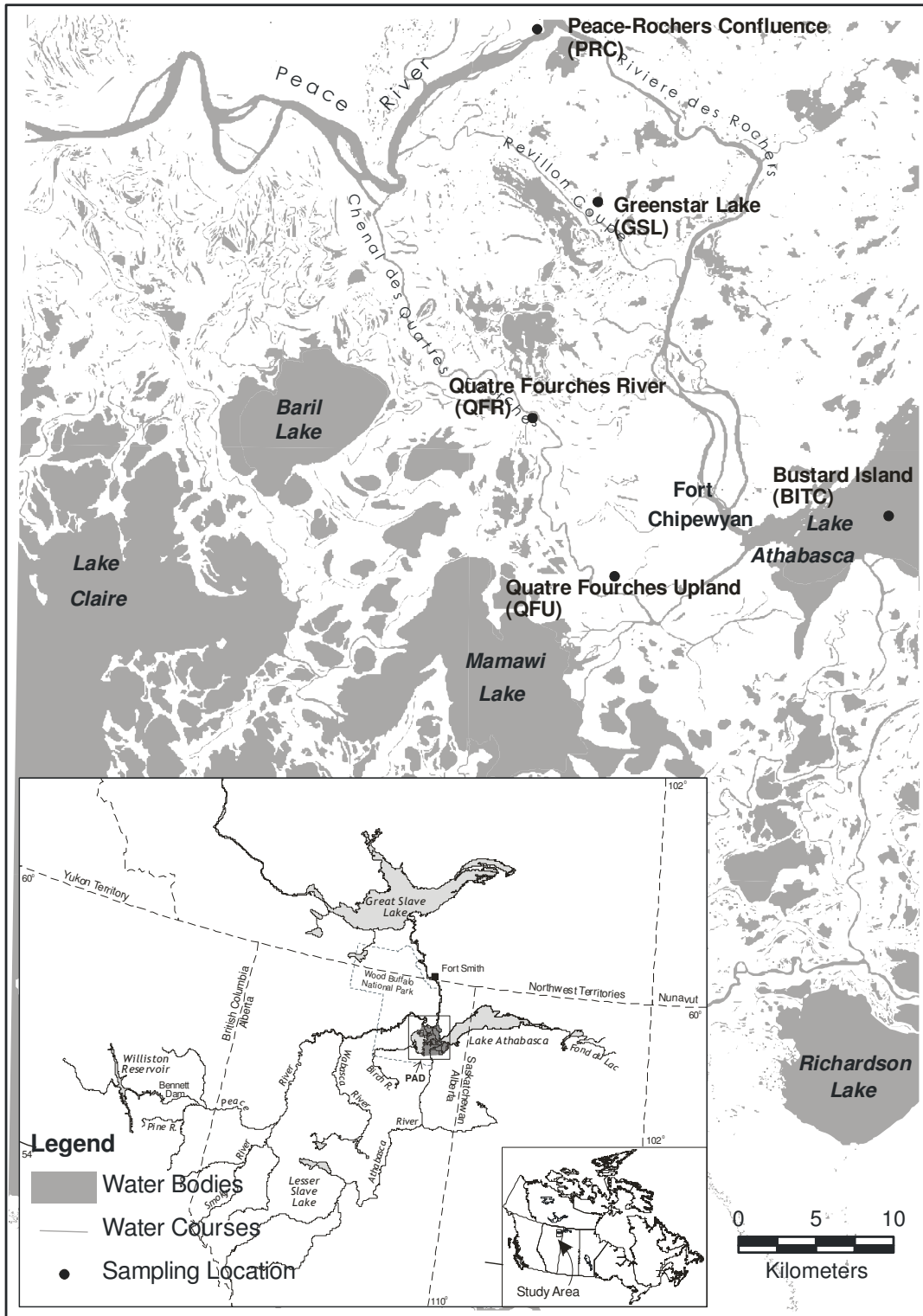
Figure I-1. The Peace Athabasca Delta (PAD), northeastern Alberta, Canada is west of Lake Athabasca.
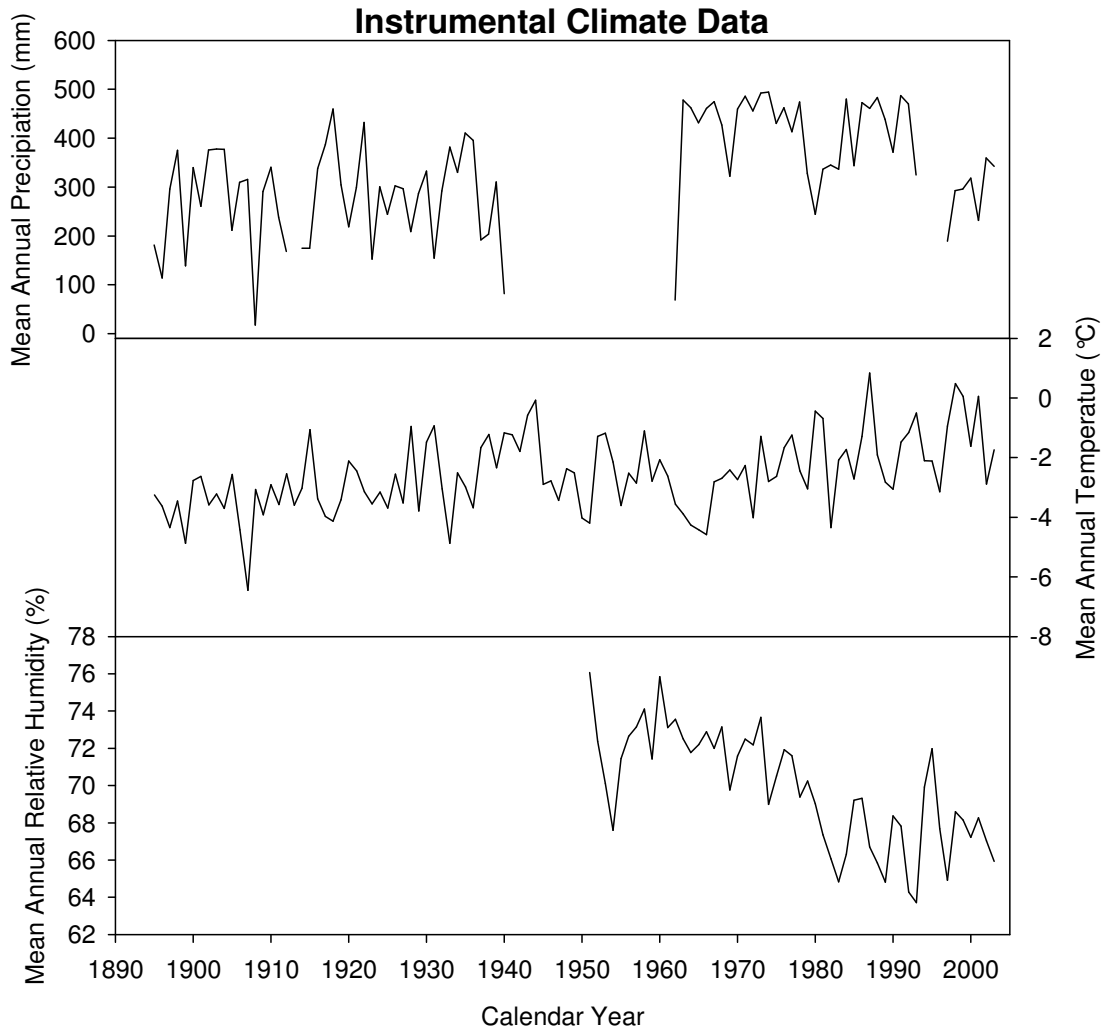
Figure I-2. The modern mean annual temperature and precipitation of Fort Chipewyan from AD 1891 – 2003 and the mean annual relative humidity measured at Fort McMurray (GOODISON and LOUIE, 1986; MEKIS and HOGG, 1997; MEKIS and HOGG, 1999; METCALFE et al., 1997; VINCENT and GULLETT, 1999).

Controls on fractionation

Influencing factors

Leaf morphology   **Irradiance**

$\delta^{13}C_{air}$

Fractionations   **Rates**

Carboxylation   Photosynthetic rate

b

-27‰

-4.4‰

a   g

Diffusion   Stomatal conductance

c_a

CO$_2$ concentrations

Air humidity

Root to leaf distance   Temperature

Xylem hydraulic conductivity   Precipitation amount and seasonality

Bark photosynthesis

Recycling of respired CO$_2$ Snow-melt

Soil freezing

Fine root network

Rooting depth   **Soil moisture status**

$$\delta^{13}C_{plant} = \delta^{13}C_{air} - \varepsilon_a - (\varepsilon_b - \varepsilon_a)(c_i / c_a)$$
$$and$$
$$c_i = c_a - A \cdot P / g_s$$

Figure I-3. Diagram of the isotopic labelling of $\delta^{13}C_{Cell}$ for C3 plants with identified isotopic labellers and a leaf cross-section. The cross-section identifies the fractionations that occur from carboxylation by rubulose-1, 5-biphosphate (RuBP) and diffusion across the leaf atmosphere interface. Diagram modified from McCarroll and Loader (2004) and includes the Farquhar et al. (1982) equations 3 and 4.
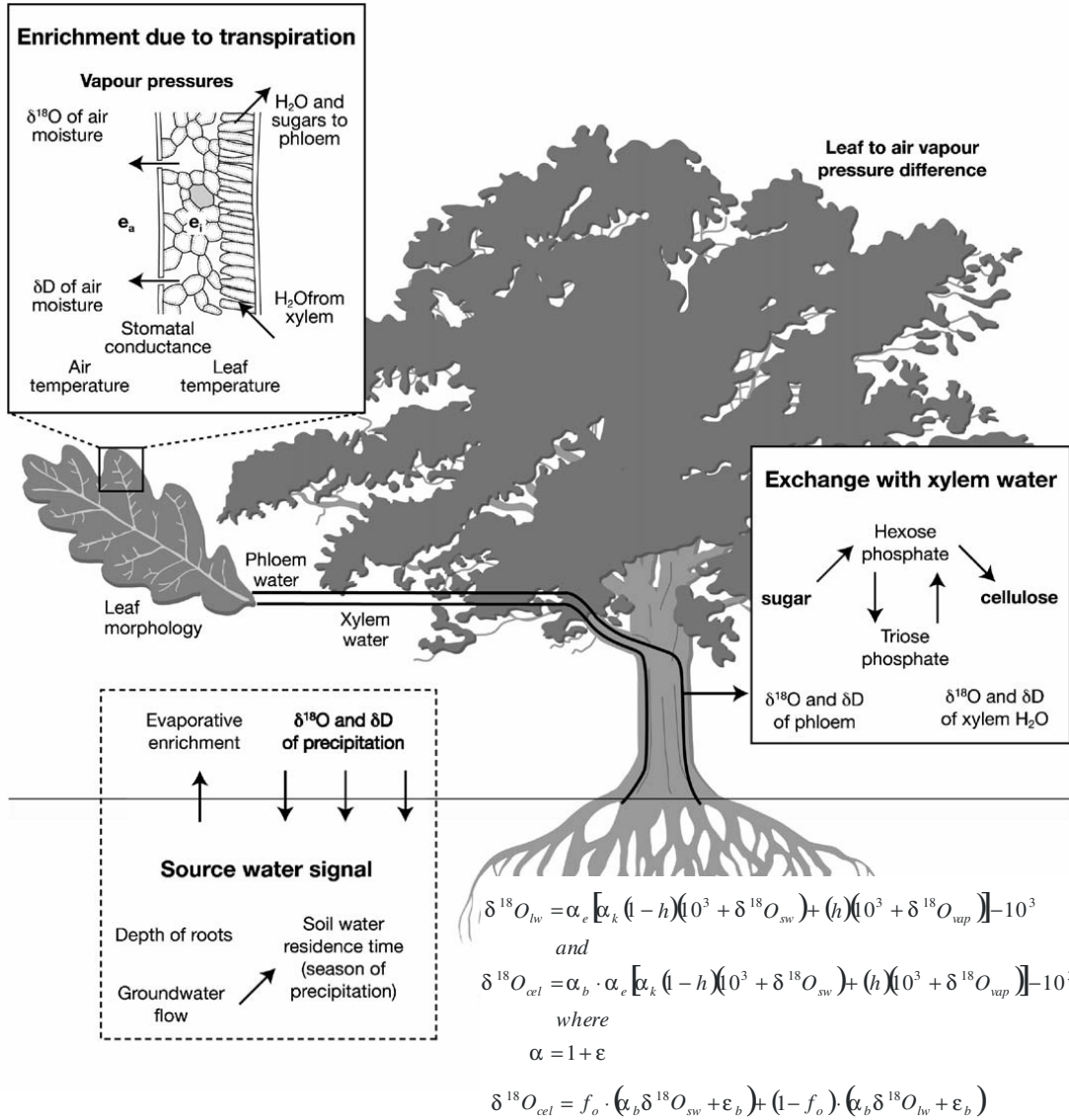
Figure I-4. Diagram of the isotopic labelling of $\delta^{18}O_{Cell}$ for C3 plants. The diagram shows a leaf cross-section and the factors that control the evaporative enrichment of leaf water. Also illustrated is a flow chart showing the exchange of leaf and xylem water. Diagram modified from McCarroll and Loader (2004) and includes the Yapp and Epstein et al. (1982) equations 8 to 10.
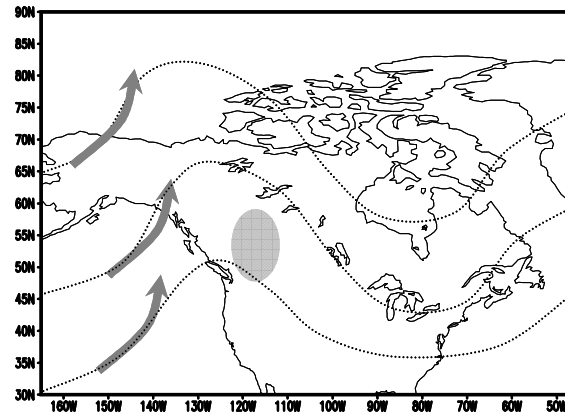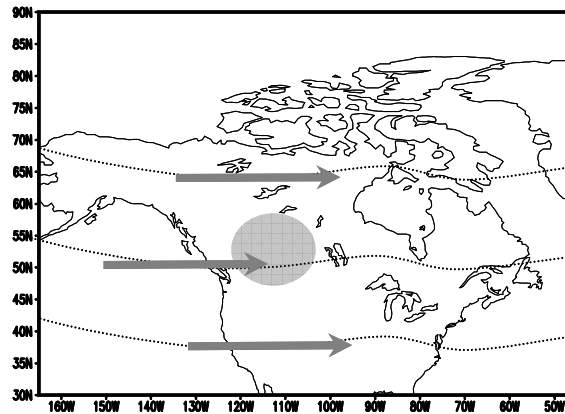
Figure I-5. Diagram illustrating the phase of atmospheric circulation (-/+) and the resulting path (dotted line) of atmospheric vapour. A schematic rain shadow due to precipitation events is illustrated by the grey oval. Diagram modified from Bailey and Edwards (2008) and original published in Birks (2003).
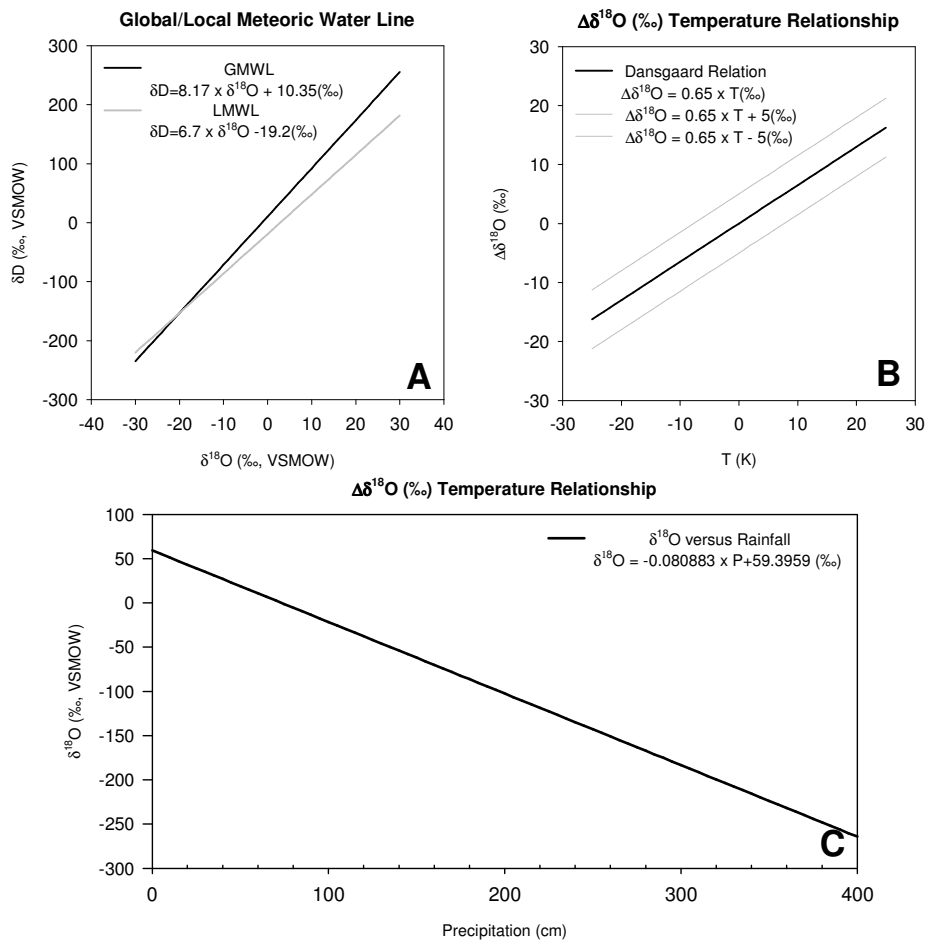
Figure I-6. *A.* $\delta^{18}O$ versus δD for the Local (LMWL) for Fort Chipewyan and Global Meteoric Water Line (GMWL) (CRAIG and GORDON, 1965; WOLFE et al., 2005). *B.* $\delta^{18}O$ versus temperature (K) relation and systematic shifts (± 5.0 ‰) in $\delta^{18}O - T$ intercept (DANSGAARD, 1964). *C.* $\delta^{18}O$ versus precipitation amount (cm) based on Lawrence and White (1991).

Table I-1. Site and core identification. Core labels are also expressed in del (δ) or delta (Δ) with units of per thousand (‰).

Location		Identifiers used in label				Data Sets Availible	
		Tree No. (Num)	Tree Core (Alph)	Carbon (‰)	Oxygen (‰)	Car	Oxy
LOWLAND	PRC	4	A	Car	Oxy	PRC.4.A.Car	PRC.4.A.Oxy
		5	AC	Car	Oxy	PRC.5.AC.Car	PRC.5.AC.Oxy
		9	A	Car	Oxy	PRC.9.A.Car	PRC.9.A.Oxy
		9	A.adj	Car		PRC.9.A.adj.Car	
			Average	Car	Oxy	PRC.Average.Car	PRC.Average.Oxy
	QFR	10	BC	Car	Oxy	QFR.10.BC.Car	QFR.10.BC.Oxy
		10	F	Car		QFR.10.F.Car	
		10	BC.F	Car		QFR.10.BC.F.Car	
		13	BD	Car		QFR.13.BD.Car	
			Average	Car	Oxy	QFR.Average.Car	QFR.Average.Oxy
UPLAND	QFU	3	B	Car	Oxy	QFU.3.B.Car	QFU.3.B.Oxy
		3	B.adj	Car		QFU.3.B.adj.Car	
		10	BC	Car		QFU.10.BC.Car	
		12	AB	Car	Oxy	QFU.12.AB.Car	QFU.12.AB.Oxy
			Average	Car	Oxy	QFU.Average.Car	QFU.Average.Oxy
	GSL	3	C	Car	Oxy	GSL.3.C.Car	GSL.3.C.Oxy
		10	A	Car		GSL.10.A.Car	
		10	B	Car	Oxy	GSL.10.B.Car	GSL.10.B.Oxy
		10	A.B	Car		GSL.10.A.B.Car	
			Average	Car	Oxy	GSL.Average.Car	GSL.Average.Oxy
ISLAND	BITC	10	AB	Car	Oxy	BITC.10.AB.Car	BITC.10.AB.Oxy
		13	ABC	Car	Oxy	BITC.13.ABC.Car	BITC.13.ABC.Oxy
			Average	Car	Oxy	BITC.Average.Car	BITC.Average.Oxy
PAD.Average			Average	Car	Oxy	PAD.Average.Car	PAD.Average.Oxy

II   Methodology and Time-Series Development

Synopsis

Part One: *Generalized step-by-step procedure for the isolation of α-cellulose from tree-rings cores. This chapter reviews the online-sampling method used at the Environmental Isotope Laboratory, University of Waterloo, for $\delta^{13}C_{Cell}$ and $\delta^{18}O_{Cell}$ analysis and the data correction techniques for quality assurance and control.*

Part Two: *Contains a description of the data adjustments that were done to the $\delta^{13}C_{Cell}$ -chronologies to account for environmental isotopic trends in labelling. This section also describes how the time-series were organized to produce the site and regional $\delta^{13}C_{Cell}$ - and $\delta^{18}O_{Cell}$ -dendrochronologies. This section describes how the instrumental temperature, relative humidity and precipitation data were grouped to form the datasets used in this and later chapters for comparison and analysis. The final sections in this chapter address the signal strength of the time-series, whether they are from an individual core or from a composite dataset.*

Part One: Methods of Sample Preparation

II.1   Cross-Dating Samples for Stable Isotope Analysis

The individual dendrochronological statistics was derived using ARSTAN (HOLMES, 2000) after the individual radii were cross-dated and verified using COFECHA (HOLMES, 2000) at the University of California at Los Angeles by Glen McDonald and David Porinchu. The cores were then returned to the University of Waterloo's Environmental Isotope Laboratory for chemical digestion and stable isotope analysis.

II.2   *Chemical Digestion Procedures*

Methods for α-cellulose preparation for isotopic analysis have been developed at the University of Waterloo's Environmental Isotope Laboratory (ELGOOD et al., 1997; HEEMSKERK and DIEBOLDT, 1994) and following Green (1963) and Sternberg (1989). All chemical extractions were performed in a fume cupboard by trained individuals. The appropriate precautions were taken to adhere to the University of Waterloo laboratory safety protocols.

II.2.1 Stage One: Sub-sampling and Milling

The chronologies were sub-sampled annually as wholewood (earlywood and latewood) using a light microscope and scalpel. Each sample was milled for four minutes, additional time was allotted for larger samples, using a Retsch MM200 and was then transferred from the milling vial to a 50 mL test tubes using de-ionized water. The samples were then placed in a convection oven at 40 ºC for 24 hours after allowing sufficient time to settle and the aspiration of excess water.

II.2.2 Stage Two and Three: Solvent Extraction

Solvent extraction to removed tannins, resins and lipids was done in two stages. The first stage began by saturating the samples with 20 mL of benzene (C_6H_6) and ethanol (C_2H_6O) (2:1) for 18 hours. If the samples retained a dark colouration, the supernatant was removed and stage one was repeated. In stage two, the samples were saturated with 20 mL of acetone (CH_3COCH_3) (reagent grade) for 18 hours. After the samples had settled, the acetone was aspirated and the samples air dried.

II.2.3 Stage Four: Bleaching

To remove lignin the samples were then bleached. The samples were placed in a 70ºC water bath with 40 mL of de-ionized water. 0.15 mL of glacial acetic acid (CH_3COOH) and 0.15 g of sodium chlorite ($NaClO_2$) were added at hourly intervals over five hours. The solution was stirred at every interval. After the final application the solution remained in the water bath for one hour before being removed. After cooling for one hour the samples were then aspirated[4] and refilled with de-ionized water and allowed to settle for 18-24 hours. Daily rinsing continued until the solution became clear and no odour remained.

II.2.4 Stage Five: Alkaline Hydrolysis

Non-glucan polysaccharides, mannan and xylan were removed using alkaline hydrolysis. 20 mL of sodium hydroxide (NaOH) (17%) were added to the wet samples after the final decanting of the bleaching solution. This solution was allowed to sit for ~45 minutes before being diluted with de-ionized water and was then aspirated and diluted after another ~45 minutes had elapsed. The solution was then diluted and aspirated daily until it reached the pH of de-ionized water, 6.5.

II.2.5 Stage Six: Freeze Drying and Weighing

After being transferred to scintillation vials and frozen, the samples were then freeze-dried for 72 hours. Samples for carbon analysis were weighed to a range of 0.090 to 0.130 mg and placed into tin capsules. A duplicate was weighed for every tenth

---

[4] as much as 25 mL was removed safely

sample. Samples for oxygen analysis were weighed out to range between 0.100 and 0.120 mg and a duplicate was weighed for each sample whenever possible. Oxygen samples were desiccated for at least 24 hours and were not allowed to sit for more than 30 minutes prior to analysis to ensure that traces of atmospheric moisture have not contaminated the sample.

II.3 *Stable-Isotope Analysis*

II.3.1 Instrumental Carbon Isotope Analysis

Purified α-cellulose samples were run for carbon isotopes on an Isochrom Continuous Flow Stable Isotope Mass Spectrometer (GVInstruments/Micromass-UK) or a Thermo Finnigan DELTA plus Continuous Flow Stable Isotope Ratio Mass Spectrometer coupled to Carlo Erba CN Elemental Analyzer at the Environmental Isotope Laboratory at the University of Waterloo, Ontario, Canada.

Samples were dropped via carousel into a tube heated to 1000ºC in a continuous flow of helium gas. A pulse of oxygen gas was then injected into the carrier gas and the combustion products passed over a series of reduction and combustion reagents. Traces of water were removed using a chemical trap before the resulting N_2 and CO_2 gas could be resolved to separate peaks by a gas chromatography column. The mass spectrometer received the sample gas via a capillary tube and open split.

Ten samples of international and internal standards, IAEA-CH6 (sugar), EIL-71 (cellulose), EIL-32 (graphite) and WB-24 (cellulose), of known isotopic composition with a range of weights were initially run to assess the reproducibility of the peaks. Standards were also placed throughout the run on every tenth sample to correct for possible machine drift. Normalizing and adjusting of the sample was achieved in the same manner as that stated below and the analytical uncertainty is ± 0.2‰.

II.3.2 Instrumental Oxygen Isotope Analysis

Purified α-cellulose samples were run for oxygen isotopes at the Environmental

Isotope Laboratory at the University of Waterloo, using a high-temperature HEKAteck furnace [1300°C] configured for oxygen pyrolysis. The furnace was connected to an elemental analyser [EA3028] which was interfaced with a GV IsoPrime Stable Isotope Ratio Mass Spectrometer set for continuous flow with a helium carrier gas. The samples were combusted in a glassy carbon tube that was packed with glassy carbon chips that provided excess carbon for the oxygen to bind to, producing CO (gas).

The CO (gas) passes through a 5Å molecular sieve-packed stainless-steel GC column held at 90°C before entering the mass spectrometer via a split capillary arranged in an open configuration. The ratio is generated by integrating the ion beams area from the CO (gas) at atomic mass 28 ($^{12}C^{16}O$) and 30 ($^{12}C^{18}O$). This ratio is then compared to a reference gas of known composition.

To maintain stability and reproducibility (standard deviation (σ) of ≤ 0.1‰), nine CO standards bracket the samples. Troubleshooting was conducted if the standard deviation was exceeded. Three internal standards [in triplicate] were run after every tenth sample [IAEA-C3 (~32‰), SIGMA (~27‰) and WB-24 (~22‰)] to monitor transient fluctuations of the system. The analytical uncertainty is ± 0.4‰.

II.3.3 Adjusting for Machine Drift in Carbon and Oxygen Isotopes

The samples were normalized to the standards stated above by linear fitting. If the measured values of the standard were greater than two standard deviations or the normalized mean value, then that value was removed. If the sample peak exceeded ~± 20% of the average peak height of the standard, then the sample was rerun.

Part Two: Methods of Time-Series Development

II.4 Stable-Isotope Adjustments for Environmental and Physiological Effects and Data Compositing

II.4.1 Suess Effect: Correcting for the Fossil-Fuel Effect on $\delta^{13}C_{ATM}$ (‰)

The combustion of fossil fuels has lowered average $\delta^{13}C_{ATM}$ by ~1.5‰ since 1850 because of dilution by $^{12}CO_2$ (FRANCEY and FARQUHAR, 1982; FRIEDLI et al., 1986; SUESS, 1970). This shift in $\delta^{13}C_{ATM}$ must be taken into account when interpreting $\delta^{13}C_{Cell}$ data from tree-rings cellulose in terms of changing discrimination against ^{13}C. The method described in McCarroll and Loader (2004) was applied in this thesis.

II.4.2 Juvenile Effects

Juvenile effect is used to refer to low values of $\delta^{13}C_{Cell}$ observed in the innermost tree-rings. Initially, this effect was thought to reflect the relationships between the partial pressure of CO_2 in the intercellular space and the ambient atmosphere surrounding the leaf (FRANCEY and FARQUHAR, 1982). Alternative hypotheses including low irradiance or reduced gas exchange due to an enclosed canopy have been proposed but were later rejected as the same effect has also been observed in trees growing in isolation (FRANCEY and FARQUHAR, 1982; GRINSTEAD, 1977). Thus, an age-related trend was proposed instead. This was noticed when comparing the

longest chronologies at PRC to the comparatively shorter ones. In this thesis, the first 30 years of each chronology were removed to amend the chronologies.

II.4.3 Stable-Isotope Composite Chronologies

The $\delta^{13}C$ and $\delta^{18}O$ time-series were organized into 12 (ten site and two regional) composite chronologies. To maintain a consistent weighting of each chronology in the composite, any trees having multiple time-series were grouped together prior to compositing to ensure that the signal was not biased by repetition in sampling. The PAD.$_{CAR}$ (Figure II-6) and PAD.$_{OXY}$ (Figure II-12) chronologies contain time-series from all five sites - Figure I-1 to Figure II-5 for $\delta^{13}C$ and Figure II-7 to Figure II-11 for $\delta^{18}O$. This method of compositing was done to reduce tree-specific noise and should help to identify common signals.

II.4.4 Climate Data Chronologies: Description & Organization

Monthly precipitation totals (1898-2005), monthly temperature (1898-2005) and hourly relative humidity (1953-2005) were obtained via the Adjusted Historical Canadian Climate Date (AHCCD) (GOODISON and LOUIE, 1986; MEKIS and HOGG, 1997; MEKIS and HOGG, 1999; METCALFE et al., 1997; VINCENT and GULLETT, 1999), courtesy of the Climate Monitoring and Data Interpretation Division, of the Climate Research Branch, a subgroup of the Meteorological Service of Canada.

The hourly values for relative humidity were averaged to reflect monthly values. Temperature and precipitation are for Fort Chipewyan airport, Alberta, Canada [58°46'11.00"N, 111°07'10.16"W], while the humidity dataset is adjusted to Fort

McMurray (airport), Alberta, Canada [56°38'59.99"N, 111°13'11.98" W]. Climate normals for 1951 to 1980 were also obtained for Fort Chipewyan, Embarras and Fort McMurray. These climate normals were used to address the annual distribution and range with respect to AHCCD values for Fort Chipewyan and McMurray with regard to relative humidity.

II.4.4.1 Temperature

The temperature data were organized into three subgroups, minimum, mean and maximum (Figure II-13). This was done to address if any variation in monthly temperature was the source of isotopic labelling in $\delta^{13}C_{Cell}$. Each subgroup displayed a similar distribution with maximum temperature values occurring in July. The lowest values occurred in January and December. January and December also show the widest range in temperature variability, $\pm$ 10°C. When compared to the climate normals for Fort Chipewyan, Embarras and Fort McMurray, the distribution and range is sufficient and gave no indication that AHCCD data quality was a concern.

II.4.4.2 Relative Humidity

The humidity data are organized into three subgroups; minimum values over 24 hours (0h00-23h00), mean daytime values (6h00-20h00) and mean values over 24 hours (0h00-23h00), Figure II-14. The distribution in all three subgroups is consistent and does not strongly co-vary with the temperature distribution described above. Minimum humidity values occur in May while maxima occur in December. The range in values is also quite variable in minimum 0h00-23h00, $\pm$ 20%.

With regard to the Fort Chipewyan, Embarras and Fort McMurray climate normals, the AHCCD data show some variability in range. The Fort Chipewyan climate normals were slightly higher in relative humidity than Fort McMurray during the early growth season. Nevertheless, the Fort McMurray time-series is believed to be a good proxy for relative humidity variability at Fort Chipewyan over the last 50 years.

The relative humidity distribution from January to December is distinct from the pattern of distribution described for temperature above. Over the calibration period of AD 1955-2000 the correlation coefficient significantly increases for minimum daytime (r = -0.84) and mean (0h00-23h00) (r = -0.59) versus mean 6h00-20h00 temperature.

II.4.4.3 Precipitation

The precipitation data were organized into rain, snow and total, **Figure II-15**. May to September precipitation events account for ~60% of the annual precipitation. There are numerous month-long gaps in the data as well as large breaks in recording between 1994 and 1996. Annual average values for mean, maximum and minimum over the calibration period are 360.6 mm, 494.4 mm and 152.9 mm.

II.4.5 Addressing Signal Strength in Isotope Chronologies

Pearson product-moment correlation coefficients (PP-MCC) (PEARSON, 1901) are used to assess the signal strength within each isotope-dendrochronology.

Correlation matrices indicate that both $\delta^{13}C$ and $\delta^{18}O$ chronologies (Table II-1, Table II-2 and Table II-3) show common signals. The mean inter-tree correlation for

43

the $\delta^{13}C_{Cell}$-chronologies is 0.54 (r, P < 0.01), while the mean inter-tree correlation

for $\delta^{18}O_{Cell}$-chronologies is 0.31 (r, P < 0.05). When the inter-site relationships are

compared, carbon has a correlation of 0.72 (r, P < 0.01), while oxygen has a mean

inter-tree correlation of 0.46 (r, P < 0.01). The marked increase in signal strength

helps to highlight that there may be notable differences from tree-to-tree, however,

signal strength is far superior when working with composite chronologies.

II.4.5.1 Data Assessment: Intra-Site Variability

To address the intra-site variability within $\delta^{13}C_{Cell}$ and $\delta^{18}O_{Cell}$ chronologies, GSL

was chosen for an in-depth comparison due to its well-documented sampling

information. A direct comparison of the variation between ring-width, $\delta^{13}C_{Cell}$ and

$\delta^{18}O_{Cell}$ chronologies is conducted below and attempts to highlight the possible

variations that can occur as a result of micro-environment and hydrological setting.

GSL.3 is located on the northwest outcrop and is exposed, while GSL.10 is located

west of GSL.3 within an old growth stand which shelters it against rain, wind and

snow, Figure II-16. Hydrologically, GSL.3 is ~1 m above the lake level and is rooted

in silty sand. A soil water $\delta^{18}O$ of ~18.5‰ was measured in 2003 and is reflective of

mean annual precipitation (Thomas W.D. Edwards, 2003 personal correspondence).

II.4.5.2   Direct Comparison of Available Chronologies

Ring-width chronology for GSL.3.C is complacent[5] and comparatively stressed (mean ring-width = 0.68 mm) with respect to GSL.10.A (mean ring-width = 0.94 mm) and GSL.10.B's (mean ring-width = 1.02 mm). The three ring-width chronologies are statistically similar, 0.75 (r, P < 0.01), GSL.3.C.RW versus GSL.10.A.RW (r = 0.63, P < 0.01), GSL.3.C.RW versus GSL.10.B.RW (r = 0.68, P < 0.01) and GSL.10.A. RW versus GSL.10.B.RW (r = 0.93, P < 0.01), Figure II-17.

$\Delta\delta$.GSL.10.A.B$_{.CAR}$[6] and $\Delta\delta$.GSL.3.C$_{.CAR}$ respond similarly to environmental stimuli (average r = 0.75, P <0.01) (Table II-1 and Table II-4). Although the two trees have distinct hydrological settings the high correlation indicates strong common environmental labellers. The $\delta^{18}O_{Cell}$ chronologies ($\Delta\delta$.GSL.3.C$_{.OXY}$ versus $\Delta\delta$ .GSL.10.B$_{.OXY}$, r = 0.53, P < 0.01) are not as significantly correlated as $\delta^{13}C$ chronologies (Table II-2 and Table II-4). The variation in ring-width, $\delta^{13}C_{Cell}$ and $\delta^{18}O_{Cell}$ chronologies is thought to be due to the variation in sampling location and overall environmental stress.

II.4.5.3   Data Assessment: Inter-Site Variability

The consistency between the $\delta^{13}C_{Cell}$ (mean r = 0.77 (P < 0.005) and $\delta^{18}O_{Cell}$ chronologies (mean r = 0.62 (P < 0.005) PP-MCC (Table II-1, Table II-2 and Table

---

[5] lacking sensitivity to changing environmental conditions

[6] $\Delta\delta$ .GSL.10.A.CAR and $\Delta\delta$ .GSL.10.B.CAR composite chronology (r = 0.89, P <0.01)

II-3) indicates that clear regional temperature and humidity signals are present in the PAD trees.

If information such as micro-environment hydrology, topography or competition was available it may be possible to identify the causes of variation in the chronologies by comparing the isotopic ratios and ring-width variation, Bailey (BAILEY, 2005).

The $\delta^{18}O_{Cell}$ chronologies have much more inter-site variation (r ranging from 0.65 to 0.90 versus PAD$_{.OXY}$) which is likely due to small variations in the isotopic composition of source-waters used by the trees.
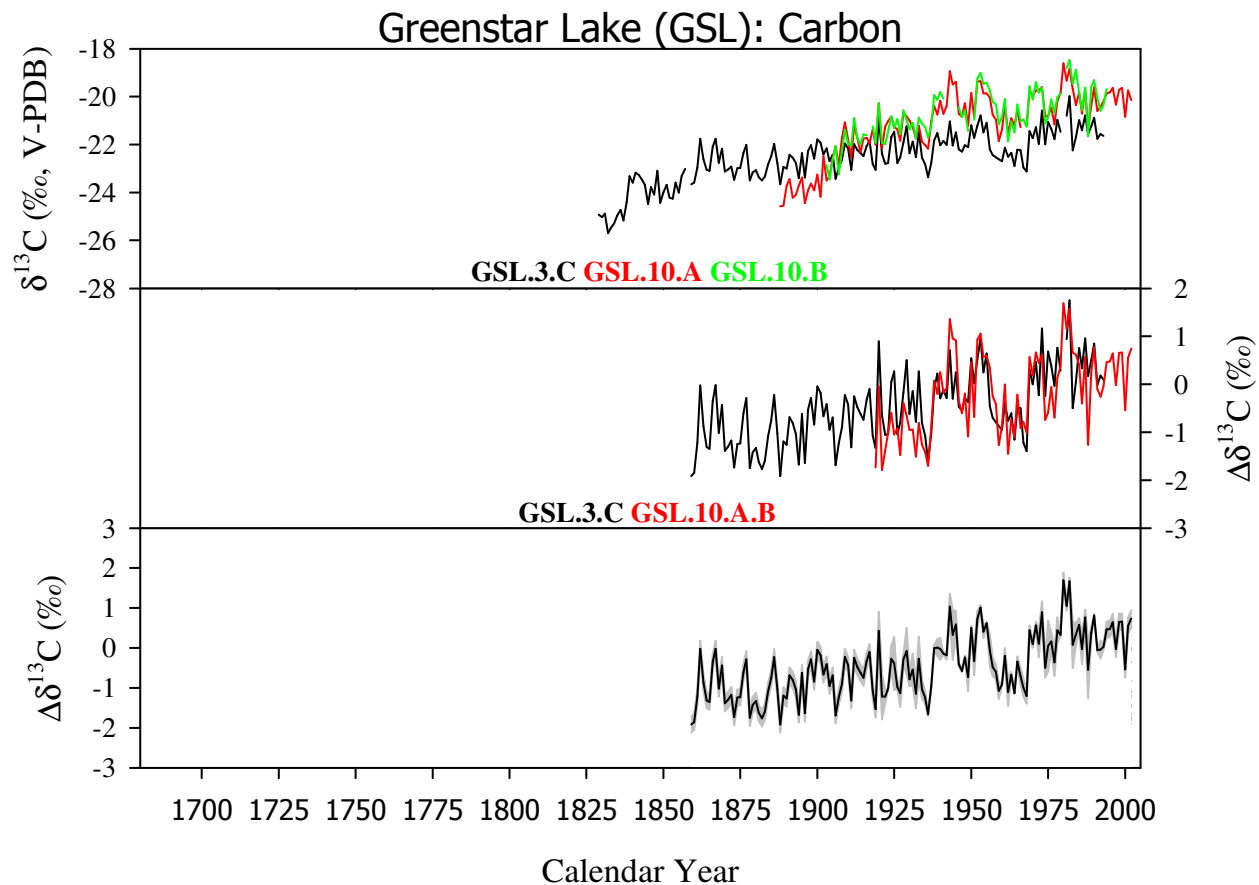
Figure II-1. Greenstar Lake (GSL) $\delta^{13}C$ **chronology (‰): A composite of three time-series from two trees. The top section shows all three chronologies vs V-PDB. The middle section shows the chronologies and a composite for GSL.10 (A.B) normalized to AD 1955-2000 and has been adjusted for juvenile and Suess effects. The bottom section shows the GSL-composite chronologies in black, with grey shading representing the variance between all three time-series. If no variance could be calculated an analytical error of ±0.2‰ is used.**
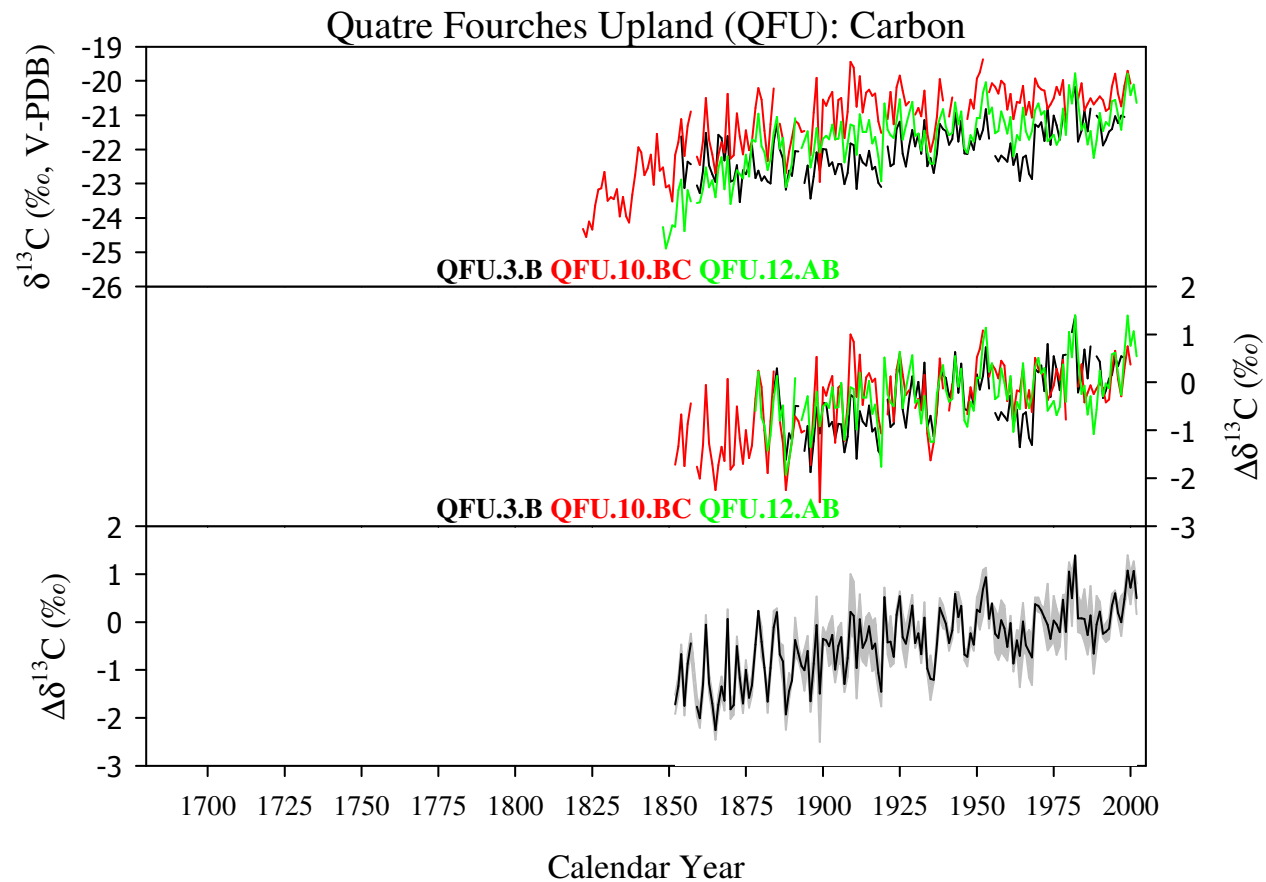
Figure II-2. Quatre Fourches Upland (QFU) $\delta^{13}C$ chronology (‰): A composite of three time-series from three trees. The top section shows all three chronologies vs V-PDB. The middle section shows the chronologies normalized to AD 1955-2000 and has been adjusted for juvenile and Suess effects. The bottom section shows the QFU-composite chronologies in black, with grey shading representing the variance between all three time-series. If no variance could be calculated an analytical error of ±0.2‰ is used.
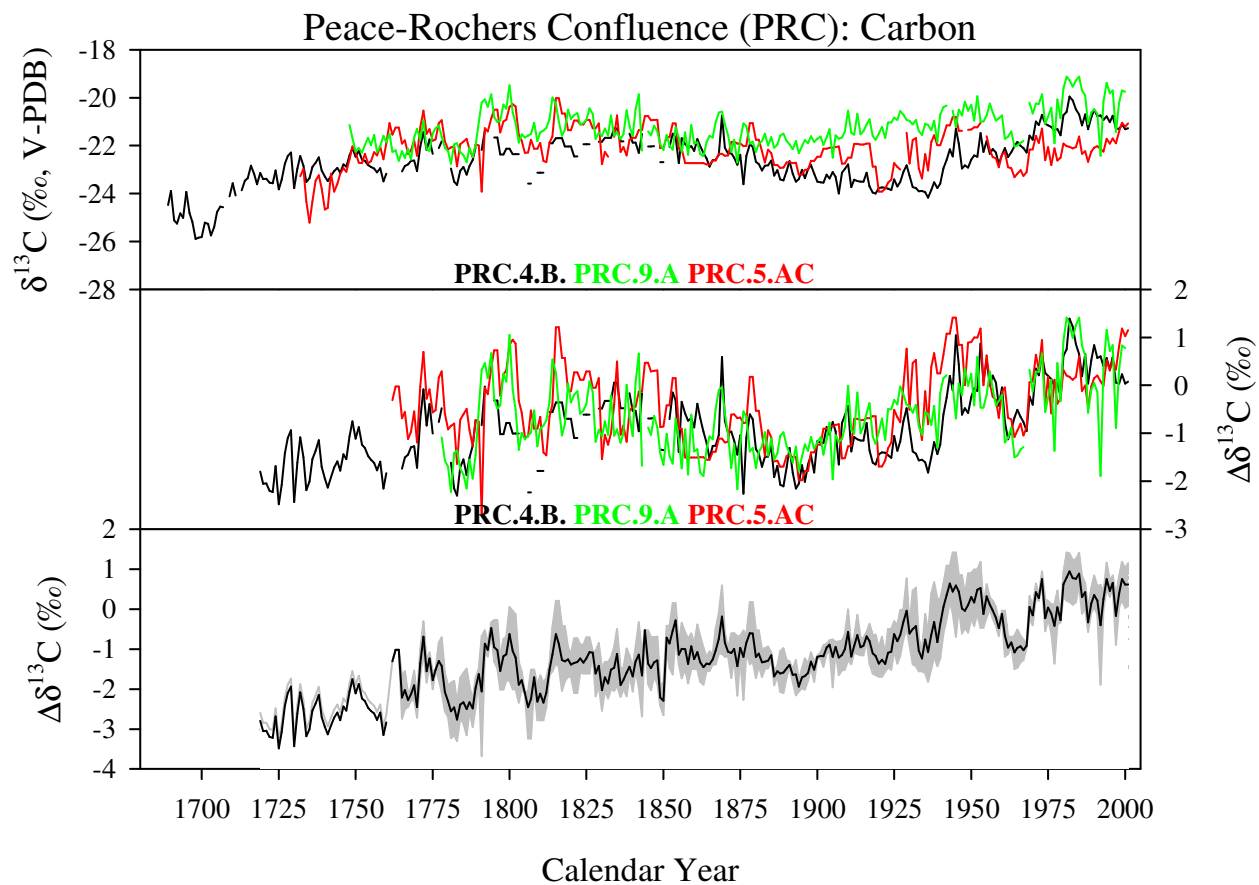
Figure II-3. Peace-Rochers Confluence (PRC) $\delta^{13}C$ **chronology (‰): A composite of three time-series from two trees. The top section shows all three chronologies vs V-PDB. The middle section shows the chronologies normalized to AD 1955-2000 and has been adjusted for juvenile and Suess effects. The bottom section shows the PRC-composite chronologies in black, with grey shading representing the variance between all three time-series. If no variance could be calculated an analytical error of ±0.2‰ is used.**
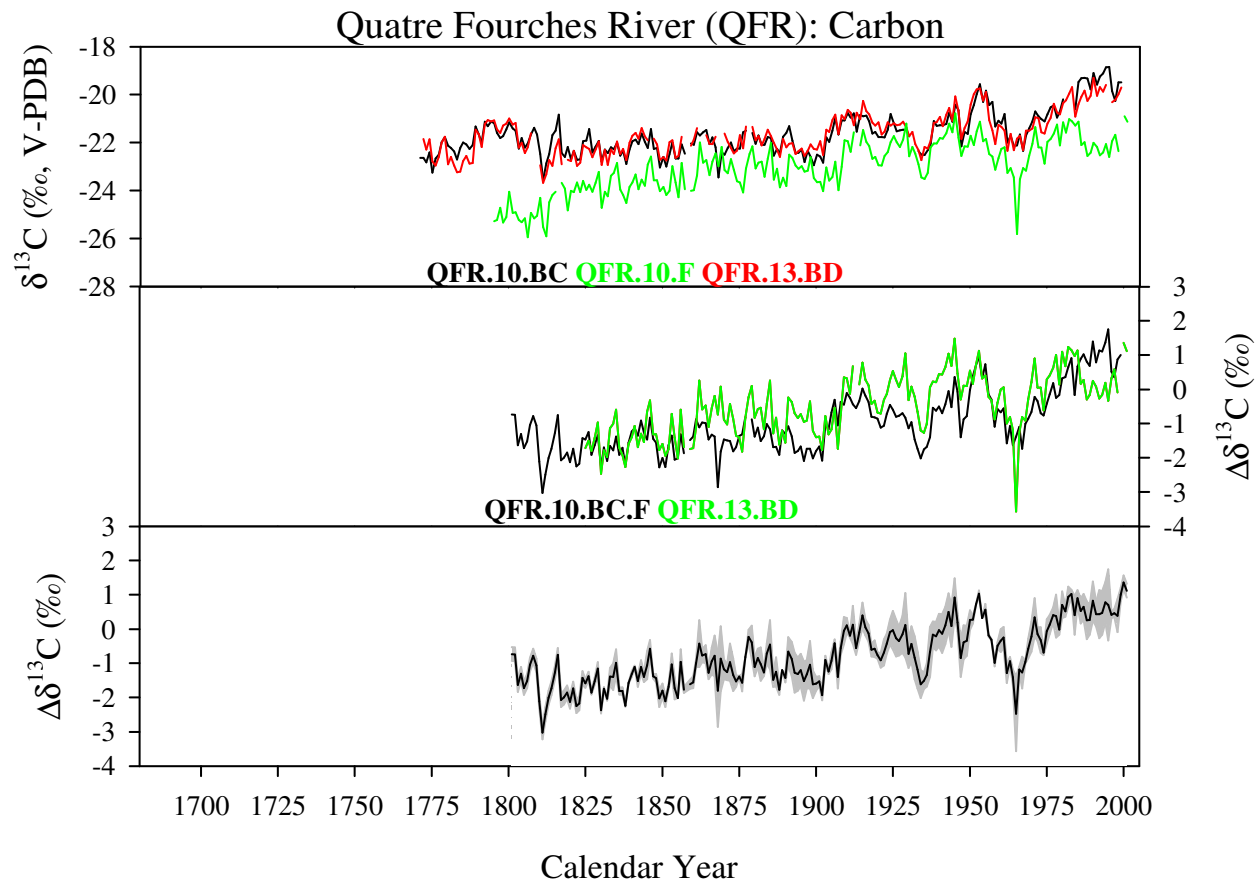
Figure II-4. Quatre Fourches River (QFR) $\delta^{13}C$ **chronology (‰): A composite of three time-series from two trees. The top section shows all three chronologies vs V-PDB. The middle section shows the chronologies and a composite for QFR.10 (BC.F) normalized to AD 1955-2000 and has been adjusted for juvenile and Suess effects. The bottom section shows the QFR-composite chronologies in black, with grey shading representing the variance between are all three time-series. If no variance could be calculated an analytical error of ±0.2‰ is used.**
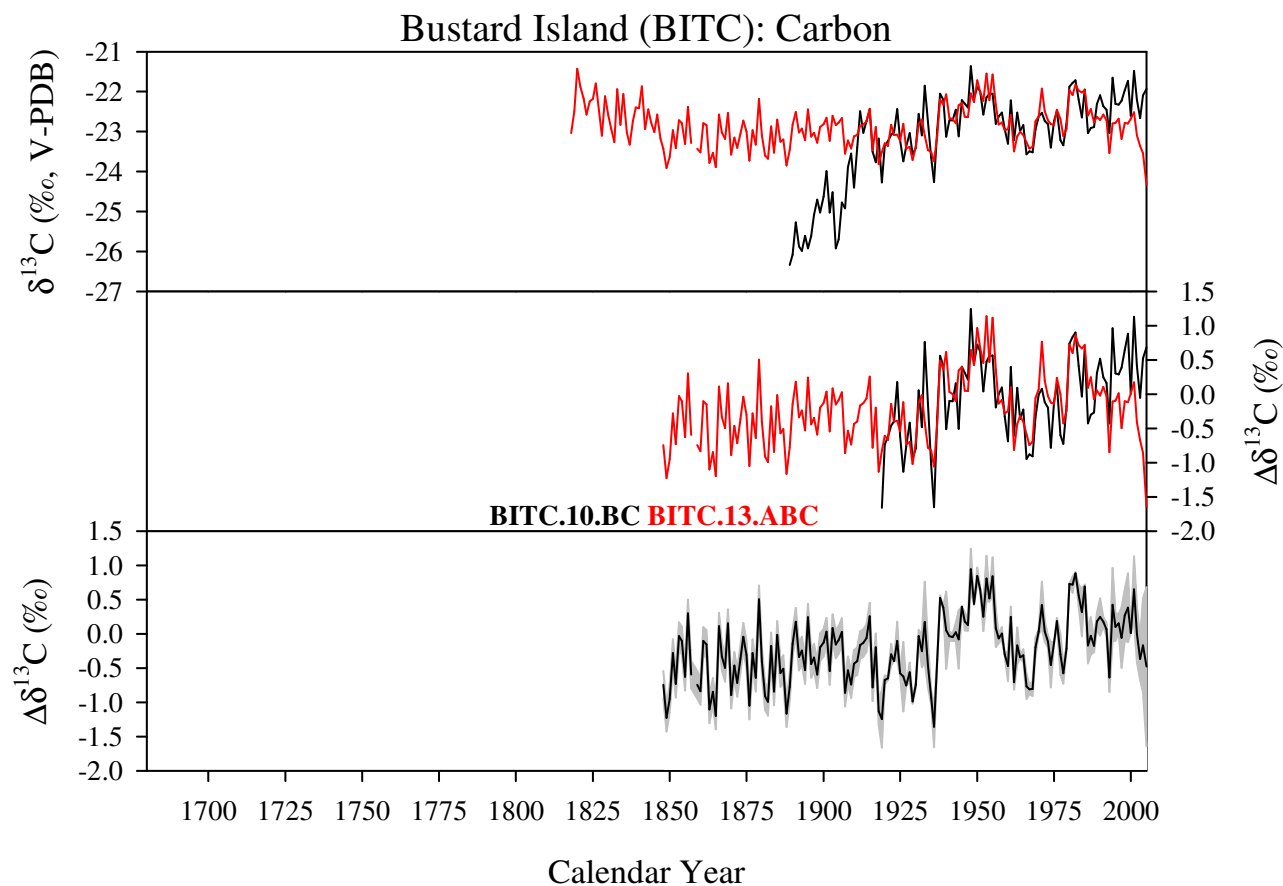
Figure II-5. Bustard Island (BITC) $\delta^{13}C$ **chronology (‰): A composite of two time-series from two trees. The *top* section shows all three chronologies vs V-PDB. The middle section shows the chronologies normalized to AD 1955-2000 and has been adjusted for juvenile and Suess effects. The bottom section shows the BITC-composite chronologies in black, with grey shading representing the variance between both time-series. If no variance could be calculated an analytical error of ±0.2‰ is used.**
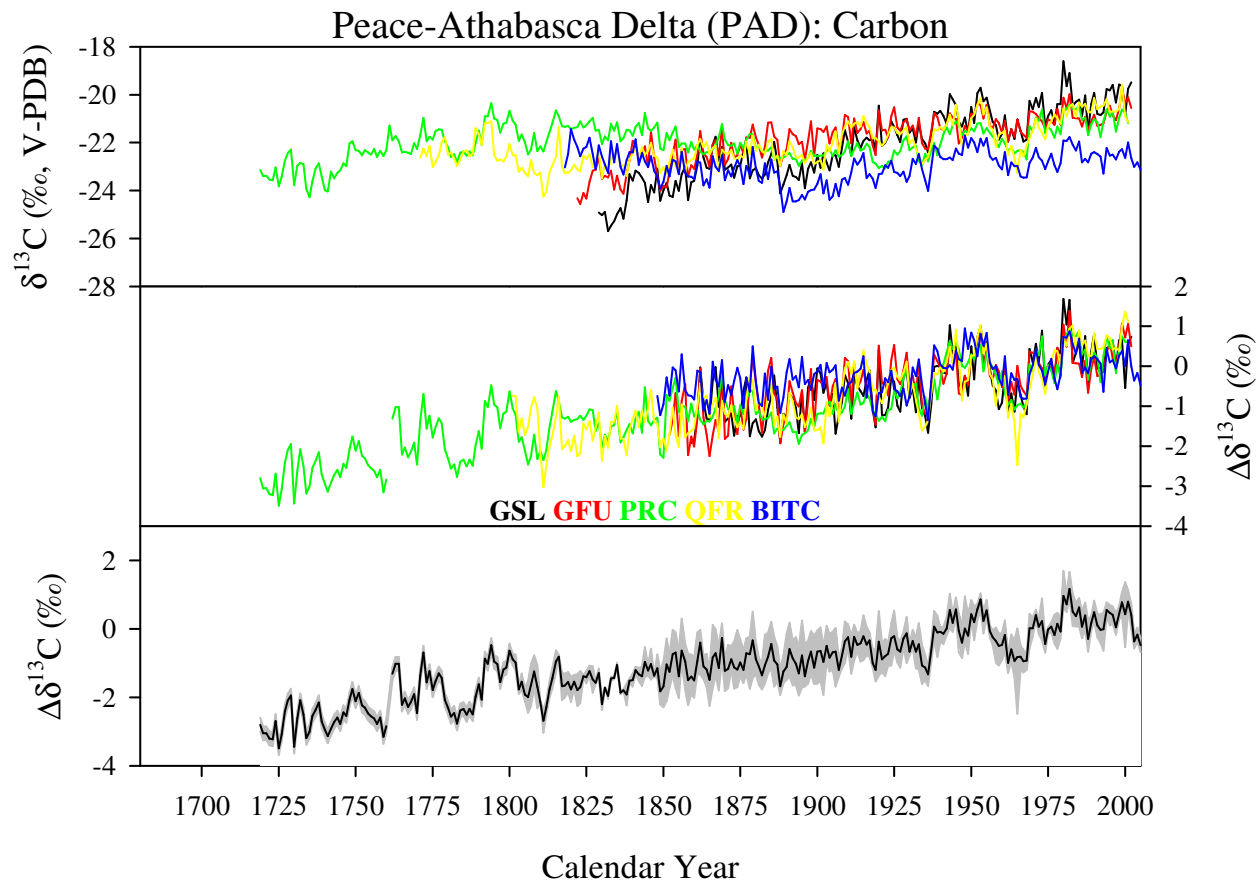
Figure II-6. Peace-Athabasca Delta (PAD) $\delta^{13}C$ **chronology (‰): A composite of five** $\delta^{13}C-$ **chronologies from within (GSL, QFU, PRC and QFR) and adjacent (BITC) to the PAD. The top section shows all three chronologies vs V-PDB. The middle section shows the chronologies normalized to AD 1955-2000 and has been adjusted for juvenile and Suess effects. The bottom section shows the PAD-composite chronologies in black, with grey shading representing the variance between all time-series. If no variance could be calculated an analytical error of ±0.2‰ is used.**
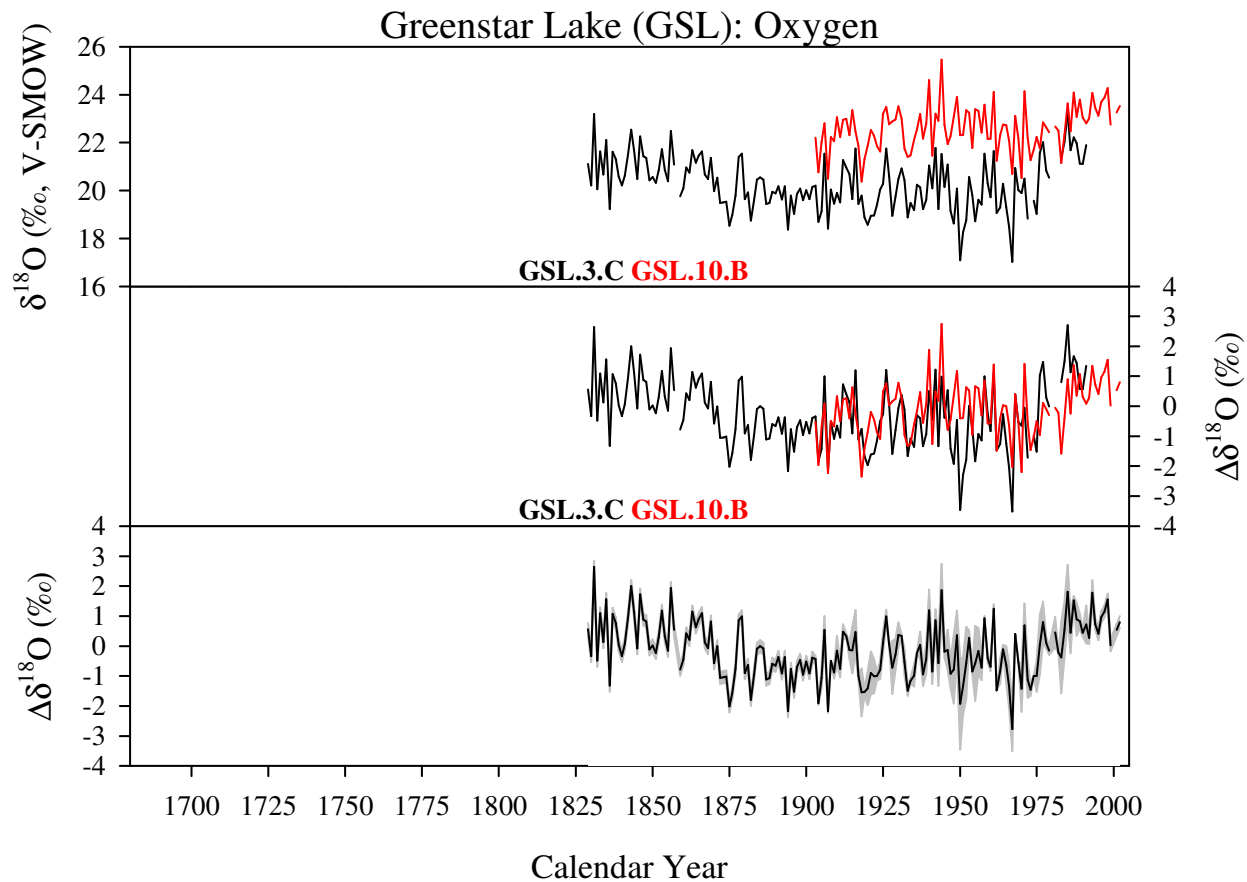
Figure II-7. Greenstar Lake (GSL) $\delta^{18}O$ **chronology (‰): A composite of two time-series from two trees. The top section shows both chronologies vs V-SMOW. The middle section shows the chronologies normalized to AD 1955-2000 and has been adjusted for juvenile effects. The bottom section shows the GSL-composite chronologies in black, with grey shading representing the variance between both time-series. If no variance can be calculated an analytical error of ±0.4‰ is used.**
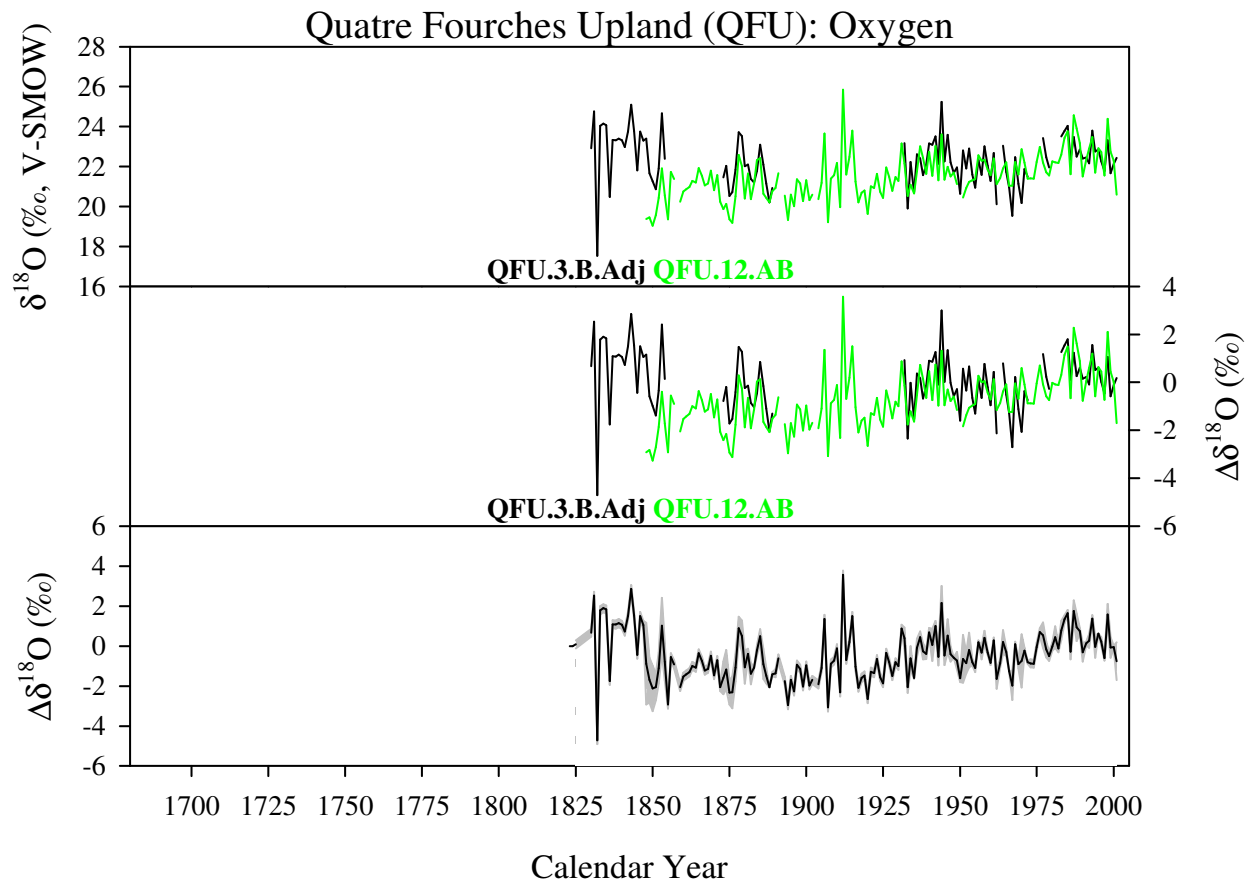
Figure II-8. Quatre Fourches Upland (QFU) $\delta^{18}O$ **chronology (‰): A composite of three time-series from three trees. The top section shows both chronologies vs V-SMOW. QFU.3.B showed some analytical drift and was adjusted to QFU.3.B.Adj. The middle section shows the chronologies normalized to AD 1955-2000. The bottom section shows the QFU-composite chronologies in black, with grey shading representing the variance between both time-series. If no variance could be calculated an analytical error of ±0.4‰ is used.**
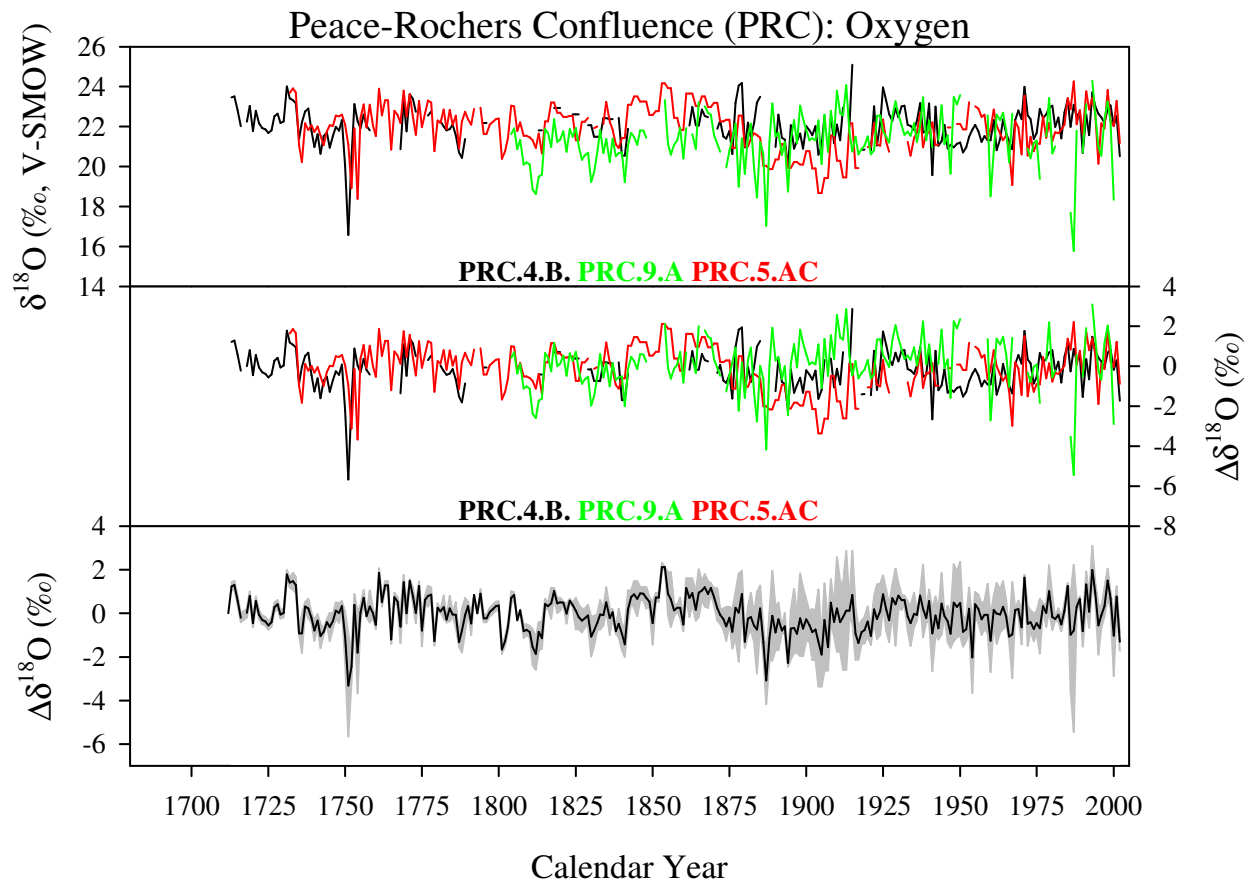
Figure II-9. Peace-Rochers Confluence (PRC) $\delta^{18}O$ **chronology (‰): A composite of three time-series from three trees. The top section shows all three chronologies vs V-NSOW. The middle section shows the chronologies normalized to AD 1955-2000. The bottom section shows the PRC-composite chronologies in black, with grey shading representing the variance between the three time-series. If no variance could be calculated an analytical error of ±0.4‰ is used.**
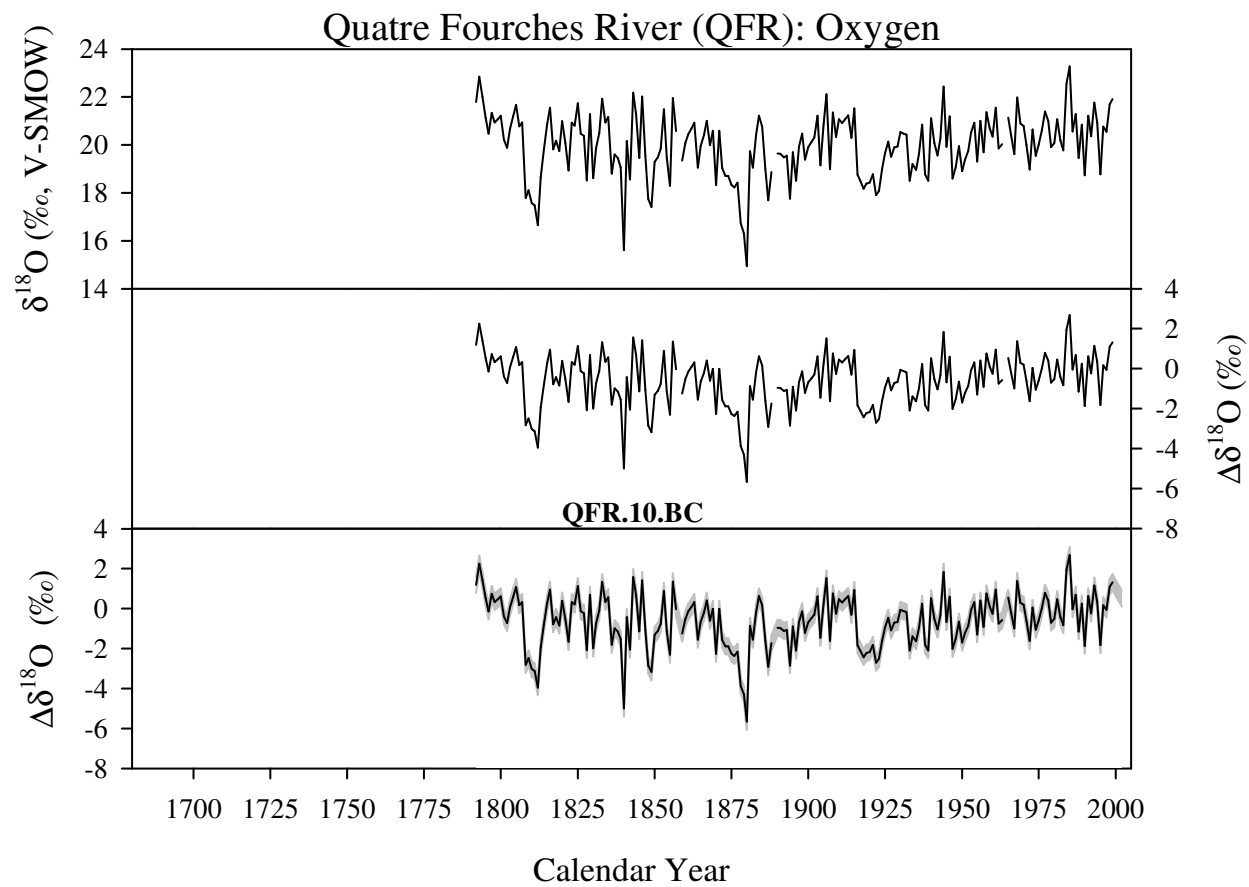
Figure II-10. Quatre Fourches River (QFR) $\delta^{18}O$ **chronology (‰): A composite of two cores from one tree. The top section shows all three chronologies vs V-SMOW. The middle section shows the chronologies normalized to AD 1955-2000. The bottom section shows the QFR-composite chronologies in black, with grey shading analytical error of ±0.4‰.**

56
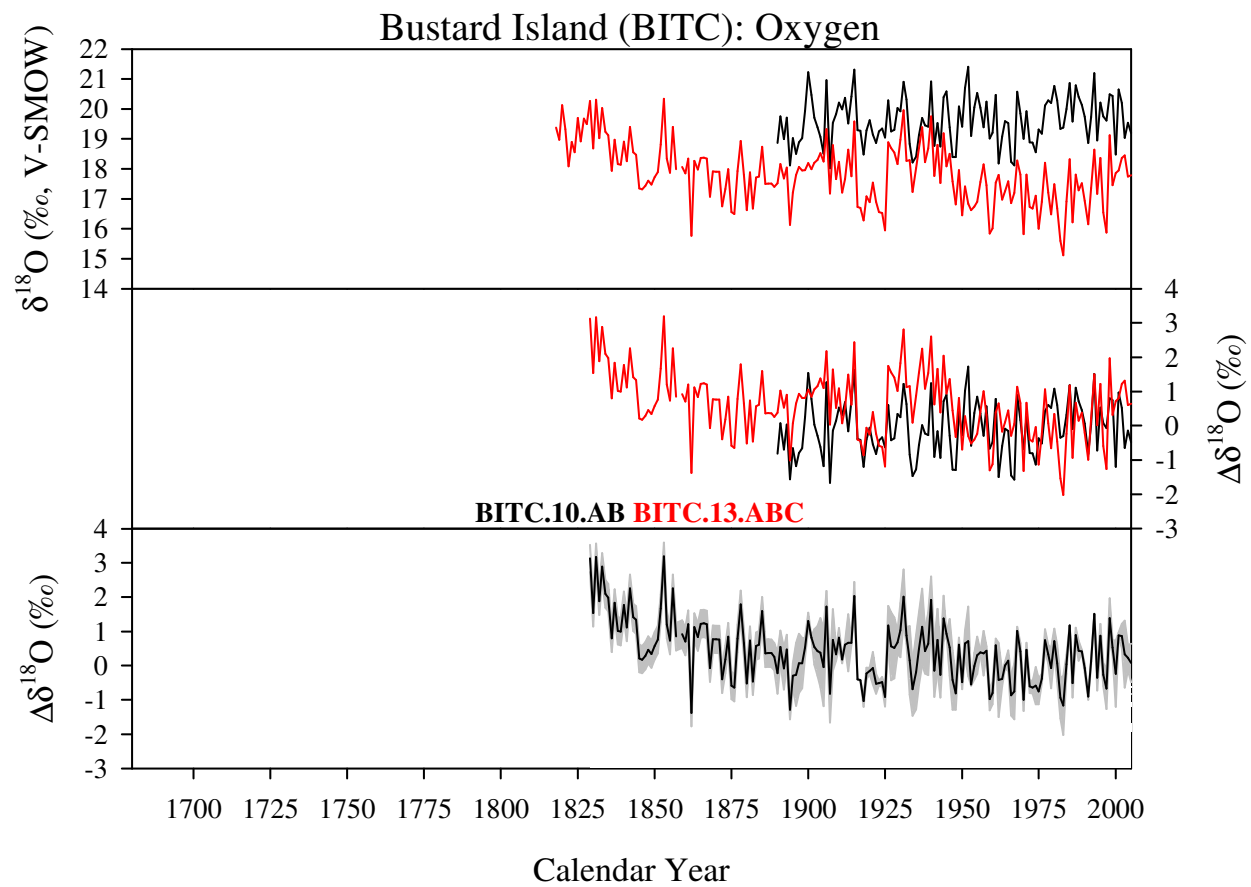
Figure II-11. Bustard Island (BITC) $\delta^{18}O$ chronology (‰): A composite of five cores from two trees. The top section shows all three chronologies vs V-SMOW. The middle section shows the chronologies normalized to AD 1955-2000. The bottom section shows the BITC-composite chronologies in black, with grey shading representing the variance between both time-series. If no variance could be calculated an analytical error of ±0.4‰ is used.
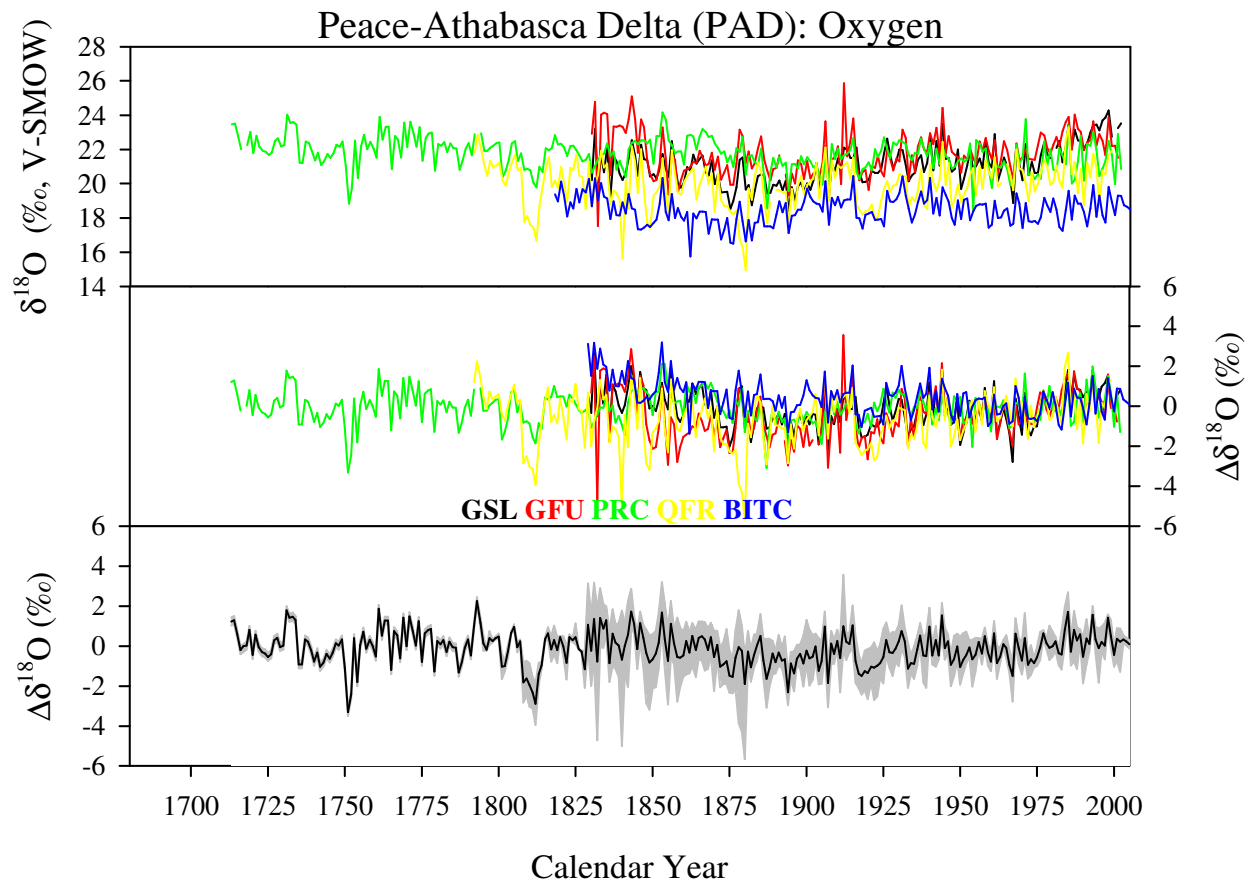
Figure II-12. Peace-Athabasca Delta (PAD) $\delta^{18}O$ chronology (‰): A composite of five $\delta^{18}O$ chronologies from within (GSL, QFU, PRC and QFR) and adjacent (BITC) to the PAD. The top section shows all three chronologies vs V-SMOW. The middle section shows the chronologies normalized to AD 1955-2000. The bottom section shows the PAD-composite chronologies in black, with grey shading representing the variance between the time-series. If no variance could be calculated an analytical error of ±0.4‰ is used.
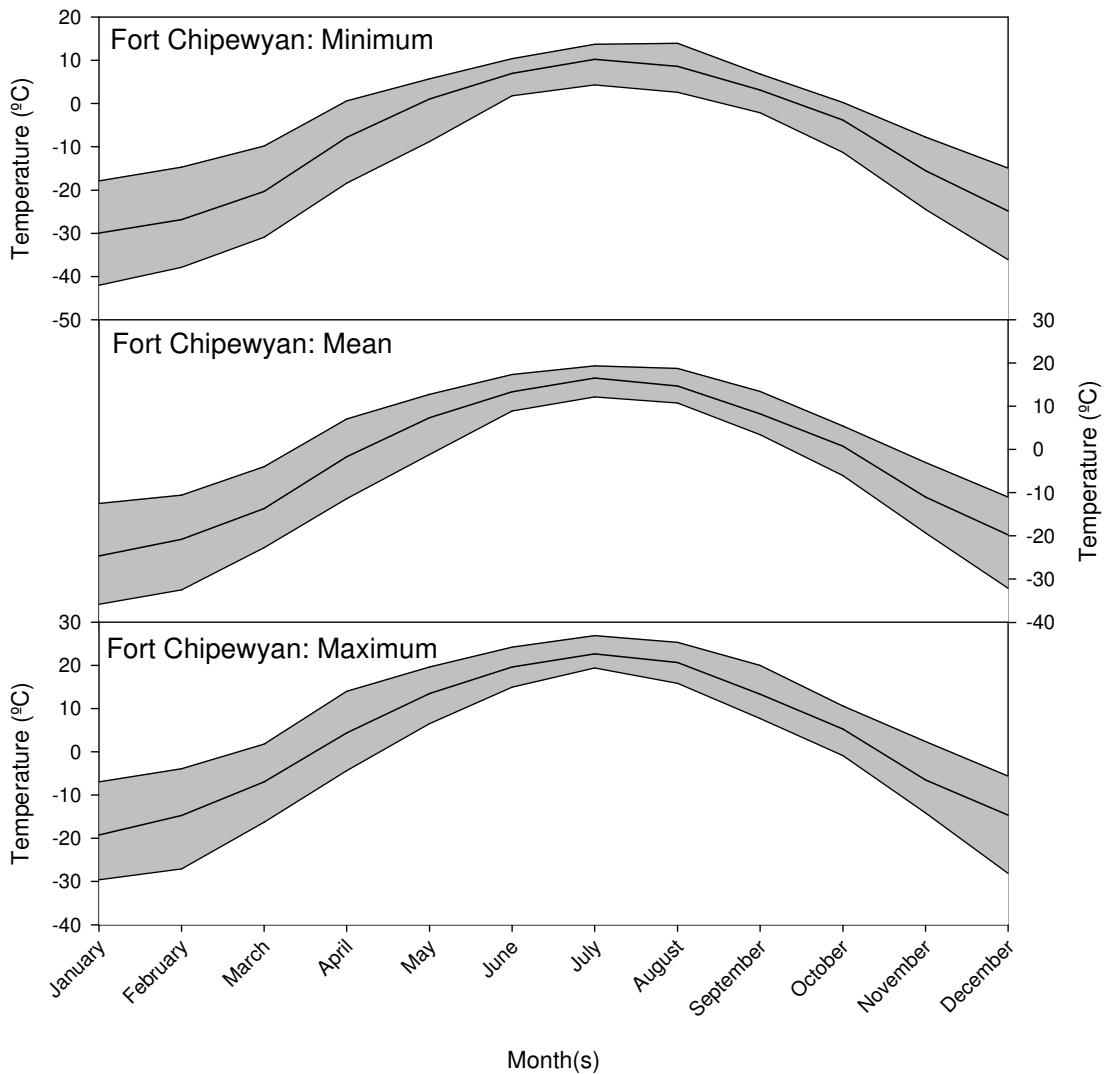
Figure II-13. Monthly averages from AD 1955 to 2000 for AHCCD temperature (ºC) for Fort Chipewyan, maximum, mean and min. The data are organized by variations in a 24 hour window. (*Top*) Averaged monthly minimum values occurring from midnight. (*Middle*) Averaged monthly mean values. (*Bottom*) Averaged monthly maximum values.
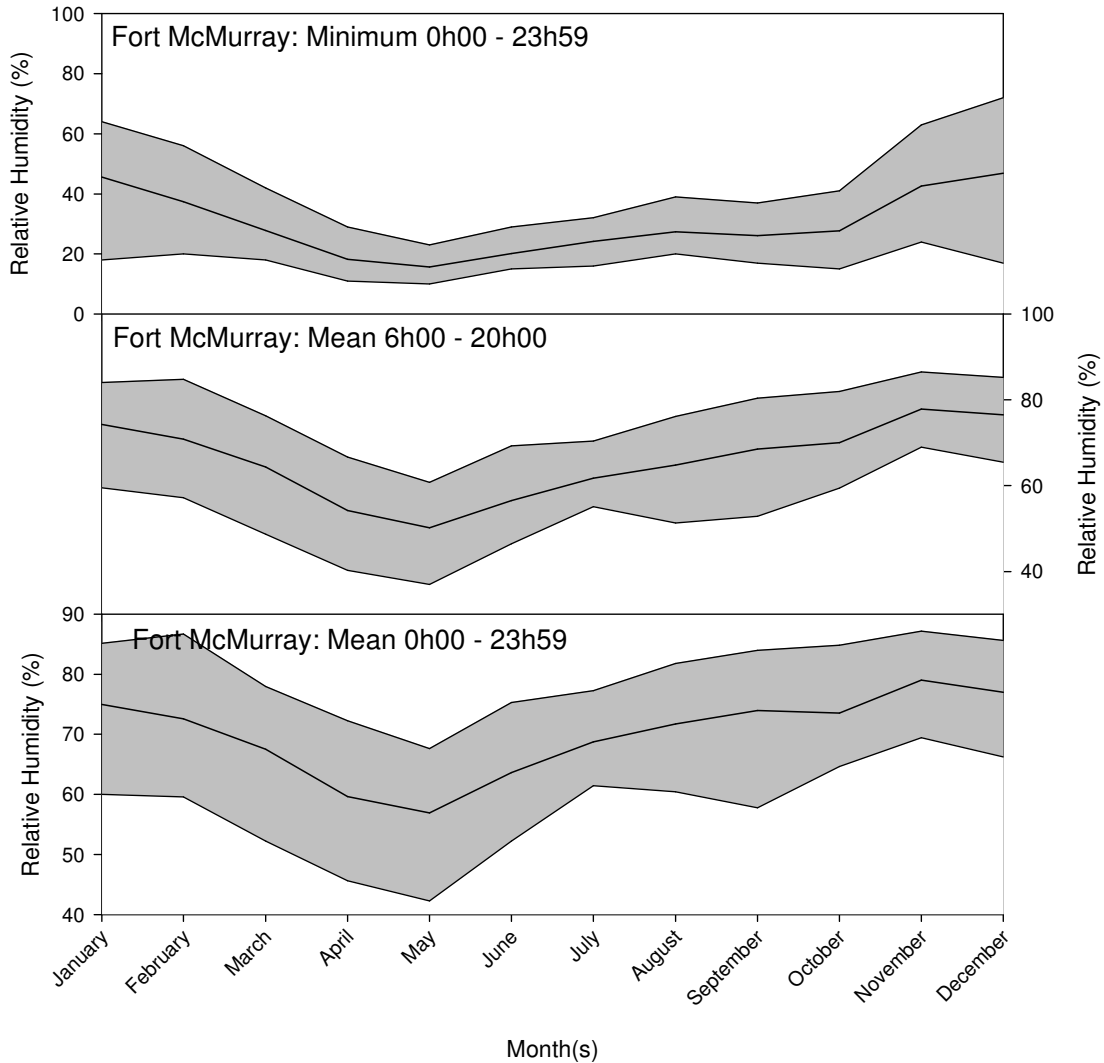
Figure II-14. Monthly averages from AD 1955 to 2000 for AHCCD relative humidity (%) for Fort McMurray. The data are organized by variations in a 24 hour window. (*Top*) Averaged monthly minimum values occurring from midnight (0h00) to midnight (23h59). (*Middle*) Averaged monthly mean values from 6 a.m. (6h00) to 8 p.m. (20h00). (*Bottom*) Averaged monthly mean values from midnight (0h00) to midnight (23h59.
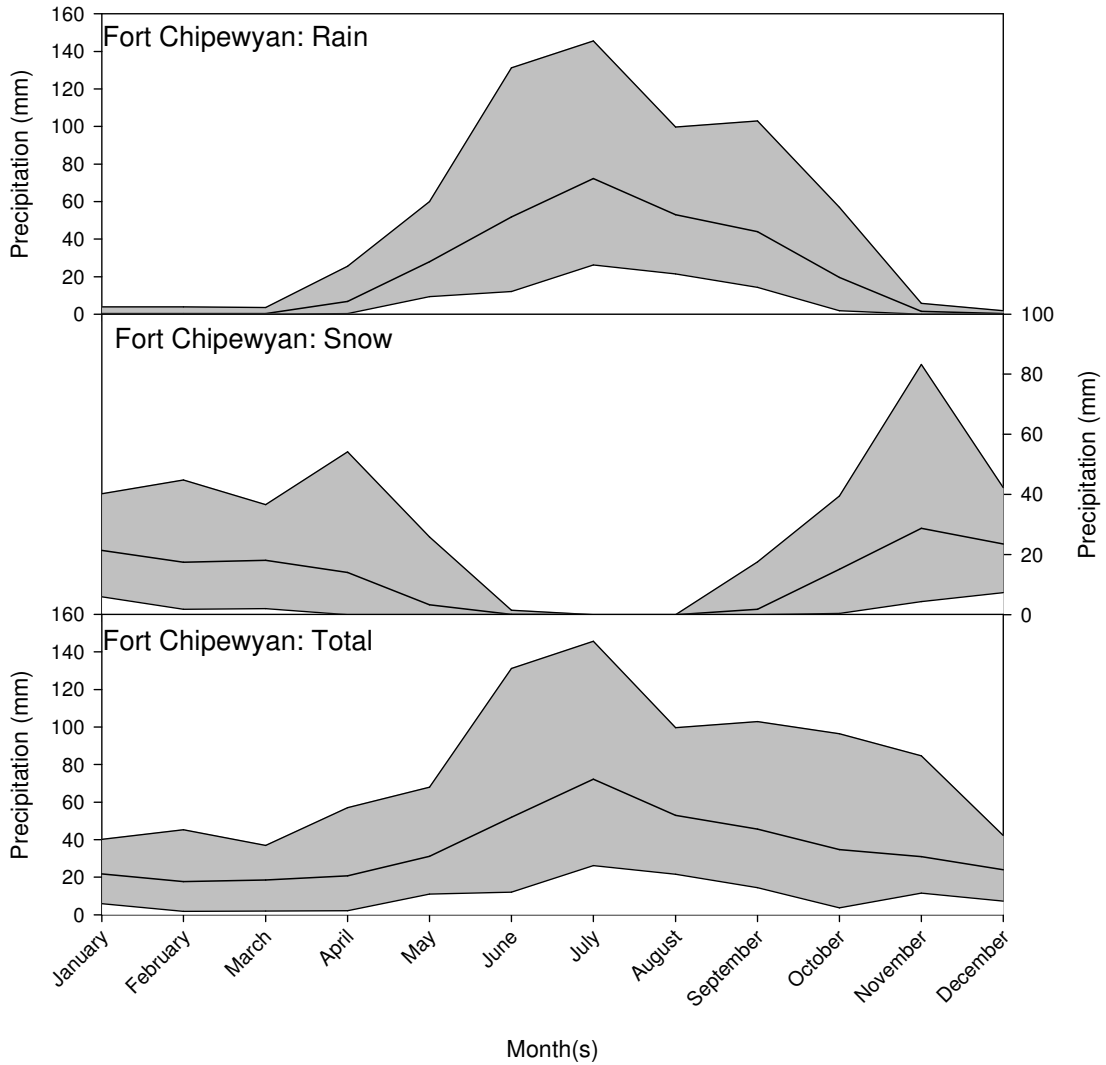
Figure II-15. Monthly averages from AD 1955 to 2000 for AHCCD for precipitation (mm) for Fort Chipewyan. The data are represented as average monthly sums. (*Top*) Averaged monthly sum of rain. (*Middle*) Averaged monthly sum of snow. (*Bottom*) Averaged monthly sum of total precipitation.
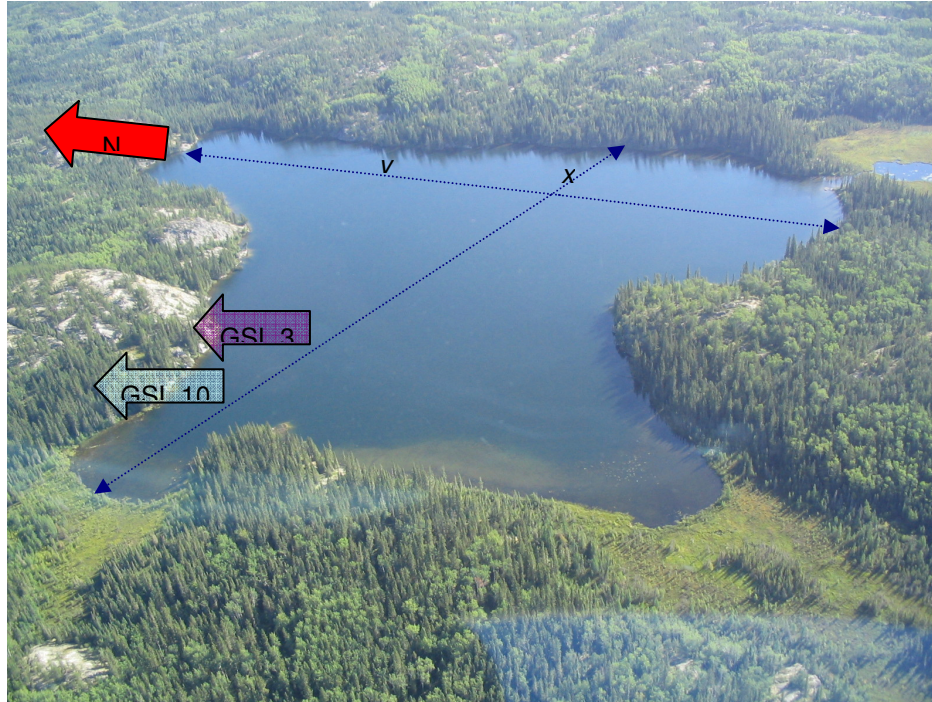
Figure II-16. Aerial view of Greenstar Lake taken from the northwest embayment with labels indicating the sampling sites for GSL.3 (purple) and GSL. 10 (blue), X- (0. 58 km) and Y- (0. 7 km) axis are also indicated and to scale to give perspective of the angle of the photograph. Photograph courtesy of Lesley-Ann Chiavaroli, August 2006.
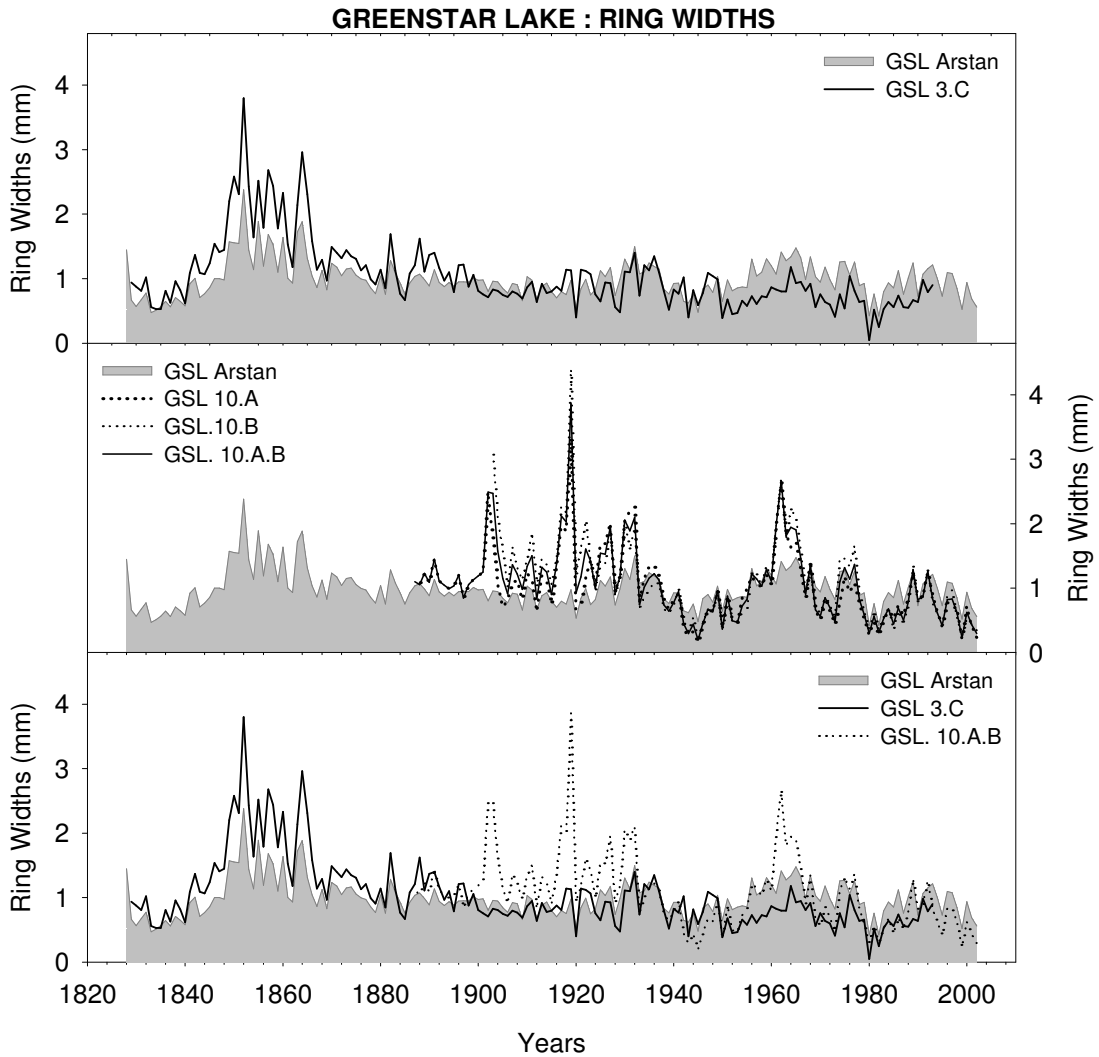
Figure II-17. Ring-width (mm) comparison of Greenstar Lake's GSL.3.C, GSL.10.A and GSL.10.B and Greenstar Lake (GSL) ARSTAN courtesy of Glen MacDonald and David Porinchu (MacDonald et al., 2005).

Table II-1. $\delta^{13}C$: Mean Pearson Product Correlation Coefficients. Inter- and Intra-site, correlation coefficients for $\delta^{13}C$ chronologies carried out on a 45-year sample set (AD 1955-2000), with comparison sample size ranging from 36–50(years). Correlation coefficients ≥ 0.36 are significant at P < 0.01 and ≥ 0.28 at P < 0.05. Maximum unrelated values for each column highlighted in bold.

	R-value		PRC			QFR				QFU			GSL				BITC	
			4A	5AC	9A	10BC	10F	10BC.	13BD	3B	10BC	12AB	10A	10B	10A.B	3C	10AB	13AB
LOWLAND	PRC	4A	1.00															
		5AC	0.56	1.00														
		9A	0.60	0.62	1.00													
		AVG	0.84	0.82	0.90													
	QFR	10BC	0.67	0.64	0.53	1.00												
		10F	0.72	0.62	0.49	0.94	1.00											
		10BC.	0.70	0.64	0.54	0.99	0.98	1.00										
		13BD	0.58	0.67	0.65	0.51	0.58	0.55	1.00									
		AVG	0.73	0.73	0.67	0.88	0.89	0.89	0.87									
UPLAND	QFU	3B	0.73	**0.72**	0.65	0.62	**0.63**	0.63	**0.66**	1.00								
		10BC	0.05	0.35	0.34	0.17	0.12	0.18	0.13	0.21	1.00							
		12AB	0.35	0.52	0.48	0.26	0.39	0.37	0.32	0.46	0.66	1.00						
		AVG	0.54	0.67	0.64	0.45	0.52	0.51	0.54	0.81	0.73	0.89						
	GSL	10A	0.68	0.62	0.65	0.46	0.54	0.52	0.49	0.73	0.29	0.65	1.00					
		10B	0.65	0.70	**0.72**	0.46	0.55	0.53	0.57	0.76	**0.45**	**0.67**	0.89	1.00				
		10A.B	0.69	0.64	0.70	0.49	0.56	0.55	0.53	0.74	0.39	0.67	0.97	0.98	1.00			
		3C	**0.75**	0.68	0.60	**0.64**	0.63	0.63	0.59	**0.97**	0.12	0.33	0.74	0.67	0.73	1.00		
		AVG	0.76	0.66	0.69	0.60	0.64	0.62	0.57	0.86	0.32	0.57	0.94	0.89	0.94	0.93		
ISLAND	BITC	10AB	0.53	0.64	0.50	0.60	0.61	**0.62**	0.44	0.56	0.38	0.63	**0.67**	0.69	**0.71**	0.54	1.00	
		13AB	0.52	0.52	0.56	0.38	0.43	0.42	0.60	0.51	0.33	0.40	0.60	**0.71**	0.68	**0.56**	0.60	1.00
		AVG	0.59	0.65	0.60	0.57	0.59	0.59	0.57	0.60	0.41	0.58	0.72	0.77	0.78	0.59	0.91	0.88
PAD.CAR			0.80	0.80	0.80	0.76	0.77	0.77	0.76	0.86	0.41	0.64	0.86	0.87	0.88	0.85	0.78	0.72

Table II-2. $\delta^{18}O$ **: Mean Pearson Product Correlation Coefficients. Inter- and Intra-site, correlation coefficients for** $\delta^{18}O$ **chronologies carried out on a 45-year sample set (AD 1955-2000), with comparison sample size ranging from 36–50(years). Correlation coefficients ≥ 0.36 are significant at P < 0.01 and ≥ 0.28 at P < 0.05. Maximum unrelated values for each column highlighted in bold.**

R-values			PRC				OFR			OFU				GSL			BITC	
			4A	5AC	9A	9A.Ad	10BC	10F	13BD	3B	3B.adi	10BC	12AB	3C	10A	10B	10AB	13AB
LOWLAND	PRC	4A	1.00															
		5AC	0.43	1.00														
		9A	0.07	-0.08	1.00	1.00												
		9A.ad	0.07	-0.08	1.00	1.00												
		AVG	0.61	0.47	0.74	0.74												
	QFR	10BC	0.43	0.50	0.05	0.05	1.00											
		10F																
		13BD																
		AVG	0.43	0.50	0.05	0.05	1.00											
UPLAND	QFU	3B	0.44	0.43	-0.06	-0.06	0.33			1.00								
		3B.adj	0.45	0.52	-0.06	-0.06	0.49			0.83	1.00							
		10BC																
		12AB	0.52	0.51	-0.14	-0.14	0.48			0.58	0.58		1.00					
		AVG	0.54	0.56	-0.12	-0.12	0.53			0.79	0.79		0.90					
	GSL	3C	0.57	0.65	-0.18	-0.18	**0.61**			**0.86**	**0.86**		**0.72**	1.00				
		10A																
		10B	0.50	**0.71**	0.01	0.01	0.33			0.47	0.47		0.47	0.53		1.00		
		AVG	0.59	0.73	-0.04	-0.04	0.51			0.77	0.77		0.66	0.92		0.85		
ISLAND	BITC	10AB	**0.58**	0.54	0.02	0.02	0.43			0.51	0.51		0.60	**0.69**		**0.73**	1.00	
		13AB	0.32	0.33	**0.13**	**0.13**	0.30			0.12	0.12		0.38	0.20		0.48	0.44	1.00
		AVG	0.52	0.51	0.09	0.09	0.41			0.35	0.35		0.57	0.51		0.69	0.83	0.87
PAD_oxy			0.68	0.71	0.17	0.17	0.74			0.68	0.68		0.73	0.85		0.75	0.77	0.53

Table II-3. $\delta^{13}C$ and $\delta^{18}O$ **: Mean Pearson Product Correlation Coefficients. Inter- and Intra-site, correlation coefficients for** $\delta^{13}C$ **and** $\delta^{18}O$ **chronologies carried out on a 45-year sample set (AD 1955-2000), with comparisons sample size ranging from 36–50(year). Correlation coefficients ≥ 0.36 are significant at P < 0.01 and ≥ 0.28 at P < 0.05. Maximum values for each column highlighted in bold.**

R-value:	PRC.AVG	QFR.AVG	QFU.AVG	GSL.AVG	BIT.AVG
PRC.AVG	1.00				
QFR.AVG	0.82	1.00			
QFU.AVG	0.72	0.59	1.00		
GSL.AVG	**0.82**	**0.71**	**0.80**	1.00	
BITC.AVG	0.71	0.67	0.70	**0.75**	1.00
PAD CAR	0.93	0.88	0.84	0.92	0.84

R-value:	PRC.AVG	QFR.AVG	QFU.AVG	GSL.AVG	BIT.AVG
PRC.AVG	1.00				
QFR.AVG	0.37	1.00			
QFU.AVG	0.31	**0.53**	1.00		
GSL.AVG	**0.50**	0.51	**0.82**	1.00	
BITC.AVG	0.42	0.41	0.59	**0.64**	1.00
PAD OXY	0.66	0.74	0.84	0.90	0.76

Table II-4. Intra-site correlation between $\delta^{13}C$ and $\delta^{18}O$ chronologies at Greenstar Lake tree specific assessment and composite-chronologies (PAD.$_{CAR}$ and PAD.$_{OXY}$). Intra-site (GSL) and regional comparisons for temperature (Temp), relative humidity (Hum) and precipitation (Precip) correlation coefficients for stable $\delta^{13}C$ and $\delta^{18}O$ chronologies carried out on a 50-year sample set (AD 1953-2003), with comparison sample size ranging from 36 – 50 (year). Correlation coefficients ≥ 0.36 are significant at P < 0.01 and ≥ 0.28 at P < 0.05. Maximum values for each month are bold.

GSL		Min	Max	Mean	Annual	Jan	Feb	Mar	Apr	May	Jun	Jul	Aug	Sept	Oct	Nov	Dec
10.A.B $_{CAR}$	Temp	-0.06	0.38	0.18	0.27	0.13	0.12	0.03	0.16	0.34	**0.38**	0.3	0.27	0.2	0.21	0.04	-0.06
	Hum	-0.44	-0.04	-0.29	-0.51	-0.12	-0.12	-0.32	-0.32	-0.44	**-0.38**	-0.35	-0.41	-0.27	-0.04	-0.34	-0.36
	Precip	-0.5	0.28	-0.17	-0.21	-0.31	-0.16	-0.21	-0.12	-0.27	-0.5	-0.11	-0.26	-0.1	-0.09	-0.11	0.28
3.C $_{CAR}$	Temp	-0.28	0.5	0.17	0.26	0.18	0.09	0.04	0.17	**0.5**	0.34	0.28	0.02	0.42	**0.28**	-0.28	0.01
	Hum	-0.43	-0.01	-0.25	-0.45	-0.01	-0.26	-0.33	-0.23	-0.35	-0.19	-0.31	-0.27	-0.43	-0.01	**-0.42**	-0.22
	Precip	-0.3	0.48	-0.04	0	-0.19	-0.26	-0.05	-0.04	-0.17	-0.14	-0.06	-0.06	-0.3	0.18	0.15	**0.48**
10.A $_{OXY}$	Temp	0	0.3	0.15	0.32	0.3	0.3	0.12	0.02	0.18	0.24	0.16	0.05	0.19	0.13	0	0.09
	Hum	-0.38	-0.13	-0.23	-0.41	-0.29	-0.21	-0.38	-0.2	-0.23	-0.16	-0.21	-0.27	-0.13	-0.2	-0.29	-0.21
	Precip	-0.37	0.23	-0.1	-0.14	-0.37	0	-0.31	-0.22	-0.07	0.1	0.1	-0.29	-0.03	-0.24	0.23	-0.11
3.C $_{OXY}$	Temp	-0.02	**0.67**	0.26	**0.67**	**0.67**	0.4	**0.58**	0.45	0.34	0.07	0.07	0.07	0.31	0.15	-0.02	0.07
	Hum	**-0.54**	-0.14	**-0.35**	-0.62	-0.24	**-0.48**	-0.54	**-0.54**	-0.2	-0.35	**-0.38**	-0.38	**-0.48**	-0.14	-0.25	-0.19
	Precip	-0.46	0.26	-0.07	-0.03	-0.16	-0.12	-0.17	-0.2	0.05	0.26	0.08	**-0.43**	-0.46	0.1	0.11	0.11
PAD$_{CAR}$	Temp	0.02	0.38	0.25	0.46	0.31	0.27	0.19	0.28	0.36	0.38	0.35	0.19	0.35	0.25	0.02	0.03
	Hum	-0.56	-0.11	-0.38	-0.69	-0.28	-0.38	-0.54	-0.56	-0.34	-0.3	-0.34	-0.43	-0.46	-0.11	-0.39	-0.48
	Precip	-0.32	0.17	-0.16	-0.18	-0.3	-0.31	-0.29	-0.17	-0.11	-0.28	-0.04	-0.26	-0.32	-0.07	0.02	0.17
PAD$_{OXY}$	Temp	0.05	0.4	0.22	0.52	0.39	0.38	0.4	0.32	0.25	0.12	0.05	0.1	0.17	0.21	0.1	0.11
	Hum	-0.45	-0.14	-0.28	-0.51	-0.23	-0.23	-0.45	-0.36	-0.14	-0.28	-0.38	-0.41	-0.2	-0.24	-0.29	-0.22
	Precip	-0.53	-0.01	-0.19	-0.26	-0.53	-0.12	-0.39	-0.2	-0.02	-0.04	-0.03	-0.37	-0.17	-0.14	-0.01	-0.23

III   The Carbon-Isotope Response Surface

Synopsis

Chapter III reviews the carbon-isotope response surface approach (^{13}C-irsa) which partitions $\delta^{13}C_{cell}$ labelling into ΔS_{MS}, Δh_{GS} and ΔT_{GS}. An April to October labelling seasons was identified for Δh_{GS} and ΔT_{GS} using a series of PP-MCC. Using the estimates for the labelling season, ^{13}C-irsa was tested and contrasted against various statistical techniques for deriving transfer functions. It was found that although a number of the regression-based techniques produced better statistical results in the short-term (50-years) reconstructions, they did not conform to the mechanistic understanding of stomatal conductance and photosynthetic rate at present and thus, any reconstruction that goes beyond the available climate data would be questionable. To achieve a better fit, modifications to the coefficients ς and τ of ^{13}C-irsa were made to capture the 50 year trend. With redefined coefficients for ^{13}C-irsa 100-year reconstructions of PAD and site-specific (Upland, Lowland and Island) Δh_{GS} were developed using ΔT_{GS} and $\Delta \delta^{13}C_{Cell}$.

III.1 Introduction

The Farquhar model (1982) (*Section I.3.3*) defines the labelling of $\delta^{13}C_{Cell}$ as a function of stomatal conductance and photosynthetic capacity, which vary with labelling season relative humidity, temperature and soil moisture status. The carbon-isotope response surface approach (^{13}C-irsa) (EDWARDS et al., 2008; EDWARDS et al., 2000) is a trivariate model which incorporates the above identified physical and biological responses to labelling season relative humidity, temperature and soil moisture status to $\delta^{13}C_{Cell}$ labelling. If soil moisture status can be ruled out as a source of stress and the season of labelling identified, ^{13}C-irsa can be simplified to a bivariate $\delta^{13}C_{Cell}$ labelling model.

To model the labelling of $\delta^{13}C_{Cell}$, the labelling seasons for temperature, relative humidity and soil moisture status should be defined. This was addressed by comparing various subgroups of environmental data against $\delta^{13}C_{Cell}$ dendrochronology (site specific and regional), 16200 comparisons. Precipitation amount (mm) was used as a proxy for soil moisture status. A labelling season of April to October with weighted smoothing over three years was identified for temperature and relative humidity, whereas soil moisture status had no discernable effect on isotopic labelling. The latter is consistent with evidence that trees in the PAD are generally not soil moisture stressed (BAILEY, 2005; COUILLARD, 2004; MELCHIN, 2007).

With these estimates of temperature and relative humidity labelling season the ^{13}C-irsa model was forward and backward modelled. The modelling results were then

compared to environmental and reconstructed datasets based on statistical univariate and bivariate models to determine if the response surface was the most apt model and could be used to reconstruct $\delta^{13}C_{Cell}$, growth season temperature and relative humidity. In the end, a modified Edwards et al. (2008) ^{13}C-irsa model was the best model that adhered to the mechanistic understanding of $\delta^{13}C_{Cell}$ labelling tested and was used to couple the response surfaces in Chapter V. The reconstructions were then separated by topographic (Upland & Lowland) and geographic (Island) location to assess whether there were any systematic differences in isotopic labelling that could be identified. It was found that although there were slight isotopic variances which may represent variation in sampling location, competition, irrigation and topography, they were not significant enough to merit independent analysis.

III.2 The Carbon-Isotope Response Surface Approach: ^{13}C-irsa

The application of ^{13}C-irsa to reconstruct paleoclimate relies on a mechanistic understanding of the relationships between $\delta^{13}C_{Cell}$ and its dependence on temperature and stomatal conductance, varying with soil moisture status, temperature and relative humidity as described by Farquhar et al. (1989). The temperature and relative humidity relationship is often reflected in significant mutually correlated univariate statistics with $\delta^{13}C_{cell}$ (FENG and EPSTEIN, 1995; LEAVITT, 1993; LIPP et al., 1991; PENDALL et al., 1999; SCHLESER et al., 1999). Due to the colinearity, the application of univariate transfer functions is being replaced with multivariate approaches such as ^{13}C-irsa (equation [20]);

$$\delta^{13}C_{cell} = \varsigma \cdot \Delta h_{GS} + \tau \cdot \Delta T_{GS} + \upsilon \cdot \Delta S_{MS} \qquad (20)$$

Here ς is the relative humidity, τ is the temperature and υ is the soil moisture status coefficients. If one parameter can be eliminated with some certainty, such as ΔS_{MS}, then the isotopic enrichment of $\delta^{13}C_{cell}$ with respect to changing Δh_{GS} and ΔT_{GS} can be expressed as a planar surface or a bivariate model.

Variations of the model have been proposed by Yakir et al. (1994) and Lipp et al. (1996) to probe climate in the Roman period at Masada, Israel. This model was advanced further when Edwards et al. (2000)conducted a series of growth chamber experiments using *Vicia faba* with the intent to resolve the temperature and relative humidity dependent signals in higher plant $\delta^{13}C_{plant}$.

The experiment was conducted by selecting seedlings germinated under identical

conditions for two weeks. The seedlings where then transferred to four climate chambers; (1) 40%/291K, (2) 40%/301K, (3) 80%/291K, or (4) 80%/301K and two irrigation treatments by weight (wet or dry).

The results indicated that the wet and dry irrigation treatments had a substantial effect on the isotopic enrichment of the samples; with the dry samples showing the least discrimination against carbon-13 in all four cases and was most likely a result of increased environmental stress due to low ΔS_{MS}. Although the irrigation treatment was not rigorously quantified and may not represent the natural range of conditions, they found that the response of the *V. faba* with respect to Δh and ΔT could be expressed on the planar surface (equation [21]);

$$\Delta \delta^{13}C_{cell} = (-0.032) \cdot \Delta h + (-0.255) \cdot \Delta T \qquad (21)$$

Edwards et al. (2000)then reanalyzed the investigation conducted on the well-irrigated (1775 mm annually (SCHLESER et al., 1999)) European silver fir (*Abies [Mill] alba*). Due to the meteorological data's mutual correlation, h and T, they concluded that based on the relationship defined for *V. faba* that the coefficients ς and τ must both be negative.

$$\Delta \delta^{13}C_{cell} = (-0.17‰/\%) \cdot \Delta h + (-0.15‰/K) \cdot \Delta T \qquad (22)$$

This was contradictory to the original assessment of the *A. alba* chronology which initially resulted in a positive τ coefficient (LIPP et al., 1991). Theoretically, a positive relationship would exist if the trees were living above their thermal optimum and thus, an increase in temperature would result in decreased isotopic discrimination. This scenario is highly unlikely in such a high-latitude environment

where temperatures rarely exceed 22ºC. One explanation for the multi-sign $\pm\tau = \text{‰}/\text{K}$ temperature coefficient, is that the $\Delta\delta^{13}C_{cell}$ and ΔT relationship is non-linear and instead is based on an optimal efficiency range (parabolic) (SCHLESER et al., 1999). Deviations away from an optimal range result in a decline in biological response and productivity which reduces discrimination against ^{13}C. This theory has implications for tree-ring reconstructions based on transfer functions generated with calibration sets in locations with environmental change. If the environment has had sufficient changes in the average temperature the slope and thus the labelling responses would not be representative of all past conditions.

III.3 Results and Discussion

III.3.1 Identifying the Seasonal Labelling of $\delta^{13}C_{Cell}$

Previous research in the PAD by Couillard (2004) and Bailey (2005) hypothesized a summer growth season and used a labelling season estimate of May to September based on average monthly temperatures. To verify this hypothesis, the above defined labelling season for soil moisture status temperature and relative humidity have to be demonstrated to have the potential to reconstruct $\delta^{13}C_{Cell}$ in PAD trees.

To clarify the labelling season and the possibility of carry-over effects the environmental data were compared against the PAD$_{.CAR}$ chronologies using PP-MCC. The environmental data were organized into 300 (possible combinations over 24 months) temperature (minimum, maximum and mean), relative humidity (minimum 0h00-23h59, mean 0h00-23h59 and mean 6h00-20h00) and precipitation (rain, snow and total [rain and snow]) groups. By organizing the environmental data, climate sensitivities to minimum or maximum values can be ruled out as a cause of stress and the identification of trees growing below their climate limits can be easily identified. All results are present as r-values (Figure III-1 and Figure III-2).

III.3.1.1 Relative Humidity Labelling Season

The relative humidity datasets (min [0h00-23h59], mean [6h00-20h00], or mean [0h00-23h59]) versus PAD$_{.CAR}$ have a similar correlation coefficient distribution to the temperature datasets (mean, min or max) versus PAD$_{.CAR}$. The comparisons show a one month shift to the left (March, Figure III-1 [Top]) with respect to temperature

datasets and two months (May) more than the hypothesized estimate. The reason for this shift is unclear and may reflect a more productive early spring growth. Humidity mean (0h00-23h59) and mean (6h00-20h00) versus PAD$_{.CAR}$ show equivalent variances. Humidity min (0h00-23h59) is similar in magnitude (r-value) and distribution (negative versus positive) of signal to the other two datasets but does show minor variations. During November and December the signal for min (0h00-23h59) decreases significantly, while the latter two approach their maximum values. This was not expected as the trees should be dormant during these months. The well-bracketed response to min (0h00-23h59) is thought to reflect the effect of low relative humidity on stomatal conductance; maximum stress and minimum discrimination. However, low humidity would only be present during peak daytime hours and would not be the only signal present. As such, mean (6h00-20h00) relative humidity although not fitting the hypothesized bounds of the labelling season will be used to estimate an April to October labelling season and thus will be used to test ^{13}C-irsa and fit the statistical models (Figure III-2 [A]).

III.3.1.2 Temperature Labelling Season

The organization of temperature (mean, min or max) versus PAD$_{.CAR}$ had little impact on the magnitude or direction of the signal over the 24-month interval (Figure III-1 [Middle] and Figure III-2 [B]). There was a consistent response throughout the 24-month interval with the exception of the winter months (November and December) of the present or previous year's growth. The most pronounced responses occur between April and October ($r \geq 0.36$, $P < 0.01$) and confirm the first estimate of a labelling season defined for mean (6h00-20h00) relative humidity. The previous (p)

year's *p*October is also seen as significant, exceeds 0.36 (r) and is likely due to photosynthate carry-over.

III.3.1.3   Precipitation Labelling Season

When looking at the Figure III-1 (bottom) and Figure III-2 (C) there is no clear growth season response that can be identified without substantial error as the precipitation datasets (rain, snow and total) versus $PAD_{.CAR}$ signals are sporadic and difficult to interpret. A previous study by McDonald et al. (2005) indicated that tree-rings (ring-width) in the PAD integrate precipitation for up to a five-year period and that in many cases, the previous years' precipitation correlated more significantly than with the current year's ring-width.

The lack of a clear precipitation labelling season response is likely due to water demand, residence times and the infiltration rates[7]. If the infiltration rate is retarded by the low hydraulic conductivity of silty outwash sands, flood deposits and seasonal freezing, then the water available at the fine root network during photosynthesis could potentially be from the previous year's late summer - early fall (*p*August) to spring precipitation (March). The resulting growth season precipitation signal would be very sporadic and unclear.

---

[7] migration from the surface to the fine root network

III.3.1.4 $\delta^{13}C_{Cell}$ Carry-Over and Autocorrelation

Due to the possibility of photosynthate storage (MACDONALD et al., 2005), an investigation of carry-over signal in $\delta^{13}C_{Cell}$ is required. The investigation consisted of comparing various weightings of the defined growth season (April to October) for temperature, humidity and precipitation over three years against PAD$_{.CAR}$ (Table III-1). The data indicate that an even three-year weighting would yield statistically significant results when introduced into a model. If evenly weighted, each year would represent 33.33 % of the signal, with the current year being Y_x and each preceding year would progress as follows, Y_{X-1}, Y_{X-2} to Y_{x-n}. After closer evaluation, a weighting towards the present-year growth season would produce a better fit and as it would be unlikely that photosynthates from two growth seasons prior (Y_{X-2}) would have an even weighting on the current year. Because of this, a three-year staggered weighting was selected; $Y_x = 50\%$, $Y_{X-1} = 30\%$ and $Y_{X-2} = 20\%$.

An autocorrelation analysis (Table III-2) was also conducted on the environmental datasets during the defined labelling season and PAD$_{.CAR}$. The results indicated that there is an autocorrelation of at least two years in the PAD$_{.CAR}$ chronology but none was present within six years in the environmental datasets. This suggests that the trees are recording a carry-over effect which is likely the result of stored photosynthates and not of gradual environmental change.

III.3.2 Application of the ^{13}C-irsa: Edwards et al. (2000) Model

When labelling season estimates for ΔT_{GS} and Δh_{GS} were introduced into ^{13}C-irsa,

the reconstructions reasonably reproduced the variability in $PAD_{.CAR}$ (r; smoothed = 0.45 and unsmoothed = 0.56, P < 0.001). The overall low-frequency trend was well captured, however, substantial deviations that generally indicated increased discrimination in the measured values versus the modelled $\Delta\delta^{13}C_{cell}$ were observed, Figure III-3 (Top).

When ^{13}C-irsa was inverted (equation [23]) to reconstruct ΔT_{GS}, significant deviations were seen between the modelled and environmental datasets, (r = -0.56), Figure III-3 (Middle). If the commonly observed statistical relationship between ΔT_{GS} and $\Delta\delta^{13}C_{cell}$ were accurate, ^{13}C-irsa may assign an inappropriate sign. Another possibility is that there is too much emphasis on Δh_{GS}-dependent labelling and the temperature coefficient, τ, should increase.

$$\Delta T_{GS} = \left(\Delta\delta^{13}C_{cell} - \varsigma \cdot \Delta h_{GS}\right)/\tau$$
$$or \qquad\qquad\qquad\qquad\qquad\qquad\qquad\qquad (23)$$
$$\Delta T_{GS} = \left(\Delta\delta^{13}C_{cell} - \left(-0.17‰/\%\right)\cdot \Delta h_{GS}\right)/\left(-0.15‰/\%\right)$$

When ^{13}C-irsa was inverted (equation [24]) to reconstruct Δh_{GS}, the model captured the high-frequency variability well and produced a significant reconstruction, 50% of the variability (r = 0.71), Figure III-3 (Bottom) of the dependent variable was explained by the independent variables. Significant deviations were also observed in the same locations as the ΔT_{GS} and $\Delta\delta^{13}C_{cell}$ reconstructions .

$$\Delta h_{GS} = \left(\Delta\delta^{13}C_{cell} - \tau \cdot \Delta T_{GS}\right)/\varsigma$$
$$or \qquad\qquad\qquad\qquad\qquad\qquad\qquad\qquad (24)$$
$$\Delta h_{GS} = \left(\Delta\delta^{13}C_{cell} - \left(-0.15‰/K\right)\cdot \Delta T_{GS}\right)/\left(-0.17‰/\%\right)$$

III.3.3 Gaussian Least Squares Model for Labelling $\Delta\delta^{13}C_{cell}$

The Gaussian Least Squares model $\Delta\delta^{13}C_{Cell}$ versus measured $\Delta\delta^{13}C_{cell}$ (Figure III-4 [Top]) fulfilled the univariate statistical relationships (positive [+] temperature and negative [-] relative humidity versus $\Delta\delta^{13}C_{cell}$ as observed in Figure III-1 and Figure III-2) and as a result violated the mechanistic model as proposed by Edwards et al. (2000) and the understanding of how plants label in the Farquhar el al. (1982) model. This model predicted 44% (r = 0.69) and 66% (r = 0.82) of the variability of the annual environmental and smoothed data. The majority of the labelling was conveyed to the temperature coefficient with humidity moderating the signal, equation (25). Mathematically this was done to equally scale both coefficients; the range in humidity values is effectively 3.5 times the variability of temperature.

$$\Delta\delta^{13}C_{cell} = \left(-0.12‰/\%\right)\cdot\Delta h_{GS} + \left(+0.40‰/K\right)\cdot\Delta T_{GS} + 0.029 \qquad (25)$$

When the models where inverted to reconstruct ΔT_{GS} and Δh_{GS} (Figure III-4 [middle] and [Bottom] respectively) there was a notable difference compared to the ^{13}C-irsa inversions. The ΔT_{GS} reconstruction was a vast improvement and captured much of the variability and trend over the 47-year comparison (r = 0.66). The Δh_{GS} reconstruction did not fare as well as it dropped by 0.09 to 0.62 (r), had no substantial deviations from the expected variability and was a near-perfect match in the low-frequency trend.

Similar signs for τ have been published (BARBOUR and FARQUHAR, 2000; DUPOUEY et al., 1993; LIPP et al., 1991; PEARMAN et al., 1976; PORTER et al., 2007; SCHLESER

et al., 1989; SCHLESER et al., 1999). Schleser et al. (1999)postulated that $\Delta\delta^{13}C_{cell}$ should enrich as the ambient temperature deviates from an ideal thermal range. In the case of Porter et al. (2007) and Barbour and Farquhar (2000) a temperature induced drought stress is thought to be the cause of the positive τ. Effectively, Porter et al. (2007) and Barbour and Farquhar (2000) both described decreased discrimination with increasing summer temperatures due to drought stress internal to the tree. A third option is that the observed temperature effect on $\Delta\delta^{13}C_{cell}$ discrimination reflects leaf versus atmospheric ΔT_{GS} differential during times of peak production (low Δh). This differential would result in the rise of c_i / c_a in response to increasing ΔT and irradiance and thus, depleted $\Delta\delta^{13}C_{cell}$.

III.3.4 Univariate Statistical Model: Temperature and Humidity

The univariate temperature model (equation [26]) was able to predict 49% (r = 0.70) of the variability in measured $\Delta\delta^{13}C_{cell}$ (Figure III-5). While the humidity based model (equation [27]) predicted 50% (r =0.71) of the variability (Figure III-6) in $\Delta\delta^{13}C_{Cell}$. These results suggest that both coefficients are being recorded equally in the tree-rings with a carry-over. Two alternative and less desirable scenarios would be that the ambient temperature or humidity are varying remarkably similarly over the calibration set (which we determined was not the case above) or that they are significantly mutually correlated (r = -0.43 and -0.53, unsmoothed and smoothed datasets) and thus, interchangeable. The latter two solutions would significantly hinder the coupling of the models if true.

$$\Delta\delta^{13}C_{cell} = (0.5906\text{‰/K})\cdot \Delta T_{GS} + 0.0315 \qquad (26)$$

$$\Delta\delta^{13}C_{cell} = (-0.1925\text{‰/\%})\cdot \Delta h_{GS} + 0.0264 \quad (27)$$

III.3.5 Modified ^{13}C-irsa:

Scaled to Reflect the Long-Term Changes in $\delta^{13}C_{cell}$

Scaling the coefficients (equation [28]) did not produce a significant statistical improvement when reconstructing measured $\Delta\delta^{13}C_{cell}$ variability with the introduction of the ΔT_{GS} and Δh_{GS} datasets. Since only the magnitude of the coefficients was varied and not the sign, there was no change in the variability (Figure III-7 [Top]).

One advantage of this model over the original was when inverted; a substantial statistical gain was observed when reconstructing ΔT_{GS} (Figure III-7 [Middle] improved to r = -0.39).

$$\Delta\delta^{13}C_{cell} = \varsigma\cdot \Delta h_{GS} + \tau\cdot \Delta T_{GS} + \upsilon\cdot \Delta S_{MS}$$
$$or \qquad\qquad\qquad\qquad\qquad\qquad\qquad (28)$$
$$\Delta\delta^{13}C_{cell} = (-0.23\text{‰/\%})\cdot \Delta h_{GS} + (-0.21\text{‰/K})\cdot \Delta T_{GS}$$

A marginal improvement in scaling was observed when reconstructing Δh_{GS} (r = 0.71, Figure III-7 [Bottom]) compared to equation (22). This reconstruction shows that the trees are experiencing higher-than-normal atmospheric moisture from AD 1900 to 1930 (small drop in AD 1915). From 1930 a progressive drop in humidity anomaly is observed till AD 1940 which continues to 1950. At AD 1950 there is a slight rebound in humidity, which ends by 1955. There is a gradual movement toward maximum humidity anomaly at 1965 and 1967 which is followed by a drop in

humidity. From AD 1967 to 1970 humidity drops to relatively average anomaly values (0) and remains relatively constant till AD 1997. Strong low-moisture events are noted in AD 1980, 1983 and 2000. The above-described pattern of variation is consistent with a moister PAD which accompanies spring ice-jam and high-stand flooding as documented by Thomson (1993) and Peterson (1994) and the reconstructed flood history by Timoney et al. (1997). Intervals or years in which the measured humidity anomalies deviate significantly (2% or more) from the reconstructed generally only occur during known drought and flood events.

The Δh_{GS} reconstruction based on ^{13}C-irsa showed promise and will be used to aid in developing the oxygen-isotope response surface approach in Chapter IV.

III.3.6 Δh_{GS} Site Comparison

Upland (GSL & QFU), Lowland (QFR & PRC) and Island (BITC) sites (Figure III-8) show consistent variability and trend throughout the comparison. The Lowland sites on average show the highest humidity, while BITC shows the lowest humidity. BITC shows low relative humidity at the turn of the twentieth century and is offset from Lowland and Island by 4%. The time-series converge toward the present. This may be the result of a longer ice-on season for Lake Athabasca in the past. Thus, in early spring when the trees began to grow the local relative humidity was lower over the lake and the island and the thawing delta was wetter. This hypothesis is supported by comparison of the Lowland, Upland and Island sites during known flood events, which shows a tendency for the Upland sites to lie midway between the Lowland and Island sites.

82

Systematic differences are also apparent between the measured and reconstructed Δh_{GS} (April-October) records, suggesting that moisture variations are buffered in the PAD compared to Fort McMurray. This is exemplified in Figure III-8.

III.4 Discussion and Conclusion

III.4.1 Temporal Isotopic Labelling of Stable Carbon in Tree-rings

May to August temperature and relative humidity values with an undefined carry-over effect were the previous growth season estimates used by Couillard (2004) and Bailey (2005). Our analysis indicates that $\Delta\delta^{13}C_{cell}$ is labelled by April to October ΔT_{GS} and Δh_{GS} with a pApril to pOctober carry-over. This will be re-evaluated using the $\Delta\delta^{18}O_{cell}$ exercise discussed in Chapter IV. The mean day humidity (6h00 to 20h00) labelling season is broader than for temperature and includes March. Minimum (0h00 to 23h59) humidity was the most statistically significant, but this time-series was rejected as the values generated would limit growth to an unreasonable short interval during the day or maximum mid-day temperatures. Minimum (0h00 to 23h59) humidity would also contradict the identified temperature labelling season. The precipitation amount analysis was inconclusive and requires further investigation. This is addressed in the $\Delta\delta^{18}O_{cell}$ labelling section for the oxygen-isotope response surface approach in Chapter IV.

Temperature, humidity and precipitation versus PAD.$_{CAR}$ displayed a carry-over signal from the previous year, which is presumed to be the result of the trees utilising stored photosynthates to initiate early spring growth or growth during unfavourable conditions. The carry-over signal was only found to occur in the $\Delta\delta^{13}C_{cell}$ and ΔT_{GS} or Δh_{GS}. However, in this analysis only three years of carry-over was found, 50-30-20 % weighting.

III.4.2 Models

The bivariate Gaussian least squares method modelled the variability in $\Delta\delta^{13}C_{cell}$ more accurately than the other four tested (r higher by 0.10-0.15). The model however, lacks mechanistic consistency and has a positive coefficient sign, τ, which is inverse to the *V. faba* growth chamber findings, Section III.2. As a result the model was discounted.

^{13}C-irsa and modified ^{13}C-irsa's low r-values for modelling $\Delta\delta^{13}C_{cell}$ may be a reflection of the input data quality not being representative of the PAD, specifically in the case of Δh, as well as the additional analytical uncertainties associated with additional parameters, whereas this is not reflected in the univariate statistical analysis of ΔT_{GS} and Δh_{GS}. The latter showed consistent and statistically significant environment-specific responses to flooding and drought conditions.

Comparison of the site-specific humidity chronologies yielded evidence of systematic local differences, but also a consistent pattern of delta-wide variability. These local differences are considered further in Chapter V in the context of the fully coupled isotopic response surface modelling.
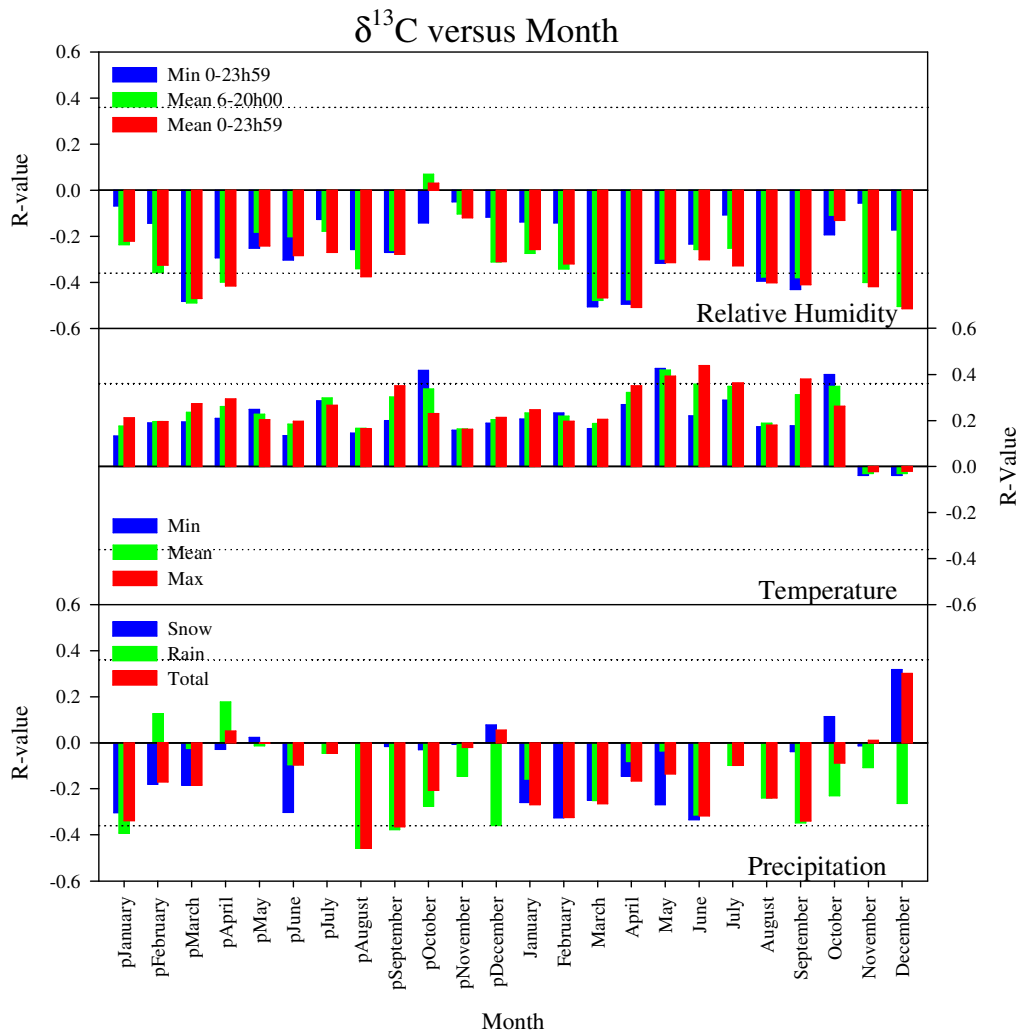
Figure III-1. $\Delta\delta^{13}C_{cell}$ vs temperature (minimum, maximum and mean), relative humidity (minimum 0h00-23h59, mean 0-23h59 and mean 6h00-20h00) and precipitation (rain, snow and total [rain & snow]). R = ± 0.36 (P < 0.01) are displayed using the grey dotted line.
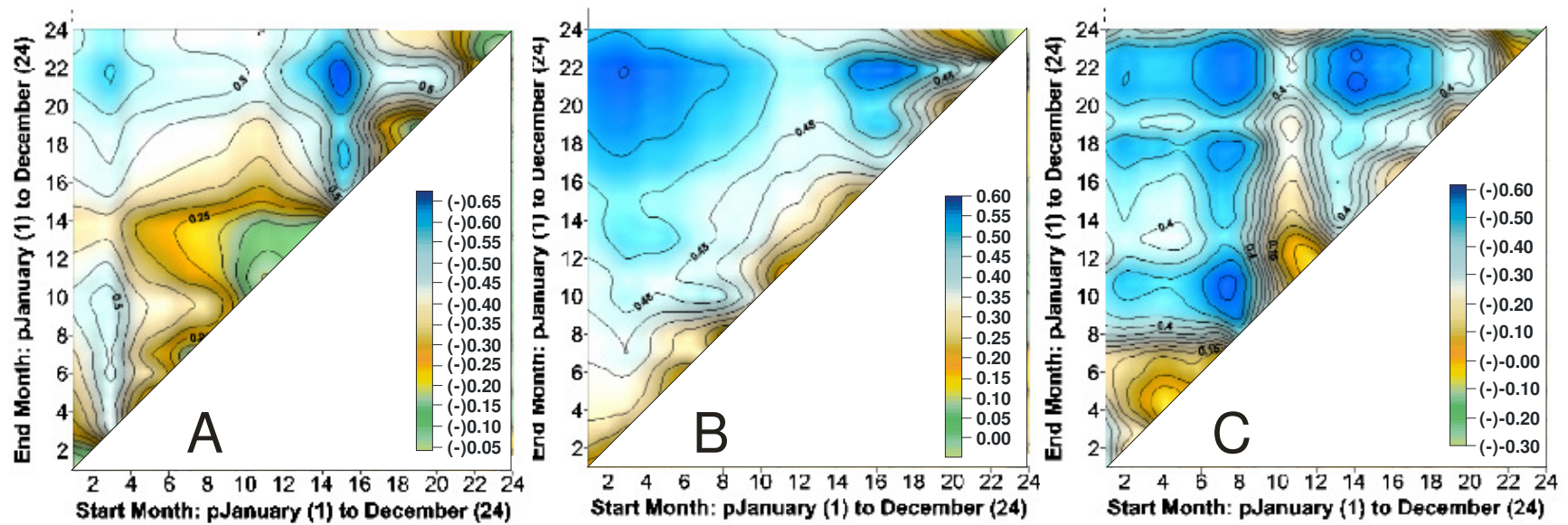
Figure III-2. $\Delta\delta^{13}C_{cell}$ vs (*A*) minimum 0h00-23h59 relative humidity, (*B*) mean temperature and (*C*) total (rain & snow) precipitation. The X-axis represents the starting month in the comparison while the Y-axis represents the ending month, with the months starting at the previous *p*January and advancing to the December of the current year's growth. The relative humidity and precipitation values have been inverted to maintain numerical consistency with the temperature values. R = ± 0.36 (P < 0.01) are deemed statistically significant.
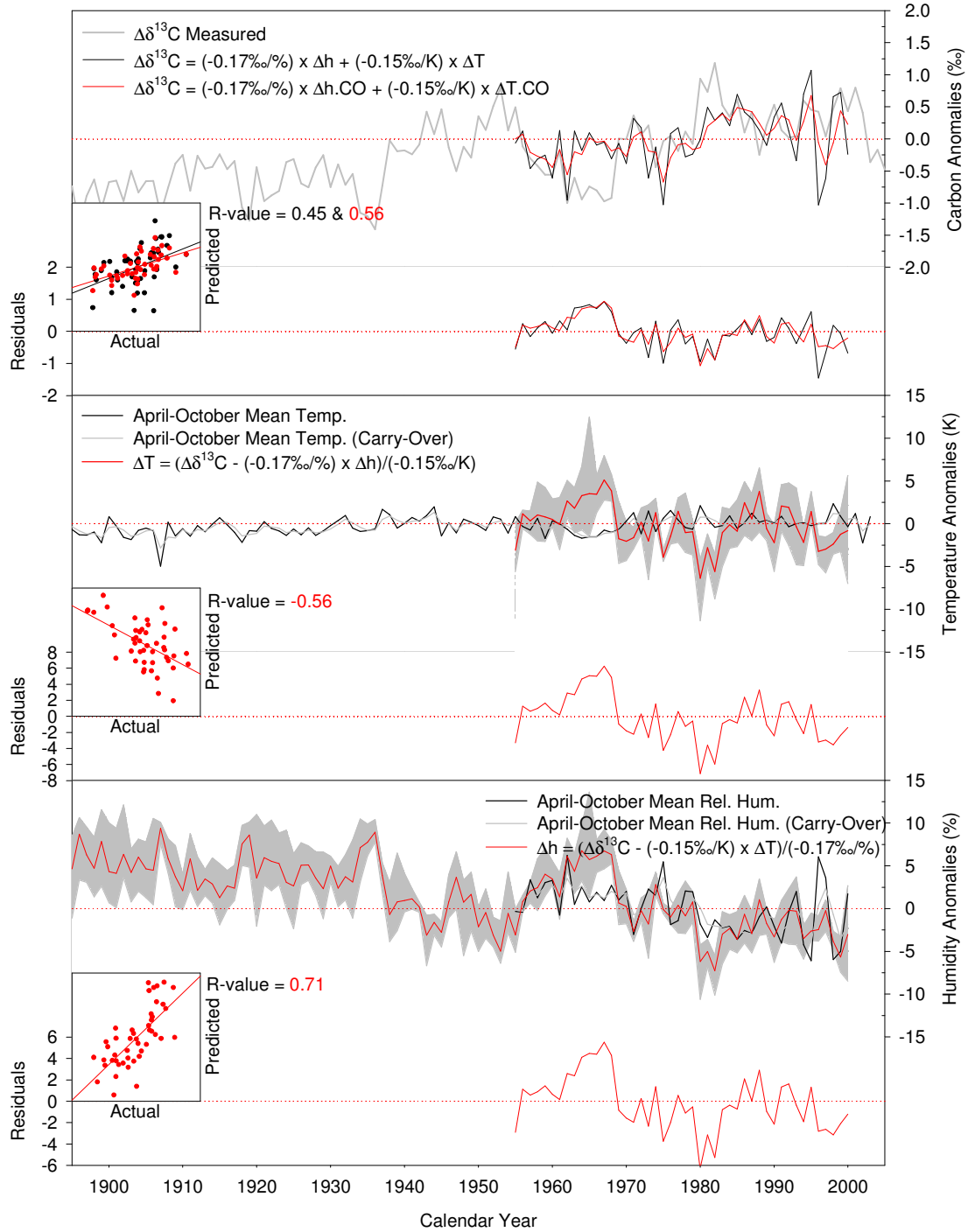
Figure III-3. Modelling and reconstruction results from the original ^{13}C-irsa with the introduction of $\Delta\delta^{13}C_{cell}$ (‰), ΔT_{GS} and Δh_{GS} (April to October) data. (*Top*) Modelling unsmoothed (black) and smoothed (red) carry-over $\Delta\delta^{13}C_{cell}$ (‰). (*Middle*) Reconstructions of carry-over ΔT_{GS} . (*Bottom*) Reconstructions of carry-over Δh_{GS} .
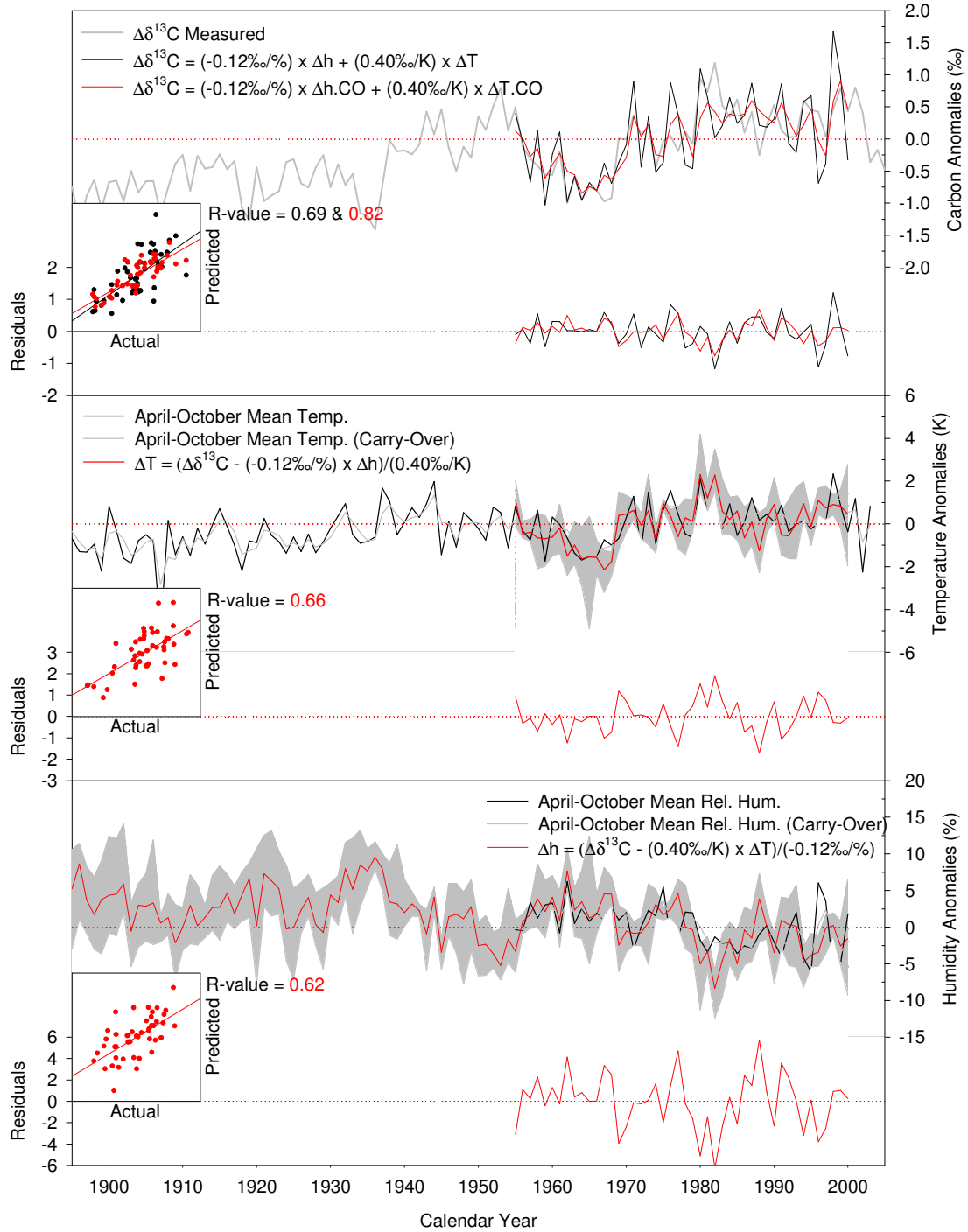
Figure III-4. Modelling and reconstruction results from a bivariate Gaussian Least Squares Model with the introduction of $\Delta\delta^{13}C_{cell}$ **(‰),** ΔT_{GS} **and** Δh_{GS} **(April to October) data. (*Top*) Modelling unsmoothed (black) and smoothed (red) carry-over** $\Delta\delta^{13}C_{cell}$ **(‰). (*Middle*) Reconstructions of carry-over** ΔT_{GS} **. (*Bottom*) Reconstructions of carry-over** Δh_{GS} **.**
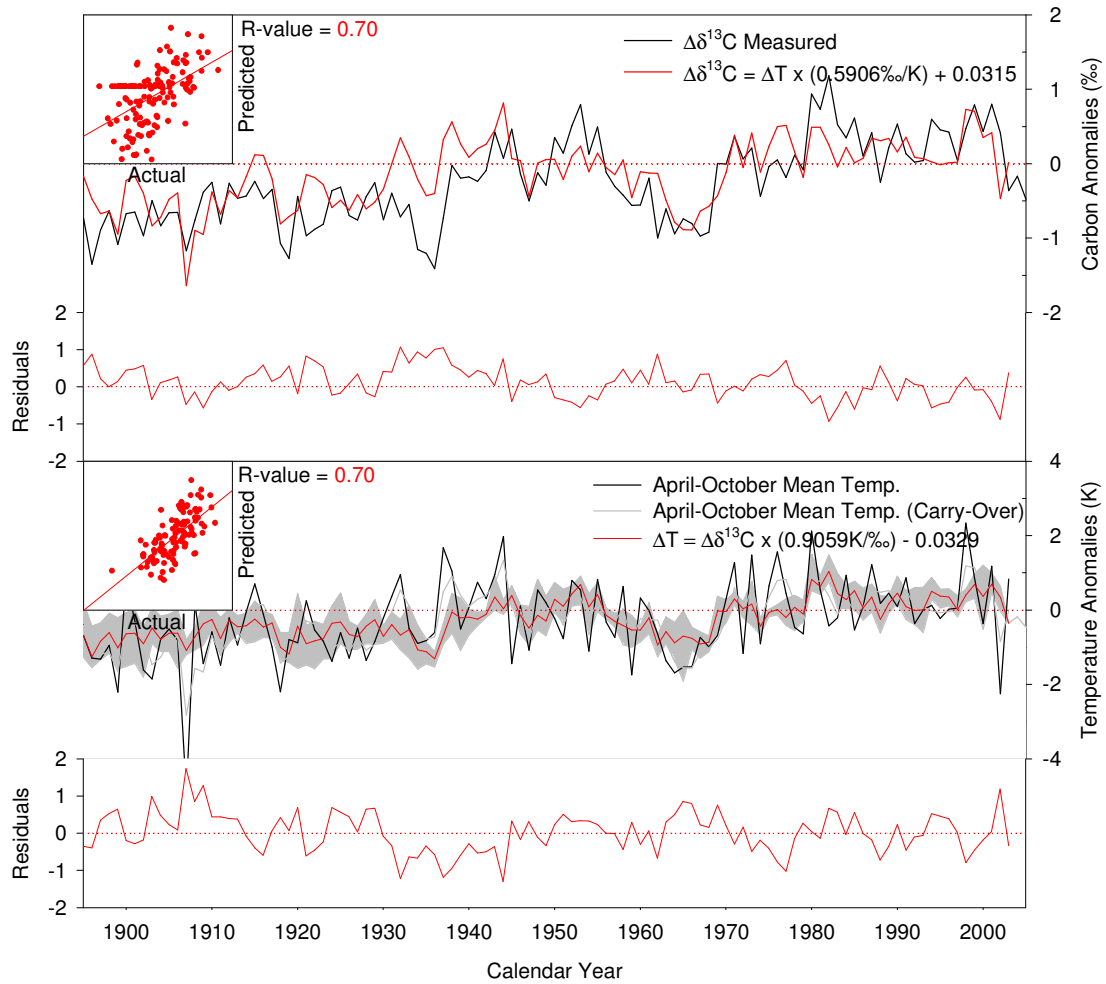
Figure III-5. Modelling and reconstruction results from a univariate Gaussian Least Squares Model with the introduction of $\Delta\delta^{13}C_{cell}$ (‰) and ΔT_{GS} (April to October) data. (*Top*) Modelling unsmoothed (black) and smoothed (red) carry-over $\Delta\delta^{13}C_{cell}$ (‰). (*Bottom*) Reconstructions of carry-over ΔT_{GS}.
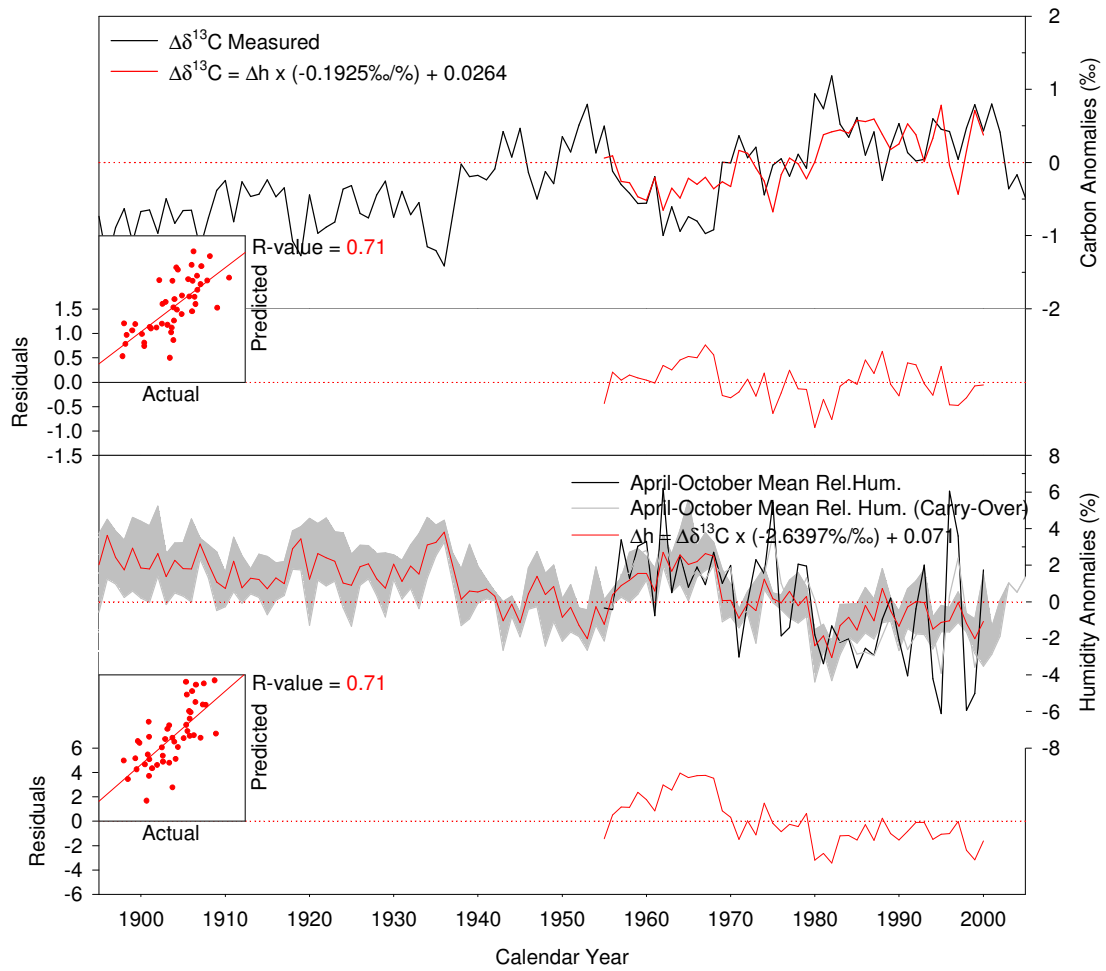
Figure III-6. Modelling and reconstruction results from a univariate Gaussian Least Squares Model with the introduction of $\Delta\delta^{13}C_{cell}$ **(‰) and** Δh_{GS} **(April to October) data. (*Top*) Modelling unsmoothed (black) and smoothed (red) carry-over** $\Delta\delta^{13}C_{cell}$ **(‰). (*Bottom*) Reconstructions of carry-over** Δh_{GS} **.**
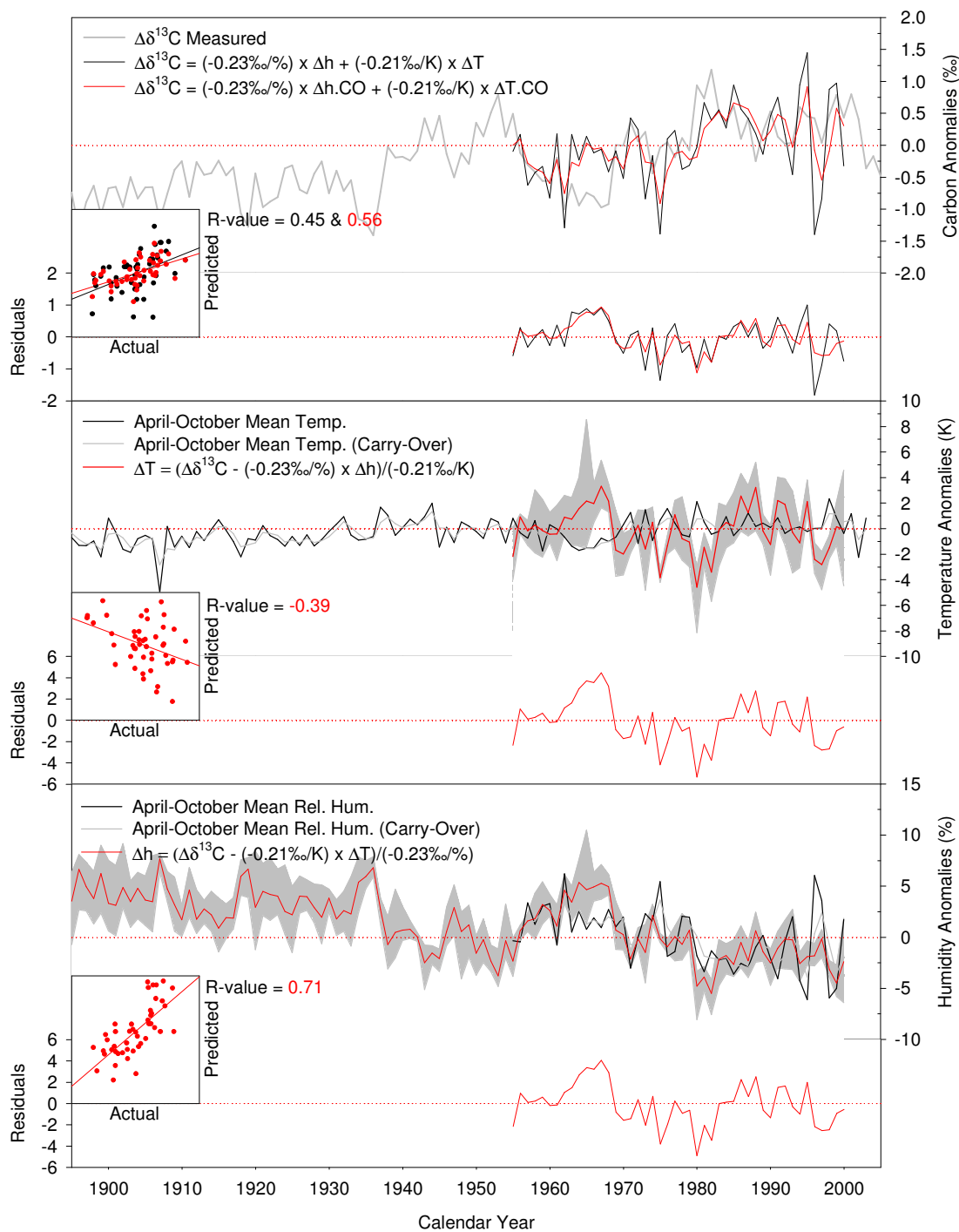
Figure III-7. Modelling and reconstruction results from the adjusted ^{13}C-irsa with the introduction of $\Delta\delta^{13}C_{cell}$ (‰), ΔT_{GS} and Δh_{GS} (April to October) data. (*Top*) Modelling unsmoothed (black) and smoothed (red) carry-over $\Delta\delta^{13}C_{cell}$ (‰). (*Middle*) Reconstructions of carry-over ΔT_{GS}. (*Bottom*) Reconstructions of carry-over Δh_{GS}.

92
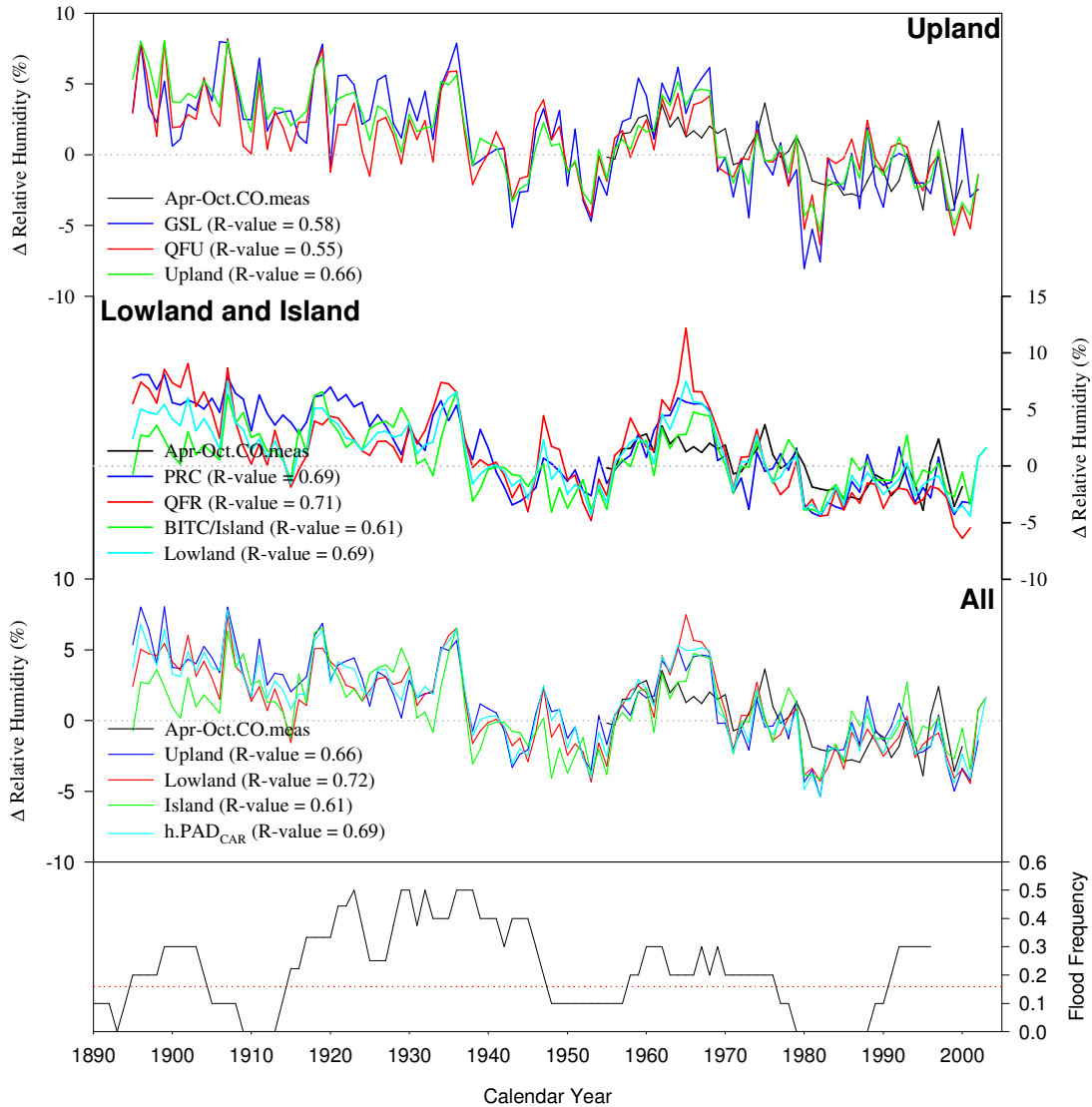
Figure III-8. Reconstructed Δh_{GS}. **Comparison of the variation in relative humidity at Upland (GSL & QFU), Lowland (PRC & QFR) and Island (BITC) locations. These reconstructions were generated from the introduction of known values of** ΔT_{GS} **and** $\Delta \delta^{13}C_{cell}$ **(‰) in to the** [13]**C-irsa with modified coefficient values fit to the** $\Delta \delta^{13}C_{cell}$ **(‰) trend and variability. A flood frequency (10-year running mean) diagram from Timoney et al. (1997) is also included for comparison with the results. R = ± 0.36 (P < 0.01) are statistically significant.**

Table III-1. PAD$_{.CAR}$ Carry-Over; PAD$_{.CAR}$ vs temperature (ΔK) and relative humidity (Δ%) [25] weighted from one to three years. All values are expressed as r-values, with values being significant at P < 0.01 and P < 0.05 when r reaches or exceeds 0.36 and 0.28 respectively.

R-value Weighting			Carbon Isotope Carry-Over: (AD) 1955-2000											
			Relative Humidity (%)						Temperature (K)					
Y_x	Y_{x-1}	Y_{x-2}	PRC	OFR	OFU	GSL	BITC	PAD	PRC	OFR	OFU	GSL	BITC	PAD
1	0	0	-0.5	-0.46	-0.58	-0.61	-0.58	-0.6	0.55	0.54	0.4	0.58	0.48	0.58
0.9	0.1	0	-0.53	-0.49	-0.59	-0.63	-0.58	-0.63	0.58	0.59	0.43	0.6	0.52	0.62
0.8	0.2	0	-0.56	-0.52	-0.59	-0.63	-0.58	-0.65	0.61	0.64	0.45	0.61	0.55	0.65
0.8	0.15	0.05	-0.57	-0.52	-0.59	-0.64	-0.59	-0.65	0.62	0.63	0.45	0.61	0.54	0.65
0.8	0.1	0.1	-0.57	-0.52	-0.59	-0.65	-0.59	-0.66	0.62	0.63	0.45	0.61	0.53	0.65
0.7	0.3	0	-0.58	-0.55	-0.58	-0.63	-0.56	-0.66	0.63	0.68	0.47	0.61	0.58	0.68
0.7	0.25	0.05	-0.6	-0.55	-0.59	-0.65	-0.57	-0.67	0.64	0.68	0.48	0.62	0.57	0.68
0.7	0.2	0.1	-0.61	-0.55	-0.6	-0.66	-0.58	-0.67	0.65	0.68	0.48	0.63	0.56	0.69
0.7	0.15	0.15	-0.61	-0.55	-0.6	-0.66	-0.59	-0.68	0.66	0.67	0.48	0.63	0.55	0.69
0.6	0.4	0	-0.6	-0.57	-0.57	-0.62	-0.53	-0.65	0.63	0.7	0.49	0.6	0.59	0.69
0.6	0.35	0.05	-0.62	-0.57	-0.58	-0.64	-0.55	-0.67	0.65	0.71	0.5	0.61	0.59	0.7
0.6	0.3	0.1	-0.63	-0.58	-0.59	-0.65	-0.56	-0.68	0.67	0.72	0.5	0.62	0.58	0.71
0.6	0.25	0.15	-0.64	-0.58	-0.59	-0.66	-0.57	-0.69	0.68	0.72	0.51	0.63	0.57	0.72
0.6	0.2	0.2	-0.65	-0.58	-0.59	-0.67	-0.58	-0.7	0.69	0.72	0.5	0.63	0.56	0.72
0.5	0.5	0	-0.6	-0.57	-0.54	-0.59	-0.49	-0.64	0.62	0.72	0.49	0.57	0.59	0.68
0.5	0.45	0.05	-0.62	-0.59	-0.55	-0.61	-0.51	-0.66	0.65	0.73	0.5	0.59	0.59	0.7
0.5	0.4	0.1	-0.64	-0.6	-0.56	-0.63	-0.52	-0.68	0.67	0.75	0.51	0.6	0.59	0.72
0.5	0.35	0.15	-0.66	-0.6	-0.57	-0.65	-0.54	-0.69	0.69	0.76	0.52	0.61	0.59	0.73
0.5	0.3	0.2	-0.67	-0.61	-0.58	-0.66	-0.55	-0.7	0.7	0.76	0.52	0.62	0.58	0.74
0.5	0.25	0.25	-0.68	-0.6	-0.58	-0.67	-0.56	-0.71	0.71	0.75	0.52	0.62	0.56	0.73
0.4	0.4	0.2	-0.68	-0.62	-0.55	-0.63	-0.51	-0.69	0.69	0.78	0.52	0.59	0.58	0.73
0.4	0.35	0.25	-0.69	-0.62	-0.55	-0.65	-0.52	-0.7	0.7	0.78	0.53	0.6	0.57	0.74
0.4	0.3	0.3	-0.7	-0.62	-0.55	-0.66	-0.53	-0.7	0.71	0.78	0.53	0.6	0.55	0.74
0.35	0.35	0.3	-0.7	-0.63	-0.54	-0.64	-0.5	-0.69	0.7	0.78	0.52	0.58	0.55	0.73
0.33	0.33	0.33	-0.7	-0.63	-0.53	-0.64	-0.5	-0.7	0.7	0.78	0.52	0.57	0.54	0.73

Table III-2. Autocorrelation of PAD$_{CAR}$, temperature and relative humidity over six years. All values are expressed as r-values, with values being significant at P < 0.01 and P < 0.05 when r reaches or exceeds 0.36 and 0.28 respectively.

			Carbon Auto-Correlation; R-values					
No.: Years lag	**Δ.T (K)**	**ΔRH (%)**	**Carbon**					
	Apr.-Oct.	**Apr.-Oct.**	**PRC**	**QFR**	**QFU**	**GSL**	**BITC**	**PAD**
Y$_{X-1}$	0.15	0.29	0.75	0.78	0.36	0.46	0.46	0.69
Y$_{X-2}$	0.16	0.35	0.66	0.71	0.36	0.49	0.3	0.63
Y$_{X-3}$	0.22	0.22	0.51	0.62	0.09	0.32	0.1	0.45
Y$_{X-4}$	0.21	0.27	0.43	0.54	0.2	0.28	0.1	0.41
Y$_{X-5}$	0.11	0.27	0.32	0.51	0.12	0.22	0.07	0.36

IV   The Oxygen-Isotope Response Surface

Synopsis

Chapter IV contains a review of the oxygen-isotope response surface approach (^{18}O-irsa) concept where $\delta^{18}O_{cell}$ is labelled by source-water isotopic composition and h-dependent leaf water enrichment. To test and apply ^{18}O-irsa correctly, the labelling seasons for source-water and Δh_{GS} were identified using a series of PP-MCC. A winter source-water labelling season of pDecember to April was identified for temperature and was confirmed in the precipitation labelling season analysis. The relative humidity labelling season of April to October for Δh_{GS} mirrored and confirmed the growth season demonstrated in Chapter III.

Using the measured values for $\delta^{18}O_{cell}$ (PAD.OXY) and newly defined labelling seasons for ΔT_{SW} and Δh_{GS}, ^{18}O-irsa was inverted to reconstruct circulation-dependent shifts in the $T - \delta^{18}O$ relation, denoted here as ΔF. It was found that ΔF and the temperature coefficient (τ) combine to represent the source-water signal in ^{18}O-irsa. ^{18}O-irsa with various circulation regimes was then tested and compared to two statistical techniques for deriving transfer functions for modelling $\delta^{18}O_{cell}$ and reconstructing ΔT_{SW} and Δh_{GS}. It was concluded that although in most cases the statistical approaches modelled $\delta^{18}O_{cell}$ well, they did not produce adequate reconstructions of ΔT_{SW} and Δh_{GS}.

IV.1 Introduction

The labelling of water isotopes in tree-ring cellulose is a function of the source-water isotopic composition and the evaporative enrichment of leaf water which varies with growth season relative humidity and temperature. The primary model of labelling for $\delta^{18}O_{Cell}$ tested in this thesis is the oxygen-isotope response surface approach (^{18}O-irsa) (EDWARDS et al., 2008). The same technique described in Chapter III for demonstrating the labelling season of $\delta^{13}C_{Cell}$, demonstrated a *p*December to April temperature and precipitation signal with a two-year water residence time. The relative humidity has a labelling season of April to October, consistent with the labelling season observed in Chapter III.

Instrumental and measured values of $\delta^{18}O_{Cell}$, T_{SW} and h_{GS} were introduced into ^{18}O-irsa to test and analyse the model's accuracy. With this model as a baseline, univariate and bivariate statistically based approaches were developed and contrasted.

[18]O-irsa was not an accurate modeller of $\delta^{18}O_{Cell}$ and displayed a highly variable frequency in the residuals. The residuals were then used to gauge the necessary variability in the circulation pattern, F, required to reduce the uncertainty in the model (EDWARDS et al., 2008). The analysis shows strong promise for reproducing circulation indices using stable isotopes from $\delta^{18}O_{Cell}$. Various circulation indices were then used as proxies for damping of the $T - \delta^{18}O_{\Pr ec}$ relation.

IV.2 The Oxygen-Isotope Response Surface Approach: ^{18}O-irsa

^{18}O-irsa was initially developed by Edwards and Fritz (1986), equation (29). Similar mechanistic approaches have been proposed by Roden et al. (2000)and Yapp and Epstein (1982).

$$\Delta\delta^{18}O_{Cell} = \varsigma \cdot \Delta h_{GS} + (\tau \cdot \Delta T_{sw})$$
$$or \qquad\qquad\qquad\qquad\qquad\qquad\qquad\qquad\qquad (29)$$
$$\Delta\delta^{18}O_{Cell} = (-0.28‰/\%) \cdot \Delta h_{GS} + ((0.65‰/\%) \cdot \Delta T_{SW})$$

Here ς and τ are the h- and T- dependent coefficients based on modified Craig and Gordon (1963)linear resistance model for a closed basin and the Dansgaard (1964) temperature relationship, respectively.

ς is based on a damped Craig and Gordon (1965)type humidity-enrichment model for a terminal body of water. The total effective liquid to vapour fractionation factor for signals from evaporative enrichment of plant waters preserved in cellulose as used but Edwards et al. (2008) is $^{18}\alpha_e \cdot ^{18}\alpha_k \cong 1.028$, yielding a humidity coefficient of $-0.28‰/\%$, which is similar to the damped coefficient used by Roden et al. (RODEN et al., 2002). τ is the slope of the temperature to oxygen-18 source-water isotopic composition at ground surface relation and is given a value of $T - \delta^{18}O_{sw} = 0.65‰/K$ in this thesis which is consistent with Dansgaard (1964).

In later iterations of the model the damping effects of variable atmospheric circulation (NAM/AO, NAO, NP and PNA) on $\delta^{18}O_{Cell}$ was identified (EDWARDS et al., 2008). To address this, the variable ΔF was incorporated, equation (30).

$$\Delta\delta^{18}O_{Cell} = \varsigma \cdot \Delta h_{GS} + \left(\tau \cdot \Delta T_{sw}\right)$$

or (30)

$$\Delta\delta^{18}O_{Cell} = \left(-0.28\text{‰}/\%\right) \cdot \Delta h_{GS} + \left(\left(0.65\text{‰}/\%\right) \cdot \Delta T_{SW} + \Delta F\right)$$

In keeping with the mechanistic approach to modelling $\delta^{18}O_{Cell}$, ΔF varies directly with the pattern and strength of atmospheric circulation (EDWARDS et al., 2008). For example, when the circulation pattern is particularly zonal, forcing the air masses east over the Canadian Cordillera, atmospheric moisture is progressively enriched in the lighter isotope due to orographic rainout ($0 < \Delta F$). At times of more meridional circulation, the trajectory of the air masses allows for migration northward around the highest parts of the Canadian Cordillera, resulting in precipitation that is relatively enriched in the heavy isotopes reaching the PAD ($0 < \Delta F$).

IV.3 Results and Discussion

IV.3.1 Identifying the Seasonal Labelling of $\delta^{18}O_{Cell}$

Since $\delta^{18}O_{Cell}$ labelling is controlled by a combination of source-water isotopic composition, which is often dependent on local temperature, and leaf water enrichment by relative humidity deficit (BURK and STUIVER, 1981), identifiable labelling seasons should be detectable in the $\delta^{18}O_{Cell}$ dendrochronology. It is hypothesized that snowmelt should provide the majority of the source-water available at the fine root network in the PAD due to the low hydraulic conductivity[8] of the overburden (BAYROCK and ROOT, 1973; PETERS et al., 2006), so temperature (T_{SW}) signals should reflect winter conditions. In Chapter III the $\delta^{13}C_{Cell}$ labelling season for both T and h were demonstrated to be from April to October. The h-dependent labelling of $\delta^{18}O_{Cell}$ should reflect the same labelling season. Because of the postulated snowmelt signal, a labelling season from pNovember (of the previous year) and April is expected for S_{ms} and T_{SW}. The same technique as described in Section III.3.1 on page 74 was applied here with PAD.$_{OXY}$. Values are displayed in Figure IV-1 and Figure IV-2 and are expressed as r-values.

IV.3.1.1   Relative Humidity Labelling Season

The mean [6h00-20h00 and 0h00-23h59] relative humidity datasets versus PAD.$_{OXY}$ was more significant than the min [0h00-23h59] dataset, however, the overall trends

---

[8] $K = 1\text{x}10^{-7}$ to $1 \text{ x } 10^{-10}$ m.s^{-1}

are similar, Figure IV-1 (Top). A h-dependent labelling season was identified for March/April with a secondary response occurring later in July/August, Figure IV-1 (Top) and Figure IV-2 (A). This is consistent with findings that the bulk of the labelling occurred at the beginning of the growth season (MELCHIN, 2007). This response also helps to justify the labelling season found in Chapter III Three for h and T. A persistent carry-over signal is also present in pMarch and pApril.

IV.3.1.2 Temperature Labelling Season

Arranging the temperature data into min, mean or max to compare against PAD$_{.OXY}$ did not help to differentiate a labelling season as there were no significant deviations in magnitude (r-value) or direction (positive versus negative) between them. Figure IV-1 (Middle) and Figure IV-2 (B) identified a distinct winter/spring, pDecember to April, response to temperature, which supports the hypothesis that the trees are incorporating snowmelt as source-water. The figures also indicate that the previous year's winter/spring temperatures are no less significant, and are consistent with carry-over effects. The late October response that was observed in the mean temperature versus PAD$_{.CAR}$ is also present.

IV.3.1.3 Precipitation Labelling Season

The precipitation (Rain, Snow and Total) versus PAD$_{.OXY}$ is variable but does show a clear response over the same labelling season as the temperature (min, max, or mean) versus PAD$_{.OXY}$ analysis. Precipitation (Total and Snow) versus PAD$_{.OXY}$ identified a winter temperature response which peaks in pJanuary and continues to April, Figure IV-1 (Bottom) and Figure IV-2 (C). A secondary summer response was also observed

during August and September.

IV.3.1.4 $\quad \delta^{18}O_{Cell}$ **Carry-Over and Autocorrelation**

Our analysis (Figure IV-1 and Figure IV-2) identified a carry-over signal in the $\delta^{18}O_{Cell}$. As the carry-over signal in $\delta^{18}O_{Cell}$ may reflect water residence time, rather than photosynthate storage, separating these effects may be problematic.

The $\delta^{18}O_{Cell}$ T-dependent carry-over analysis (Table IV-1) indicates that the majority (70%) of the source-water signal is from the previous winter's precipitation. $PRC_{.OXY}$ and $GSL_{.OXY}$ were exceptions and suggested only a ~50% carry-over in the source-water signal. However, the lack of a carry-over signal in $\delta^{18}O_{Cell}$ h and the presence of one for $\delta^{18}O_{Cell}$ T suggests that the use of stored photosynthates is not the cause of a carry-over since it should affect both parameters. Instead it is likely that the carry-over signal identified for temperature is the result of water residence time in the soil, which also accounts for the heavier weighting to the present year's temperature and precipitation values.

There is some uncertainty regarding the lack of a $\delta^{18}O_{Cell}$ h-dependent carry-over as both a T- and h-dependent carry-over were identified for $\delta^{13}C_{Cell}$. One possible explanation is that post-photosynthetic exchange is so significant that a photosynthate carry-over signal is not recorded. This is unlikely as the calculated exchange is only ~13% (Calc. 2 in Appendix Appendix One: Application of the Dongmann Model) assuming that we have a representative value of winter snowmelt.

IV.3.2 Application of the Original ^{18}O-irsa: Edwards et al. (2008) Model

The ^{18}O-irsa reconstruction (Figure IV-3) overestimated the trend and range of variability in the measured $\delta^{18}O_{Cell}$ time-series. In most instances however, ^{18}O-irsa was a good predictor of annual variability and change, r = 0.57 and 0.60, when annual and smoothed T and h were introduced, respectively. The model's overestimation is likely due to the static $T - \delta^{18}O_{\Pr ec}$ relation, $0.65‰/K$, and may require re-scaling to fit the PAD.

The two inversions (equations [30] and [31]) of ^{18}O-irsa are not consistent reconstructions of mean winter temperature (pDecember to April) and mean growth season relative humidity (April to October) (6h00 to 20h00) (Figure IV-3). The temperature reconstruction shows increasing variability in the late 20th century and indicates a shallow but consistent increase in temperature since AD 1957. The humidity reconstruction is inverse to the mean growth season relative humidity dataset and indicates an increasing relative humidity. Since neither temperature nor humidity reconstruction captured the variation in range or variability (r = 0.17 and -0.38, respectively) sufficiently, ^{18}O-irsa as presented requires modification.

$$\Delta T_{sw} = \left(\Delta\delta^{18}O_{Cell} - \varsigma \cdot \Delta h_{GS}\right)/\tau$$
$$or \hspace{4cm} (31)$$
$$\Delta T_{sw} = \left(\Delta\delta^{18}O_{Cell} - \left(-0.28‰/\%\right)\cdot \Delta h_{GS}\right)/\left(0.65‰/\%\right)$$

and

$$\Delta h_{GS} = \left(\Delta\delta^{18}O_{Cell} - \left(\tau \cdot \Delta T_{sw}\right)\right)/\varsigma$$
$$or \hspace{4cm} (32)$$
$$\Delta h_{GS} = \left(\Delta\delta^{18}O_{Cell} - \left(0.65‰/\%\right)\cdot \Delta T_{sw}\right)/\left(-0.28‰/\%\right)$$

IV.3.3 Defining a Local $T - \delta^{18}O_{\mathrm{Pr}ec}$ Relation

The $T - \delta^{18}O_{\mathrm{Pr}ec}$ relation at Fort Smith, Alberta, Canada (60º00'20 N, 111º52'51 W; 203 masl) was estimated using $\delta^{18}O_{\mathrm{Pr}ec}$, $\delta^{18}H_{\mathrm{Pr}ec}$ and available mean monthly temperature from AD 1960 to 1969 (BIRKS et al., 2004) (Figure IV-4 and Figure IV-5). Fort Smith's proximity to Fort Chipewyan (~148 km) makes it a reasonable analogue to test the variation in the $T - \delta^{18}O_{\mathrm{Pr}ec}$ relation with varying pattern and strength of circulation.

$T - \delta^{18}O_{\mathrm{Pr}ec}$ relations of 0.30‰/K and 0.25‰/K were calculated for mean-annual and -winter (*p*December to April) temperature, respectively (Figure IV-4). The winter labelling season (demonstrated above to be the primary season of source-water labelling) is 0.40‰/K lower than the 0.65‰/K "Dansgaard" relation indicated above in equations 30 to 32. By analogy with the observations of Birks (2003), this may reflect the influence of varying circulation regime on temperature-dependent isotopic labelling of winter precipitation. It is thus hypothesized that the local $T - \delta^{18}O_{\mathrm{Pr}ec}$ relation incorporates shifts in circulation that damp the apparent temperature-dependent effects. Similar variations in the slope and intercept of $T - \delta^{18}O_{\mathrm{Pr}ec}$ have been documented at several stations in western Canada (e.g. at Gimli, Manitoba, Canada [50°37'59 N, 96°59'46 W; 223 masl]). Birks (2003) observed that a negative (annual average -0.48 of July 1978 to June 1979) PNA, associated with westerly (zonal) air mass circulation, produced $T - \delta^{18}O_{\mathrm{Pr}ec}$ slopes that were steeper and led to lower $\delta^{18}O_{\mathrm{Pr}ec}$ values for a given winter temperature. Conversely, a positive (annual

average +0.49 of April 1980 to March 1981) PNA, consistent with meridional air mass circulation, led to a shallower slope and relatively enriched precipitation for a given winter temperature. Circulation-dependent shifts in $\delta^{18}O_{\mathrm{Pr}ec}$ have also been inferred from ice-cores and lake sediment records from the 19th century in southwestern Yukon (FISHER et al., 2004). Although the data from Fort Smith are sparse, equivalent signals can be discerned in Figure IV-6. This can be accommodated in the ^{18}O-irsa model by introducing an offset in the intercept of the "Dansgaard" relation that varies with circulation regime (*cf.* Hammarlund et al., 2002; Edwards et al., 2008). Therefore, the observed local relation can be adjusted using ΔF as a circulation proxy;

$$T - \delta^{18}O_{\mathrm{Pr}ec} = 0.25\text{‰/K} = \tau \cdot \Delta T_{sw} + \Delta F = 0.65\text{‰/K} + \Delta F \qquad (33)$$

IV.3.3.1   Reconstructing Circulation Indices $\left(\Delta F\right)$

If the error (measured versus reconstructed) in the $\Delta\delta^{18}O_{Cell}$ anomaly reconstruction using ^{18}O-irsa is the result of neglecting the isotopic shifts in source-water due to changing circulation regime, ^{18}O-irsa (with ΔF) can then be used to calculate (50- and 100-years [based on h-reconstruction from PAD.CAR in Chapter III]) PAD circulation regime shifts, ΔF.

$$\Delta F = \Delta\delta^{18}O - \varsigma \cdot \Delta h_{GS} - \tau \cdot \Delta T_{sw}$$
$$or \qquad\qquad\qquad\qquad\qquad\qquad\qquad\qquad\qquad\qquad\qquad (34)$$
$$\Delta F = \Delta\delta^{18}O - \left(-0.28\text{‰/\%}\right)\cdot \Delta h_{GS} - \left(0.65\text{‰/\%}\right)\cdot \Delta T_{sw}$$

Using equation (33) and the demonstrated labelling season values for Δh_{GS}, ΔT_{WIN} and $\Delta\delta^{18}O_{Cell}$, a local ΔF time-series was calculated for the PAD and compared

against winter (pDecember to April) NAO, PNA, NAM and NP. Three of the four indices (NAO, NP and PNA) produced statistically significant reconstructions (r < 0.36) from AD 1955 to 2000 and 1900 to 2000 (Figure IV-7 and Table IV-3). The strongest long-term correspondence occurs between the smoothed NP and the reconstructions (r = 0.46, 0.50 and 0.45 for F .18 [unsmoothed], ΔF .18 [smoothed, to reflect the carry-over identified in Chapter III] and ΔF .18.13 [smoothed], respectively). The PNA was the best reconstruction of high-frequency variability, although it had the shortest comparison interval (r = -0.54, -0.58 and -0.50 for F .18, ΔF .18 and ΔF .18.13 respectively). Continued in-depth analysis used the longer NP and NAO records as proxies for ΔF .

IV.3.4 Application of the ^{18}O-irsa: The Introduction of a Circulation Index as a Proxy for Isotopic Shifts in Precipitation (ΔF)

Two modified ^{18}O-irsa reconstructions were developed by introducing scaled NAO and NP indices as a proxy for ΔF . Use of the NAO ΔF in the ^{18}O-irsa produced a better reconstruction of $\delta^{18}O_{Cell}$ (r = 0.60, AD 1957 to 2000) in terms of trend, variability and range than the original ^{18}O-irsa. However, the use of the NP ΔF slightly weakened the reconstruction from AD 1957 to 2000, but reproduced the overall range of values and trend reasonably well (r = 0.39, AD 1957 to 2000). All four ^{18}O-irsa (two with NAO and two with NP) inversions were greatly improved. The temperature reconstruction with NAO ΔF captured the variability and trend with improved accuracy (r = 0.17 to 0.46, AD 1900 to 2000). Notably, the NP ΔF temperature inversion captured the variability and high frequency statistical trend

remarkably well over the full 100 years (r = 0.56).

The NAO ΔF humidity inversion was improved; however it was not statistically significant and under-predicted much of the variability. The NP ΔF humidity inversion was only slightly less statistically significant than the original (r decrease of 0.04) but was more accurate in reconstructing range and trend.

The relative influence of NP and NAO ΔF seemed to vary over time as the NP ΔF with a five-year running mean captured most of the variability from ~AD 1900-2000 (r = -0.42), ~AD 1955-2000 (r = -0.32) and for ~AD 1900-1955 (r = -0.33), while the NAO ΔF with a five-year running mean captured the signals at the opposite intervals ~AD 1900-2000 (r = -0.09), for ~AD 1955-2000 (r = -0.58) and for ~AD 1900-1955 (r = 0.40). The NAM index also showed promise in reconstructing temperature (r = -0.26 [annual] and -0.40 [smoothed over 5-years]), however, the correlation is thought to reflect the teleconnection between the NAM and the NAO and thus was not investigated further.

IV.3.5 Gaussian Least Squares Model for Labelling $\Delta \delta^{18}O_{Cell}$

The Gaussian least squares model predicted the smallest range of variability in reconstructed $\Delta \delta^{18}O_{Cell}$ of all four modelling methods. This may reflect under-scaled coefficients; a statistical inability to separate the gradual enrichment in source-water isotopic composition. The majority of the labelling is imparted to winter temperature (0.18‰/K) and results in a coefficient similar to the one calculated for the $T - \delta^{18}O_{\Pr ec}$ relation. This model captures the variability in oxygen anomalies well and with consistency (r [annual] = 0.56 and unsmoothed 0.61). The temperature

inversion of the model over-predicted much of the variability and produces values which are unrealistic when compared to the measured values (r = 0.55). The humidity inversion was unrealistic due to over-prediction. Values of ~ ±60% for Δh are recorded at some times in the reconstruction. If it is assumed that the mean value for humidity is 50%, the model would produce values of -10 and 110% humidity which is obviously unrealistic.

IV.3.5.1   Univariate Statistical Model: Temperature and Humidity

Two univariate models were developed to model oxygen anomalies using ΔT_{sw} and Δh_{GS}. The ΔT_{sw}-based model (Figure IV-11) predicts a transfer function of 0.58‰/K which is similar to the default value of 0.65‰/K used by Edwards et al. (2008) for the $T - \delta^{18}O_{\Pr ec}$ relation. This model predicts the change in the $\Delta\delta^{18}O_{Cell}$ anomaly consistently and captures the trend. The temperature anomaly reconstruction captured the variability and predicts the gradual rise in winter temperature throughout the 20th century (r = 0.59).

The Δh_{GS}-based model (Figure IV-12) has a transfer function of -0.39‰/% which is lower than expected for the h-dependent transfer function used by Edwards et al. (2008). The model predicted the change in the trend of the $\Delta\delta^{18}O_{Cell}$ anomaly satisfactorily but did not match the variability at high frequency. The inversion of the model to reconstruct Δh_{GS} did not produce an accurate representation of the observed instrumental variability and under-predicted the long-term trend (r = 0.40).

IV.4 Discussion & Conclusion

IV.4.1 Temporal Isotopic Labelling of Stable-Oxygen in Tree-rings

Temperature and humidity seasonal isotopic labelling of $\Delta\delta^{18}O_{Cell}$ is predictable and consistent. The analysis indicates that there is a temporal offset between the primary labellers of oxygen isotopes. Our estimates place source-water precipitation as winter (*p*December to April), which precedes the growth season by four to six months. This winter signal was confirmed during the precipitation (used as a proxy for S_{ms}) analysis and indicates a two-year carry-over. The humidity labelling season was identified as the growth season (April to October) and showed no signs of carry-over, unlike $\Delta\delta^{13}C_{Cell}$.

IV.4.2 Models

^{18}O-irsa was shown to be a reliable predictor of $\delta^{18}O_{Cell}$ anomalies in tree-rings in the PAD when shifts in circulation regime were incorporated into the model. The selection of circulation regimes was found to be an important factor, as regimes that strongly correlate to local precipitation patterns at Fort Smith (our analogue for the PAD) were found to yield the best results. However, the location of measurement for the indices may not be optimal for measuring the atmospheric forcing placed on the system in this particular environment. The trees have also been found to be natural smoothers and thus, would not reconstruct annually resolved indices. With respect to the PAD the circulation strength and its interaction with the Canadian Cordillera are a

key concern as rapid change in elevation of air masses results in enhanced precipitation from adiabatic cloud formation. And, since most of the circulation regimes have been statistically detrended, the annual variability and not the long-term trend being reconstructed may be the only way to compare the $\delta^{18}O_{Cell}$-based reconstructions. The relationship between $\delta^{18}O_{Cell}$ and circulation regime cannot be well-defined without further investigation at various locations so that the degree of enrichment can be understood.

It is suggested that the modified ^{13}C-irsa and the ^{18}O-irsa with ΔF as defined in Chapters III and IV be coupled in Chapter V to extract the h and T signals.
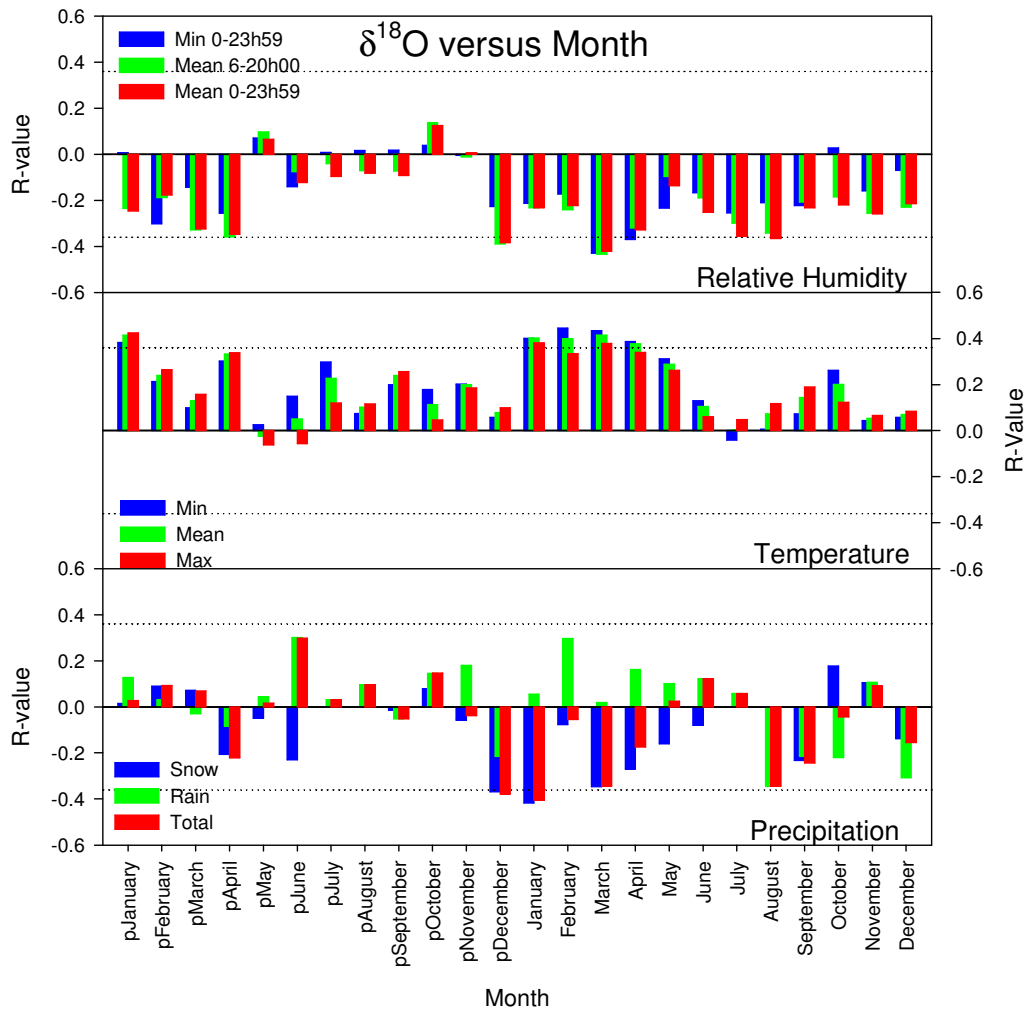
Figure IV-1. PAD.OXY versus relative humidity (Top) (minimum 0h00-23h59, mean 0-23h59 and mean 6h00-20h00), temperature (Middle) (minimum, maximum and mean) and precipitation (bottom) (rain, snow and total [rain & snow]). R = ± 0.36 (P < 0.01) are displayed using the grey dotted line.
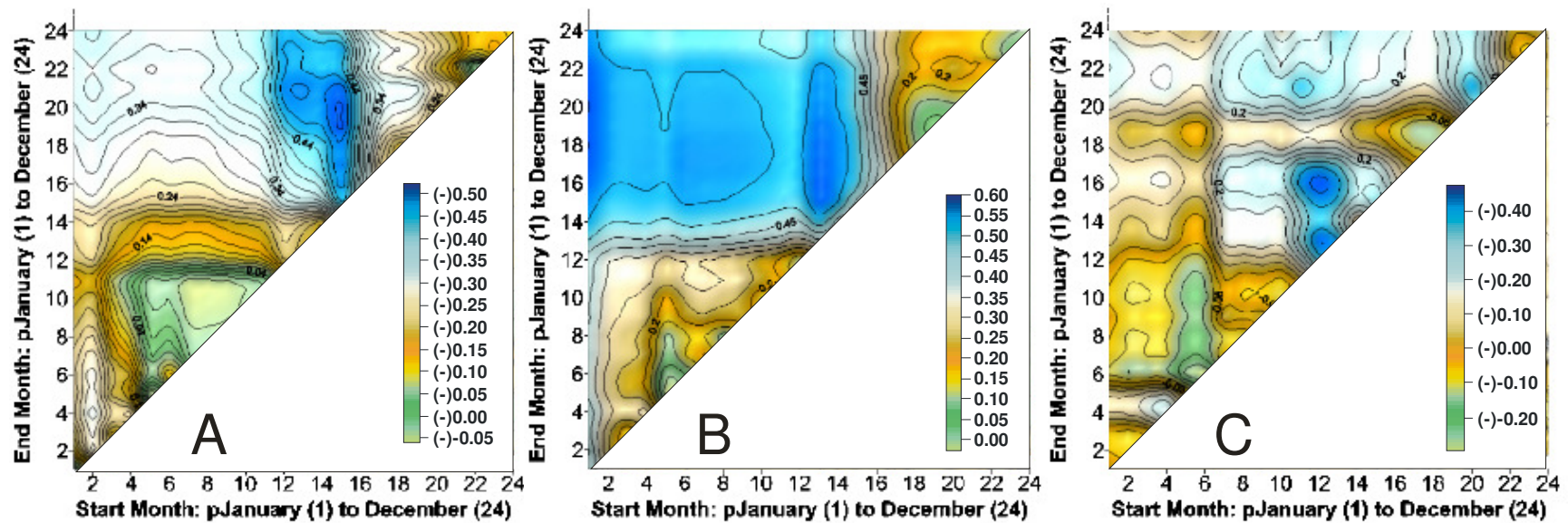
Figure IV-2. PAD_{.OXY} versus (*A*) relative humidity, (*B*) mean temperature, minimum 0h00-23h59 and (*C*) precipitation total (rain and snow). The X-axis represents the starting month in the comparison while the Y-axis represents the ending month, with the months starting at the previous (p) January and advancing to the December of the growth year. The relative humidity and precipitation values have been inverted to give positive r-values for comparative purposes. r = ± 0.36 (P < 0.01) are deemed statistically significant.
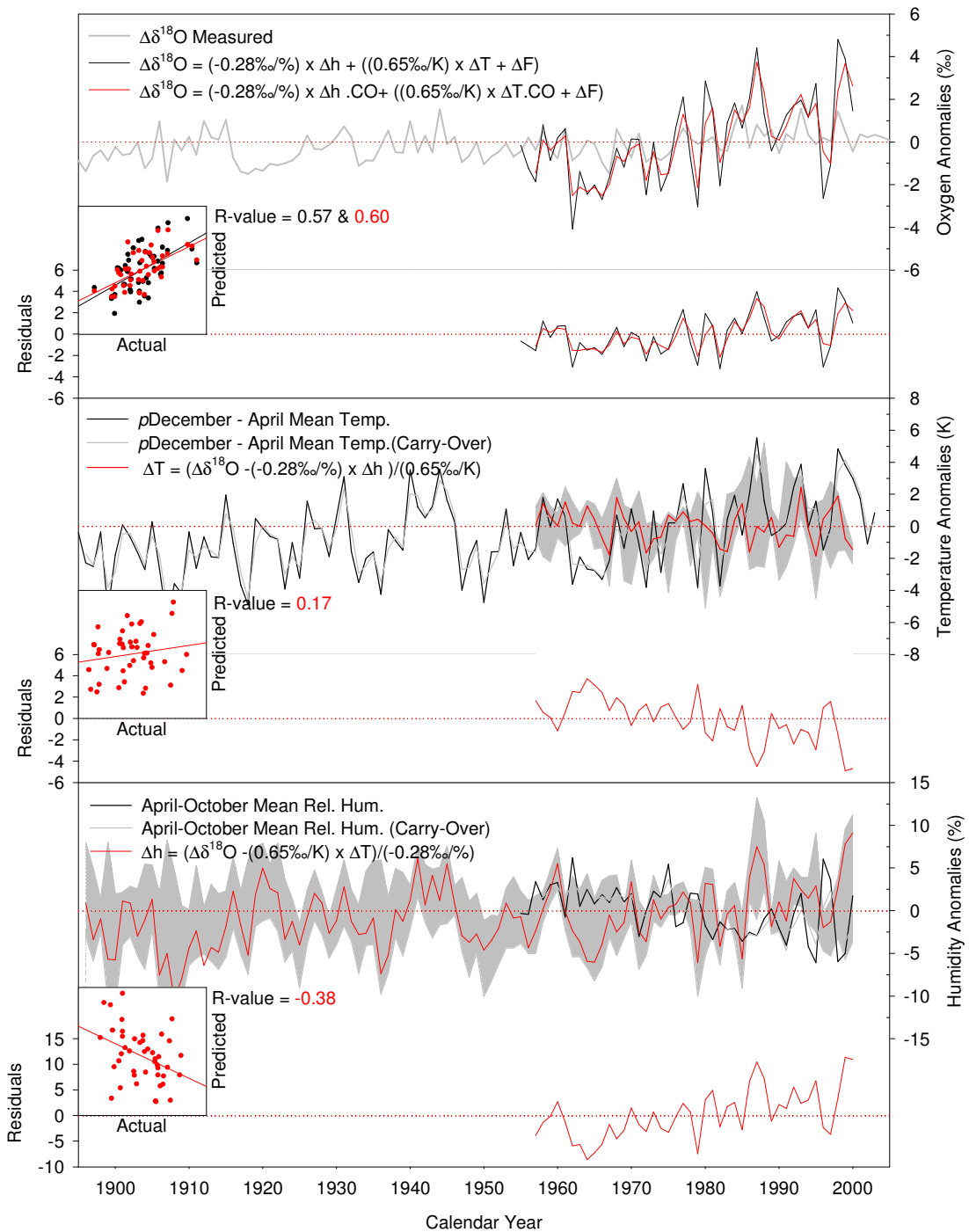
Figure IV-3. Modelling and reconstruction results from the original ^{18}O-irsa with the introduction of $\Delta\delta^{18}O_{Cell}$ (‰), ΔT_{sw} (pDecember to April) and Δh_{GS} (April to October) data. (*Top*) Modelling unsmoothed (black) and smoothed (red) carry-over $\Delta\delta^{18}O_{Cell}$ (‰). (*Middle*) Reconstructions of carry-over ΔT_{sw}. (*Bottom*) Reconstructions of carry-over Δh_{GS}.
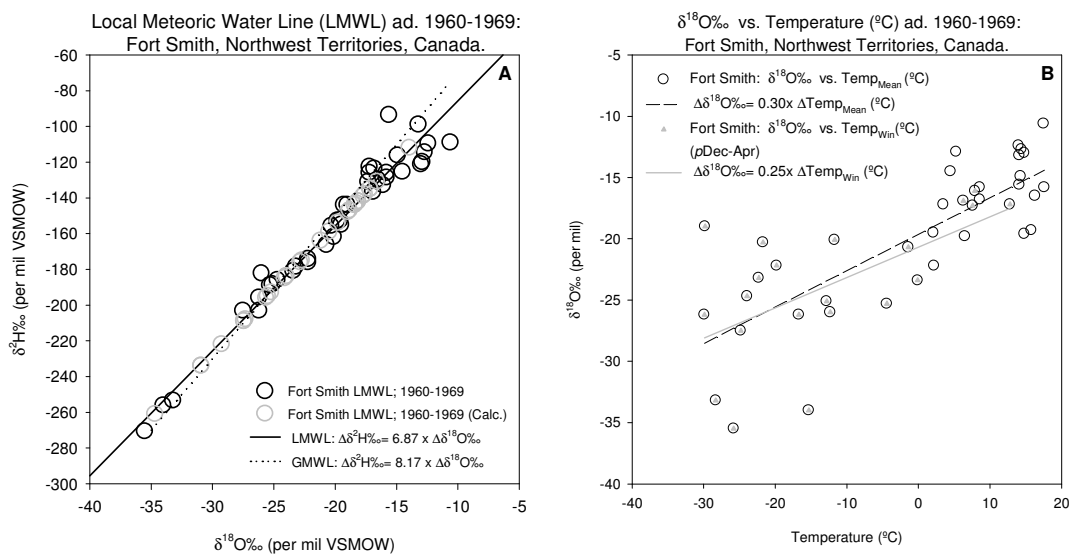
Figure IV-4. Examination of relationships between water isotopes (hydrogen and oxygen) and temperature (mean annual and winter [*p*December to April]) at Fort Smith, Alberta, Canada. (*A*) Examination of local meteoric water line and its relation to the global meteoric water line. (*B*) Examination of oxygen isotope and temperature (mean annual and winter).
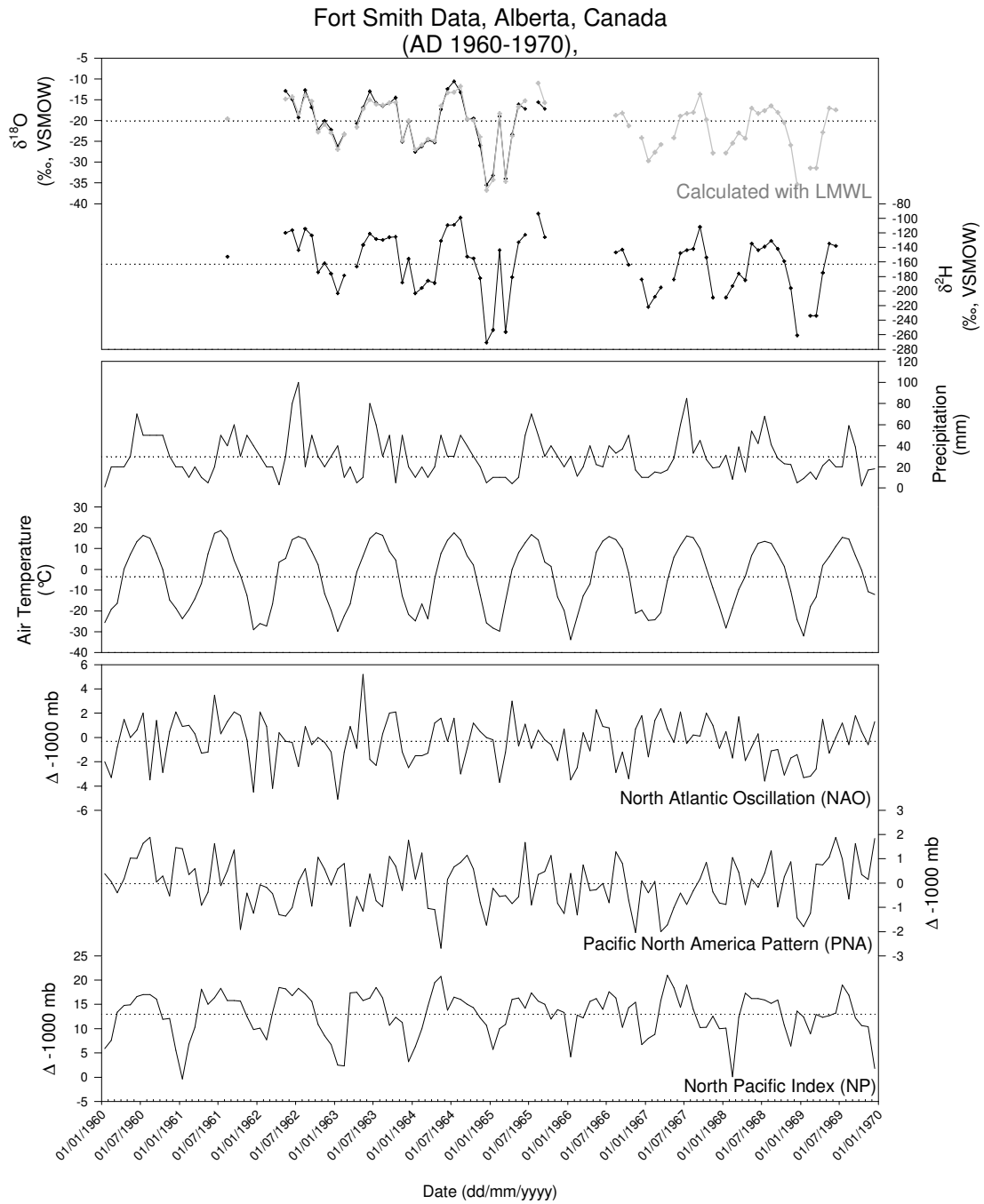
Figure IV-5. Diagram illustrating the variability and seasonality in (*A*) water isotopes (hydrogen and oxygen), (*B*) instrumental temperature and precipitation amount and (*C*) circulation indices (PNA, NAO, NP) at Fort Smith, Alberta, Canada.
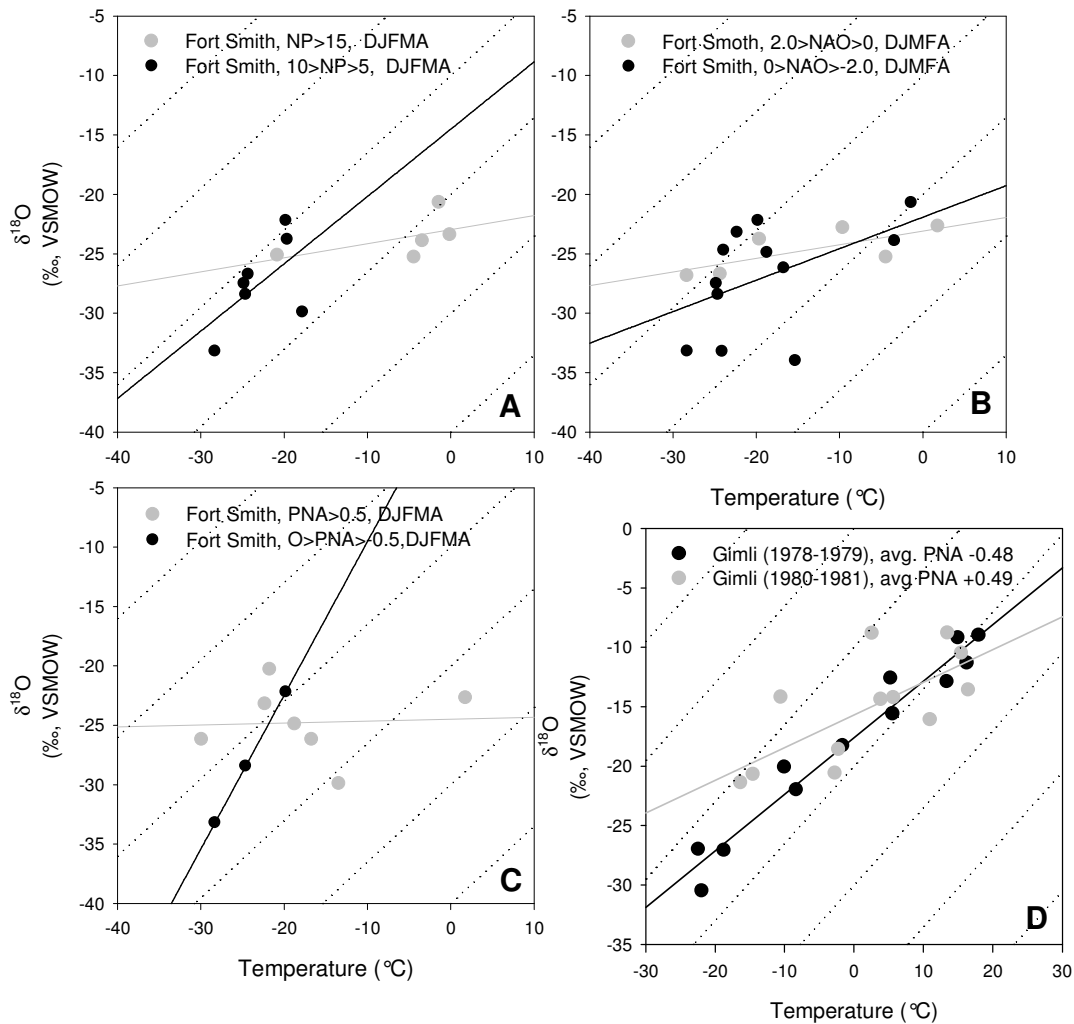
Figure IV-6. (A [NP], B [NAO], C [PNA]) Comparison of winter (*p*December [D] to April [A]) temperature and $\delta^{18}O_{\mathrm{Pr}\,ec}$ at Fort Smith, Alberta, Canada and annual (Δ PNA = -0.48 [July 1978 to June 1979] and = +0.49 [April 1980 to March 1981]) at Gimli, Manitoba, Canada (Figure D courtesy of Birk, 2004, Excerpt of Figure 3.15). Dotted lines represent the default "Dansgaard" relation (1964) with a varying intercept of *n* x 10 ‰; where *n* is a whole number.

116
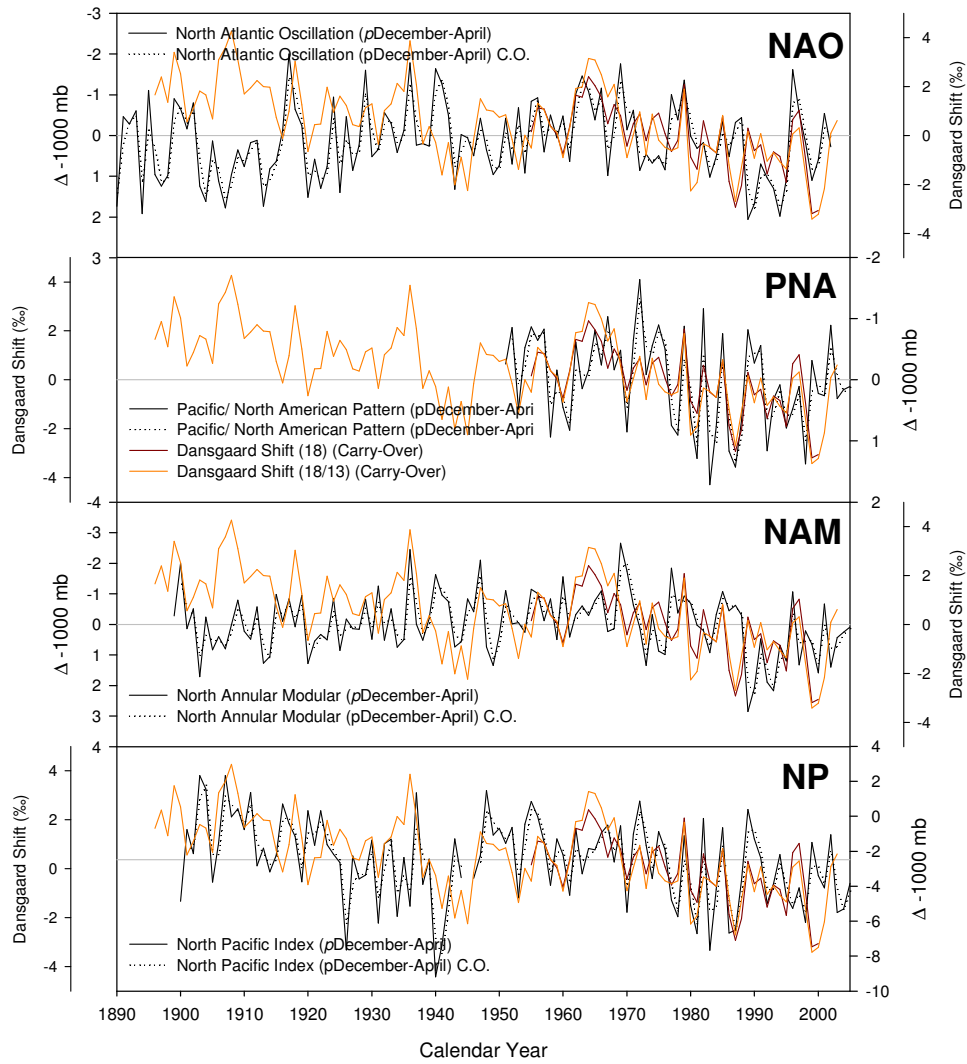
Figure IV-7. Reconstruction of the circulation proxy, ΔF, using instrument ΔT_{sw} (*p*December to April) and Δh_{GS} (April to October) and ^{18}O-irsa. C.O. indicates a two year carry-over as defined for the carbon tree-ring chronology in Chapter III.

117
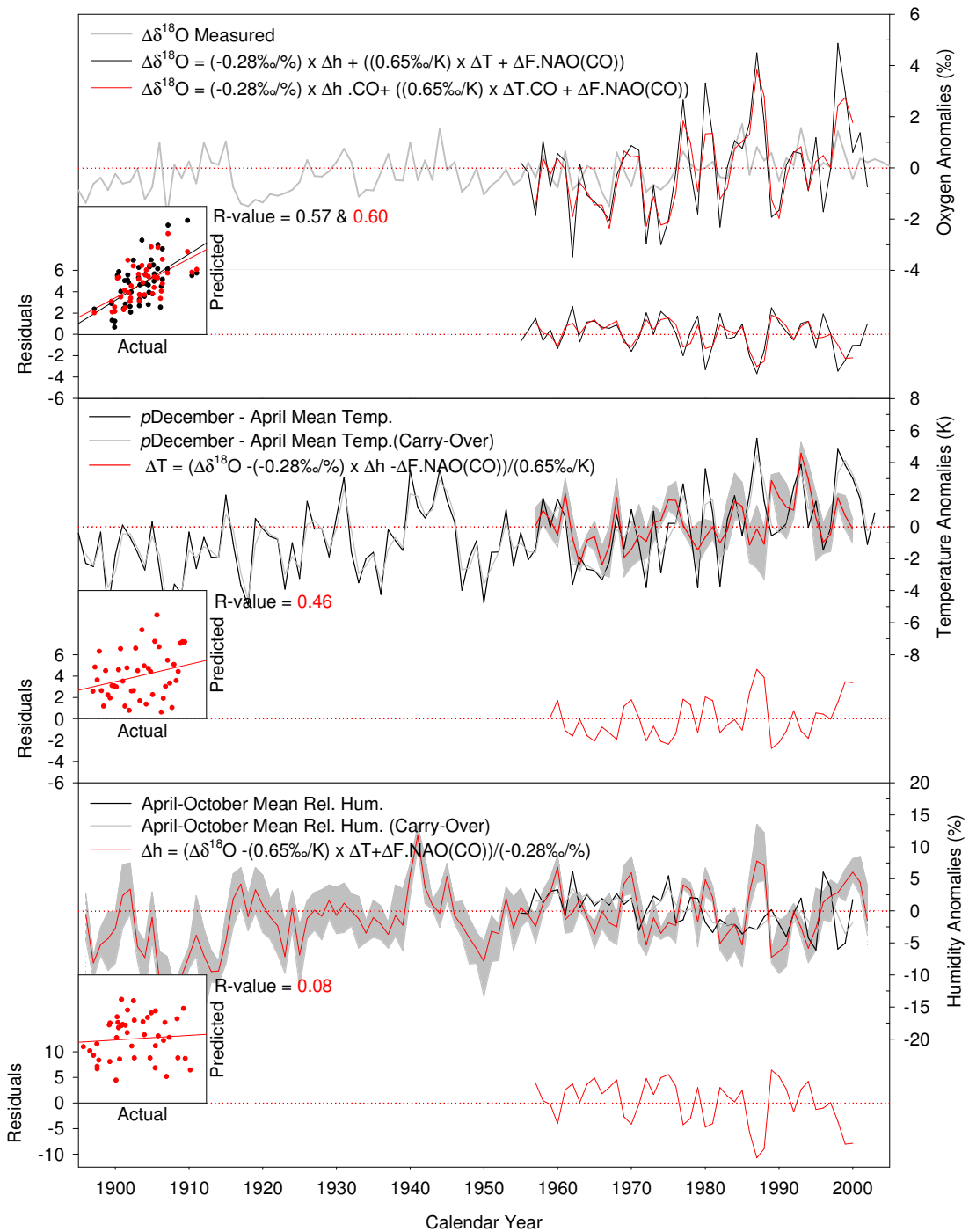
Figure IV-8. Modelling and reconstruction results from the original ^{18}O-irsa and NAO index with the introduction of $\Delta\delta^{18}O_{Cell}$ (‰), ΔT_{sw} (pDecember to April) and Δh_{GS} (April to October) data. (*Top*) Modelling unsmoothed (black) and smoothed (red) carry-over $\Delta\delta^{18}O_{Cell}$ (‰). (*Middle*) Reconstructions of carry-over ΔT_{sw}. (*Bottom*) Reconstructions of carry-over Δh_{GS}.
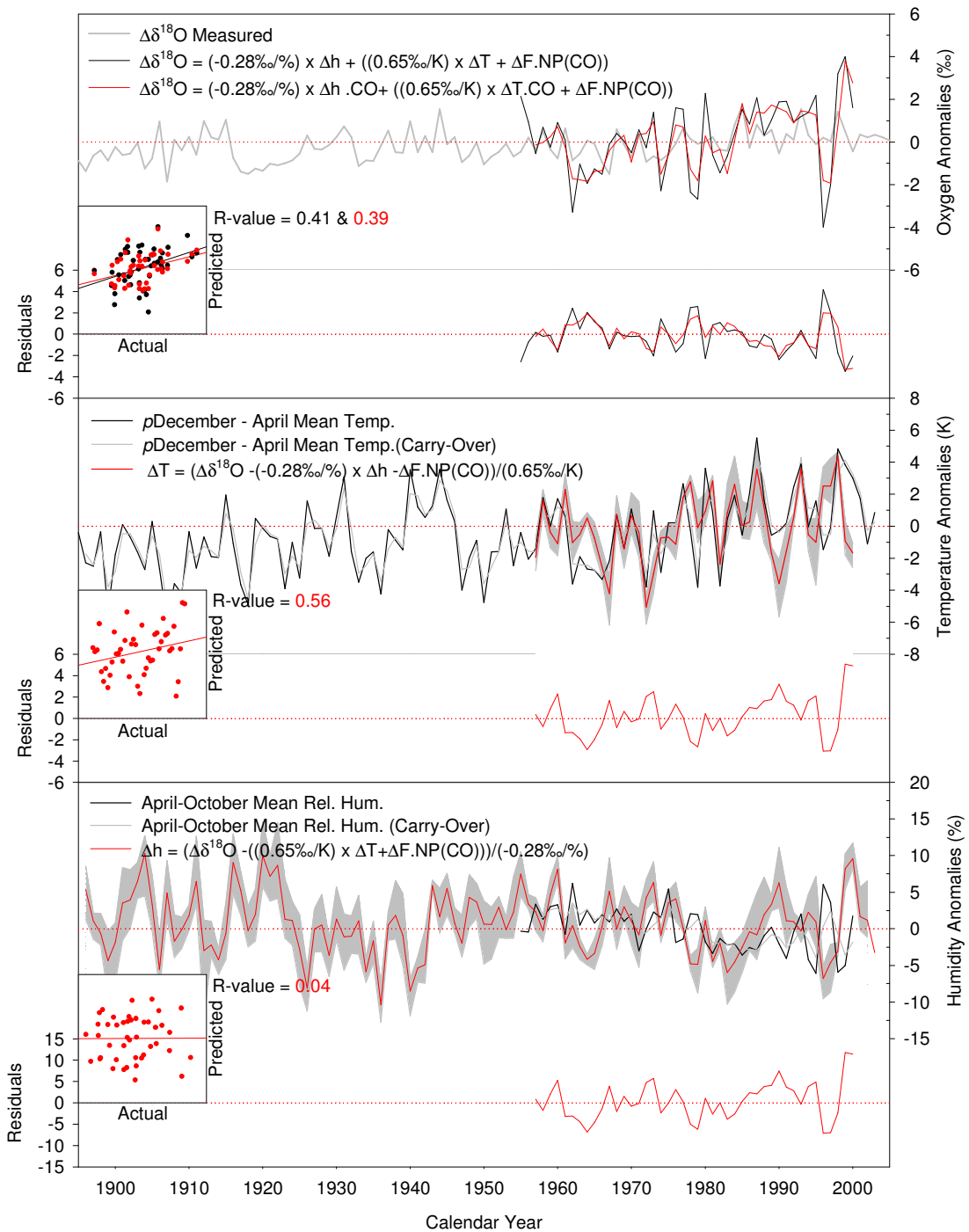
Figure IV-9. Modelling and reconstruction results from the original ^{18}O-irsa and NP index with the introduction of $\Delta\delta^{18}O_{Cell}$ (‰), ΔT_{sw} (pDecember to April) and Δh_{GS} (April to October) data. (*Top*) Modelling unsmoothed (black) and smoothed (red) carry-over $\Delta\delta^{18}O_{Cell}$ (‰). (*Middle*) Reconstructions of carry-over ΔT_{sw}. (*Bottom*) Reconstructions of carry-over Δh_{GS}.

119
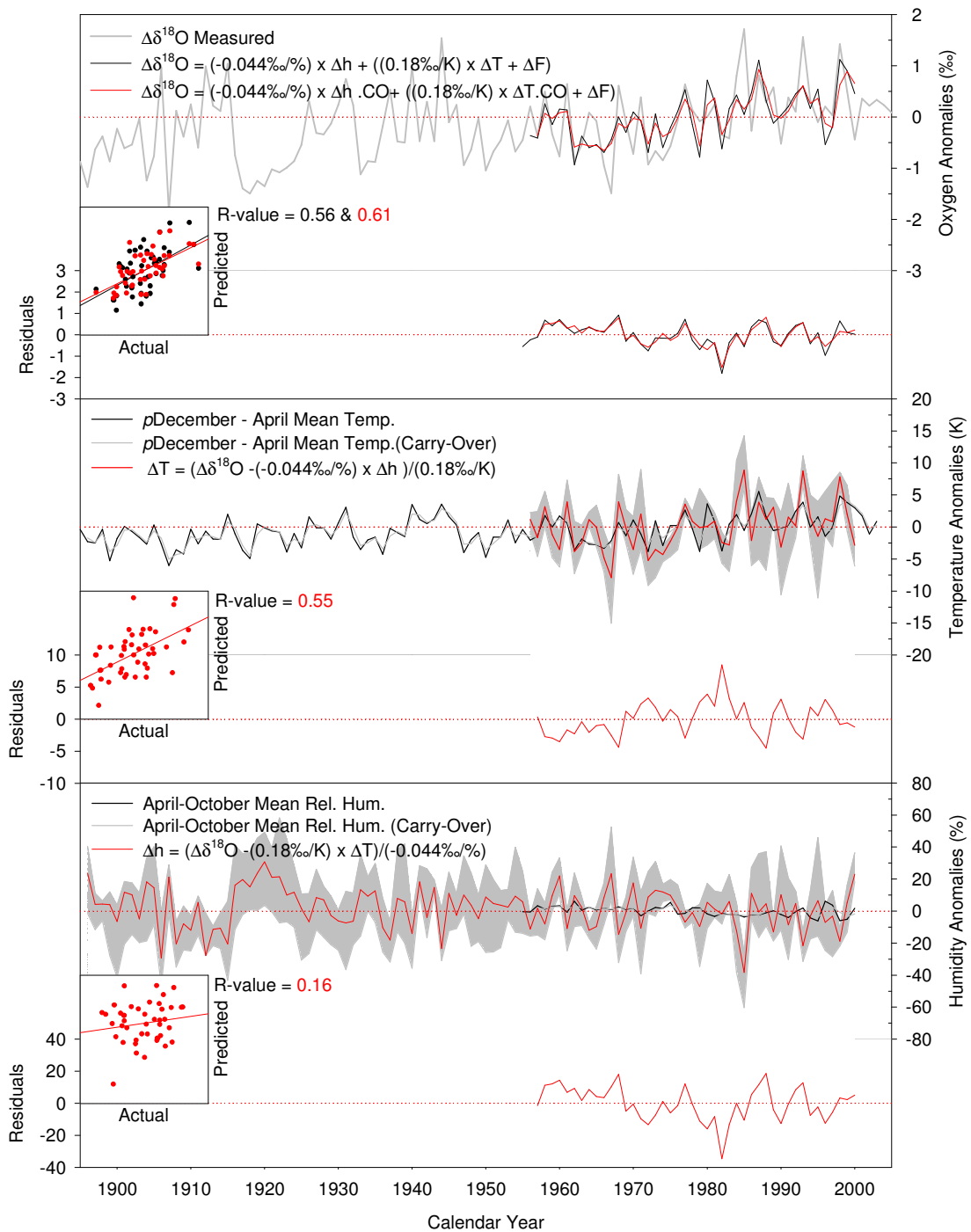
Figure IV-10. Modelling and reconstruction results from a bivariate Gaussian Least Squares Model with the introduction of $\Delta\delta^{18}O_{Cell}$ **(‰),** ΔT_{sw} **(pDecember to April) and** Δh_{GS} **(April to October) data. (*Top*) Modelling unsmoothed (black) and smoothed (red) carry-over** $\Delta\delta^{18}O_{Cell}$ **(‰). (*Middle*) Reconstructions of carry-over** ΔT_{sw}. **(*Bottom*) Reconstructions of carry-over** Δh_{GS}.
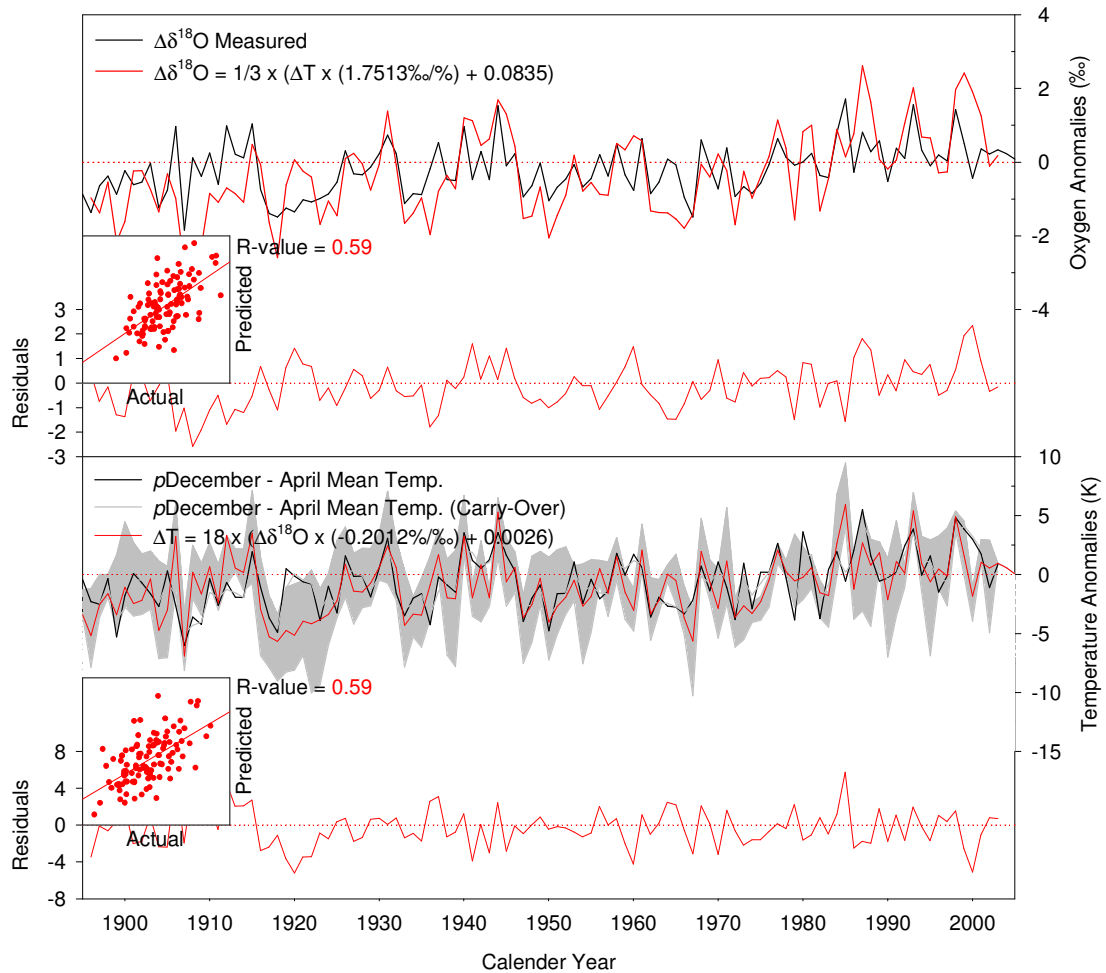
Figure IV-11. Modelling and reconstruction results from a univariate model with the introduction of $\Delta\delta^{18}O_{Cell}$ (‰), ΔT_{sw} (*p*December to April) data. (*Top*) Modelling unsmoothed (black) and smoothed (red) carry-over $\Delta\delta^{18}O_{Cell}$ (‰). (*Bottom*) Reconstructions of carry-over ΔT_{sw}.
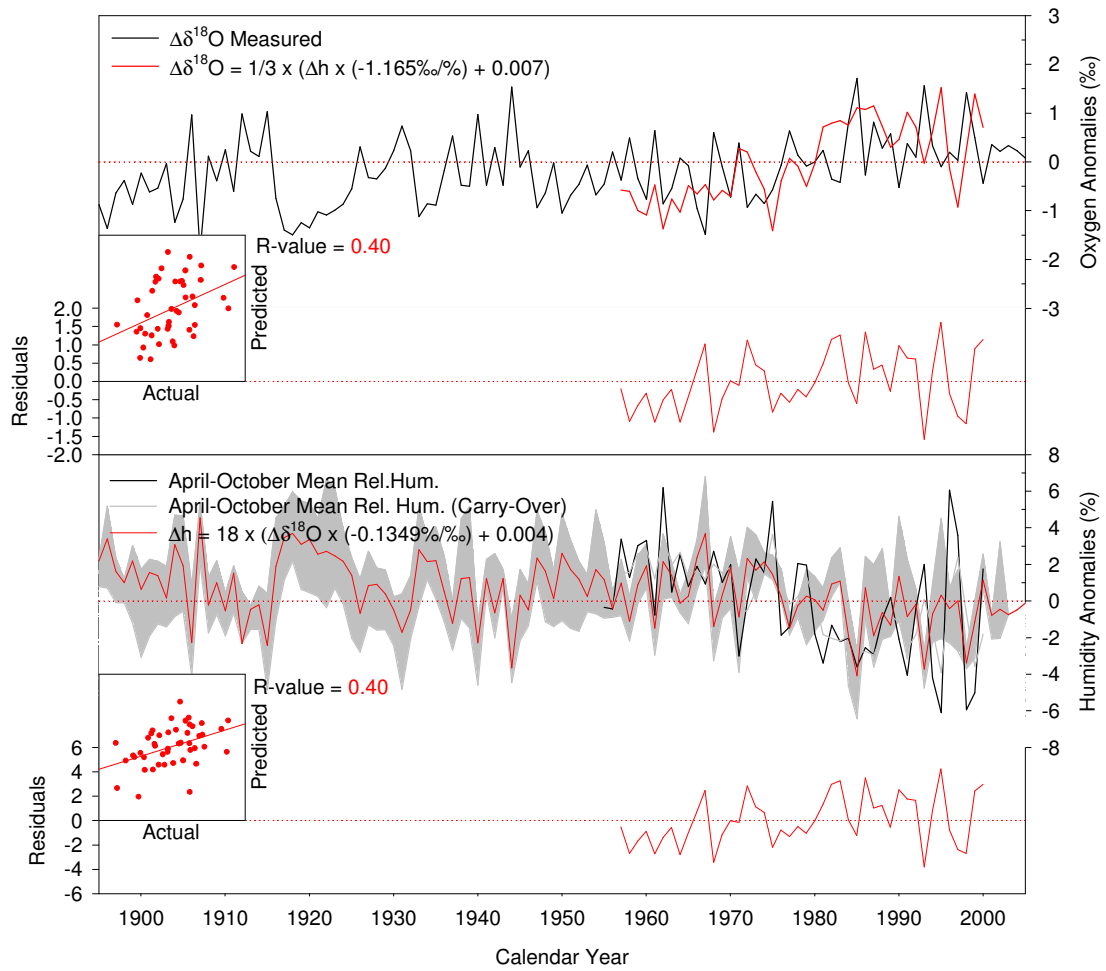
Figure IV-12. Modelling and reconstruction results from a univariate model with the introduction of $\Delta\delta^{18}O_{Cell}$ (‰), Δh_{GS} (April to October) data. (*Top*) Modelling unsmoothed (black) and smoothed (red) carry-over $\Delta\delta^{18}O_{Cell}$ (‰). (*Bottom*) Reconstructions of carry-over Δh_{GS}.

Table IV-1. PAD OXY Carry-Over (a); Carry-Over; PAD$_{OXY}$ vs temperature and relative humidity [25] weighted from one to three years. All values are expressed as r-values, with values being significant at P < 0.01 and P < 0.05 when r reaches or exceeds ±0.36 and ±0.28 respectively.

R-value Weighting			Oxygen Isotope Carry-Over: (AD) 1955-2000											
			Relative Humidity (%)						Temperature (K)					
Y_X	Y_{X-1}	Y_{X-2}	PRC	QFR	QFU	GSL	BITC	PAD	PRC	QFR	QFU	GSL	BITC	PAD
1	0	0	-0.13	-0.23	-0.46	-0.32	-0.24	-0.35	0.19	0.49	0.59	0.56	0.52	0.59
0.9	0.1	0	-0.11	-0.22	-0.47	-0.31	-0.23	-0.35	0.22	0.5	0.6	0.58	0.53	0.61
0.8	0.2	0	-0.1	-0.21	-0.47	-0.3	-0.22	-0.33	0.25	0.51	0.61	0.61	0.54	0.63
0.8	0.15	0.05	-0.1	-0.21	-0.47	-0.31	-0.22	-0.33	0.24	0.49	0.61	0.61	0.53	0.62
0.8	0.1	0.1	-0.1	-0.21	-0.46	-0.31	-0.21	-0.33	0.22	0.47	0.61	0.6	0.52	0.61
0.7	0.3	0	-0.08	-0.19	-0.46	-0.28	-0.21	-0.31	0.28	0.52	0.61	0.63	0.54	0.64
0.7	0.25	0.05	-0.08	-0.19	-0.46	-0.29	-0.21	-0.31	0.27	0.5	0.62	0.63	0.53	0.64
0.7	0.2	0.1	-0.08	-0.2	-0.46	-0.3	-0.2	-0.31	0.25	0.48	0.62	0.63	0.53	0.62
0.7	0.15	0.15	-0.08	-0.19	-0.45	-0.3	-0.19	-0.31	0.24	0.45	0.61	0.62	0.52	0.61
0.6	0.4	0	-0.05	-0.17	-0.44	-0.26	-0.19	-0.28	0.3	0.51	0.6	0.64	0.52	0.64
0.6	0.35	0.05	-0.05	-0.17	-0.45	-0.27	-0.19	-0.28	0.29	0.49	0.61	0.64	0.52	0.64
0.6	0.3	0.1	-0.05	-0.17	-0.45	-0.27	-0.18	-0.29	0.28	0.47	0.61	0.64	0.52	0.63
0.6	0.25	0.15	-0.05	-0.17	-0.44	-0.28	-0.17	-0.28	0.27	0.45	0.61	0.64	0.51	0.62
0.6	0.2	0.2	-0.05	-0.17	-0.44	-0.28	-0.17	-0.28	0.25	0.42	0.61	0.64	0.5	0.6
0.5	0.5	0	-0.03	-0.14	-0.42	-0.23	-0.17	-0.25	0.32	0.49	0.57	0.63	0.5	0.62
0.5	0.45	0.05	-0.03	-0.14	-0.42	-0.24	-0.16	-0.25	0.32	0.47	0.58	0.64	0.5	0.62
0.5	0.4	0.1	-0.03	-0.14	-0.42	-0.24	-0.16	-0.25	0.31	0.45	0.59	0.65	0.49	0.62
0.5	0.35	0.15	-0.03	-0.15	-0.42	-0.25	-0.15	-0.25	0.29	0.43	0.59	0.65	0.49	0.61
0.5	0.3	0.2	-0.03	-0.15	-0.42	-0.26	-0.15	-0.25	0.28	0.4	0.59	0.65	0.48	0.59
0.5	0.25	0.25	-0.03	-0.15	-0.42	-0.26	-0.14	-0.25	0.26	0.37	0.59	0.64	0.47	0.57
0.4	0.4	0.2	0	-0.12	-0.39	-0.22	-0.12	-0.21	0.3	0.37	0.55	0.64	0.44	0.57
0.4	0.35	0.25	0	-0.12	-0.39	-0.23	-0.11	-0.21	0.28	0.34	0.55	0.63	0.43	0.55
0.4	0.3	0.3	0	-0.12	-0.39	-0.23	-0.11	-0.21	0.27	0.3	0.55	0.63	0.42	0.53
0.35	0.35	0.3	0.02	-0.1	-0.37	-0.21	-0.09	-0.19	0.27	0.28	0.52	0.62	0.4	0.51
0.33	0.33	0.33	0.02	-0.1	-0.36	-0.21	-0.08	-0.18	0.26	0.25	0.51	0.6	0.38	0.49

Table IV-2. Autocorrelation of PAD$_{OXY}$, temperature and relative humidity over six years. All values are expressed as r-values, with values being significant at P < 0.01 and P < 0.05 when r reaches or exceeds ±0.36 and ±0.28 respectively.

			Oxygen Auto-Correlation; R-values						
No.: Years lag	**Δ.T (K)**	**ΔRH (%)**	Oxygen					
	Apr.-Oct.	**Apr.-Oct.**	**PRC**	**QFR**	**QFU**	**GSL**	**BITC**	**PAD**
Y$_{X-1}$	0.24	0.29	0.05	0	0.29	0.35	0.01	0.13
Y$_{X-2}$	0	0.35	0.04	-0.01	0.3	0.32	-0.25	0.06
Yx-3	0.18	0.22	0.03	-0.18	0.31	0.47	0.11	0.17
Yx-4	0.12	0.27	0.01	-0.14	0.34	0.28	-0.1	0.2
Yx-5	0	0.27	0.12	-0.04	0.34	0.33	-0.07	0.18

Table IV-3. Pearson Product Mean Correlation Coefficients of proxy ΔF versus various measured and reconstructed circulation indices; NAO (North Atlantic Oscillation), NP (North Pacific), NAM (Northern Annular Mode) and PNA (Pacific-North America pattern).

R-value		$\Delta F(18)_A(1955\text{-}2000)$	$\Delta F\,18_A(1975\text{-}2000)$	$\Delta F(18)_A(1955\text{-}1974)$	$\Delta F_A(13/18)_A(1897\text{-}2000)$	$\Delta F_A(13/18)_A(1950\text{-}2000)$	$\Delta F_A(13/18)_A(1975\text{-}2000)$	$\Delta F_A(13/18)_A(1950\text{-}1974)$	$\Delta F_A(13/18)_A(1925\text{-}1949)$	$\Delta F_A(13/18)_A(1900\text{-}1924)$
NAO.DJFMA (Hurrell et al., 1995)	Original	-0.46	-0.31	-0.39	-0.11	-0.39	-0.28	-0.26	-0.16	0.17
	2-Year CO (0.70-0.30)	-0.51	-0.32	-0.45	-0.13	-0.44	-0.25	-0.36	-0.17	0.15
	5-Year (RM)	-0.5	-0.18	-0.52	-0.04	-0.46	-0.01	-0.5	0.02	0.31
NAO (Glueck and Stockton 2001)	Original	-0.25	0.1	-0.31	-0.03	-0.33	0.05	-0.38	0.2	-0.09
	2-Year CO (0.70-0.30)	-0.27	0.09	-0.33	-0.05	-0.35	0.02	-0.4	0.11	-0.05
	5-Year (RM)	-0.45	-0.43	-0.31	-0.07	-0.52	-0.51	-0.44	0.14	-0.12
NP.DJFMA (Trenberth and Hurrell 1994)	Original	0.49	0.4	0.2	0.39	0.46	0.36	0.2	0.22	0.08
	2-Year CO (0.70-0.30)	0.5	0.36	0.1	0.47	0.48	0.33	0.15	0.27	0.29
	5-Year (RM)	0.38	-0.22	0.04	0.49	0.41	-0.19	-0.11	0.49	0.43
TR-NP (D'Arrigo.et.al 2005)	Original	0.31	0.22	0.03	0.22	0.29	-0.04	0.05	0.08	0.15
	2-Year CO (0.70-0.30)	0.3	0.17	-0.05	0.26	0.32	-0.01	0.06	0.17	0.18
	5-Year (RM)	0.44	0.32	0.23	0.29	0.43	0.22	0.17	0.41	0.16
NAM.DJFM. (Hurrell et al., 1995b)	Original	-0.28	-0.1	0.03	-0.14	-0.27	-0.1	-0.01	-0.07	-0.07
	2-Year CO (0.70-0.30)	-0.3	-0.11	0.07	-0.14	-0.28	-0.09	0.02	-0.07	0.03
	5-Year (RM)	-0.47	-0.24	-0.13	-0.18	-0.41	-0.14	-0.16	0.44	0.11
PNA.DJFM (Hurrell et al., 1995)	Original	-0.57	-0.53	-0.35	-0.5	-0.51	-0.45	-0.33	N/A	N/A
	2-Year CO (0.70-0.30)	-0.59	-0.52	-0.3	-0.52	-0.52	-0.42	-0.28	N/A	N/A
	5-Year (RM)	-0.39	0.08	-0.12	-0.36	-0.38	0.16	-0.03	N/A	N/A

V   The Coupled-Isotope Response Surfaces

Synopsis

Chapter V examines the two temperature labelling seasons denoted in Chapter III and IV. Although the two labelling seasons are distinct and offset, the dominant signal is the winter labelling season of pDecember to April. By applying an external circulation regime the coupling of the response surfaces was used to generate a 280-year record of April to October relative humidity, temperature and source-water $\delta^{18}O$ anomalies.

V.1 Introduction

The isotopic labelling seasons for $\delta^{13}C_{Cell}$ and $\delta^{18}O_{Cell}$ were defined in Chapters III and IV, respectively. By applying the identified labelling seasons (h_{GS}, T_{GS} and T_{SW}) to ^{13}C-irsa and ^{18}O-irsa it allowed for the testing and modification of the mechanistic relations for *P. glauca* in each model. The subscripts 13 and 18 have been added to the $\delta^{13}C_{Cell}$ and $\delta^{18}O_{Cell}$ coefficients, respectively, to identify them when the models are coupled in equations 28 to 29.

$$\Delta\delta^{13}C_{Cell} = \varsigma_{13} \cdot \Delta h_{GS} + \tau_{13} \cdot \Delta T_{GS}$$
$$and \qquad\qquad\qquad\qquad\qquad\qquad (28) \text{ and } (29)$$
$$\Delta\delta^{18}O_{Cell} = \varsigma_{18} \cdot \Delta h_{GS} + \left(\tau_{18} \cdot \Delta T_{SW} + \Delta F\right)$$

with appropriate substitutions,

$$\Delta\delta^{13}C_{Cell} = \left(-0.23‰/\%\right)\cdot \Delta h_{GS} + \tau_{13} \cdot \left(-0.21‰/K\right)$$
$$and \qquad\qquad\qquad\qquad\qquad\qquad (28) \text{ and } (29)$$
$$\Delta\delta^{18}O_{Cell} = \left(-0.28‰/\%\right)\cdot \Delta h_{GS} + \left(\left(0.65‰/K\right)\cdot \Delta T_{SW} + \Delta F\right)$$

The models were tested to determine whether coupling of the models could generate practical reconstructions of paleotemperature (equation 35) and relative paleohumidity (equation 36) in the PAD. The NP ΔF proxy data used in the final reconstructions is scaled from Trenberth and Hurrell (1994) (AD 1900-2007) and D'Arrigo et al. (2005)(AD 1719-1899).

$$\Delta T_{SW/GS} = \frac{\Delta\delta^{13}C_{Cell} \cdot \varsigma_{18} - \Delta\delta^{18}O_{Cell} \cdot \varsigma_{13} + \varsigma_{13} \cdot \Delta F}{\varsigma_{18} \cdot \tau_{13} - \varsigma_{13} \cdot \tau_{18}} \qquad (35)$$

and

$$\Delta h_{GS} = \frac{\Delta \delta^{13} C_{Cell} \cdot \tau_{18} - \Delta \delta^{18} O_{Cell} \cdot \tau_{13} + \tau_{13} \cdot \Delta F}{\varsigma_{13} \cdot \tau_{18} - \varsigma_{18} \cdot \tau_{13}} \qquad (36)$$

128

V.2   Temperature Data

One concern in coupling the isotope response surfaces (C-irsa) is the validity of the
resulting temperature reconstruction. In Chapter III a summer (April to September)
labelling season was identified for temperature, while in Chapter IV a winter
(*p*December to April) source-water labelling season was identified. If the two
temperature signals are not identical matches, is it still valid to couple the response
surfaces to reconstruct paleotemperature and relative paleohumidity? If the
paleotemperature is not valid when coupled, will that affect the accuracy of the
relative paleohumidity reconstruction? These questions will be addressed below;
however, first the similarities and differences in the winter and summer temperature
records need to be characterized and identified.

The winter and growth season temperature records are not identical over the
calibration period of AD 1955 to 2000. There are significant differences between the
ranges of the two datasets which is likely due to seasonality. Both labelling seasons
show some similarities due to common drivers (r = 0.64, P < 0.01, AD 1895-2003
and 0.63, P < 0.01, AD 1955 to 2000), Figure V-1. Both datasets show increasing
temperatures over the 20th century. Winter temperatures have risen by 3.0 K while
growth season temperatures have risen by 1.5 K. Over the 45-year (~AD 1955-2000)
calibration period a similar trend in rising temperature is observed, however, the
change is occurring more rapidly with winter temperature rising by 3.6 K and
summer by 1.2 K.

If the reconstructions were expressed as z-score it may slightly alleviate uncertainty

in assuming that the $\delta^{13}C_{Cell}$ and $\delta^{18}O_{Cell}$ temperature labelling seasons are close enough to be coupled. By doing this the temperature season only needs to vary in the same direction and maintain a constant magnitude differences, which we know is not the case for the PAD. If this was true, the decadal scale z-score method used by Edwards et al. (2008) to reconstruct temperatures in the Canadian Cordillera could be applied here. For the purpose of the following analysis, winter and growth season temperatures were assumed to vary in parallel although this is beyond the scope of the current study.

V.3   Results and Discussion

Final Reconstructions

The C-irsa h- and T-reconstructions were developed using composite chronologies for $\delta^{13}C_{Cell}$ and $\delta^{18}O_{Cell}$. The isotopic shifts in circulation regime, ΔF, were assumed to be zero (NC, Figure V-2) or estimated using instrumental index data from AD 1900 to 2007 (HURRELL, 1995b) and tree-ring width-based proxy reconstructions from AD 1719 to 1899 (HURRELL, 1995a) for the NAO (Figure V-3). For NP, instrumental index data was used to estimate ΔF shifts for AD 1900-2007 (TRENBERTH and HURRELL, 1994) and tree-ring width-based proxy for AD 1719-1899 (D'ARRIGO et al., 2005) (Figure V-4). The proxy-based indices used to estimate ΔF for NAO and NP were adjusted to fit the instrumental index data over overlapping intervals, range and average value. When appropriately fitted, the index proxies were smoothed to 70% (current year) - 30% (previous year) to reflect source-water carry-over identified in section IV.3.1.4 on page 102.

There are similarities between the $T_{SW/GS}$ and h_{GS}. The C-irsa NC ΔF reconstructions (Figure V-2) was a statistically reasonable h_{GS}-reconstruction, but the $T_{SW/GS}$ reconstruction was not a good predictor of the instrumental data trend or variability. The C-irsa NAO ΔF reconstructions predicts the last 75 years (AD 1925-2000) of the instrumental record trend and variability for both $T_{SW/GS}$ and h_{GS} with remarkable accuracy. However, the C-irsa NP ΔF reconstruction (Figure V-4) is clearly superior for the full 100-year instrumental period, thus supporting the use of the D'Arrigo et al. (2005) NP reconstruction as a basis for interpreting the longer-

term isotope records. Statistics for the reconstructions and instrumental data are presented in Table V-1 and Table V-2.

V.3.1 The Temperature Reconstruction (NP)

The 280-year trend indicates that temperatures have decreased by 0.0021 K/year since AD 1750, Figure V-4, the range of winter temperatures during the modern period is consistent with the Little Ice Age[9]. Instrumental and reconstructed temperatures have been increasing rapidly over the last 50 years of the 20th century, than during any other period in the last ~300 years, according to the reconstruction. Since 1900 and 1955 (to present) average winter temperature has risen by 0.010 K/year (r = 0.51, P < 0.01) and 0.035 K/year (r = 0.53, P < 0.01), respectively. The warmest year during the reconstruction, 3.92 K, occurred in AD 1805 during the Little Ice Age. The minimum temperatures occurred in the late 1800s and have been progressively warming since. The warmest intervals also occur during the Little Ice Age, AD 1775 - 1785 and 1840 - 1850. A number of warm (1919, 1935 and 1978) and cold (1921 and 1961) years that are recorded in the Fort Chipewyan instrumental records were also captured. Notably, pre-instrumental incidences of cold temperatures events occurring within one or two years of major volcanic events were also evident, including Laki (Iceland-1783), Tambora (Indonesia-1815), Babuyan (Philippines-1831), Coseguina (Nicaragua-1835) and Krakatau (Indonesia-1883) (ZEREFOS et al., 2007), Figure V-5.

The $T_{SW/GS}$-reconstruction also has a roughly 40-year cycle that is characterized by

---

[9] AD *c*. 1550 to 1900

oscillations in temperature. Such oscillations are observed on three separate occasions in the reconstruction; 1800 to 1860, 1880 to 1930 and 1940 to 1980.

During the major incidences of increased flood frequency in the PAD (TIMONEY et al., 1997), highlighted in dark grey in Figure V-5, a general warming is observed. The $T_{SW/GS}$-reconstruction is generally consistent with the Rocky Mountain headwater (Figure V-5 E) (EDWARDS et al., 2008) T-reconstructions during the modern climate interval, AD 1900 to present. The warming observed in both reconstructions is consistent with the warming observed in the northern hemisphere (FOLLAND et al., 2001; MANN et al., 1999). However, there are two notable limitations in comparing the Rocky Mountain headwaters chronologies present by Edwards et al. (2008) to the shorter PAD $T_{SW/GS}$-reconstruction. One, the Edwards et al. (2008) is coarsely resolved (10-year resolution) and thus only the overall trends and large scale patterns of variability can be compared. Second, the Edwards et al. (2008) step-shift at c. AD 1900 to represent the transition from the predominantly meridional circulation of the Little Ice Age to the zonal modern circulation is too abrupt to accurately reflect the variability or the gradual transition observed in the instrumental and reconstructed circulation indices (D'ARRIGO et al., 2005; HURRELL, 1995a; HURRELL, 1995b; THOMPSON and WALLACE, 2001; TRENBERTH and HURRELL, 1994; WALLACE and GUTZLER, 1981). As shown in Figure VII-1, incorporation of a variable ΔF in the reconstruction of Edwards et al. (2008) provides a much better fit to the instrumental record at Fort Chipewyan, which is also consistent with Northern Hemisphere temperature records (FOLLAND et al., 2001; MANN et al., 1999).

The previous hypothesis that the $T_{SW/GS}$-reconstruction should be predominantly a winter source-water labelling signal, pDecember-April, with minor over-prints by the atmospheric summer temperature signal, April-October, is strongly supported by the similarity between reconstructed temperature and instrumental winter temperature, rather than instrumental growth season temperature.

V.3.2 The Relative Humidity Reconstruction (NP)

The h_{GS}-reconstruction shows a consistent long-term drying of -0.05%/year in the PAD over the entirety of the chronology. The trend appears to be in two phases; the first phase having a saddle-shape, with two minima occurring in the late 1700s and the early-mid 1800s and an overall drying of -0.04%/year from AD 1719 to 1882. The second phase has more pronounced drying of -0.08%/year from 1883 to present. Overall, the h_{GS}-reconstruction was a good predictor of instrumental variability, r = 0.48, AD 1955 to 2000. The drying trends in the h_{GS}-reconstruction are consistent with increasing westerly circulation (Figure V-6 B). Notably the NC ΔF reconstruction, which does not have a dependence on ΔF, depicted the same drying trends with a marginally smaller range of variability (see Figure V-3).

When the PAD h_{GS}-reconstruction was compared to the Edwards et al. (2008) RH_{grs} time-series over the common interval, it is clear that the overall trends are inverted. The Edwards et al. (2008) reconstructions indicates increasing relative humidity during the 18th to 20th century, Figure V-6 E and Figure V-9 B. The relatively high values of relative humidity in the PAD during the Little Ice Age, although

inconsistent with the climate in the headwaters as shown by the RH_{grs}-reconstruction, are consistent with independent diatom paleolimnological evidence that large portions of the PAD were inundated under a shallow embayment of Lake Athabasca from ~AD 1600 to 1860 (SINNATAMBY, 2006). Subsequent episodes of elevated water levels are also captured in the h_{GS}-reconstruction; e.g., around AD 1917 (MOLLARD et al., 2002; SINNATAMBY, 2006).

Unlike the PAD temperature reconstruction there appears to be no periodic pattern in the h_{GS}-reconstruction that would indicate that the 20th century trend of drying will end soon. However, both the instrumental record and reconstruction indicate a slowing of the trend since 1980. The AD 1975 to 2000 interval is 4.53% below the 280-year mean of 2.68%. The recorded AD 1968-1971 drought during the filling of the Williston Reservoir is clearly visible in the instrumental and reconstructed h_{GS} time-series. This is a strong indication that the delta- and western Canada-wide climatic and hydrologic drought during the filling of the reservoir was a result of natural effects and not of river regulation (TIMONEY, 2002), although the latter may have exacerbated drying in the delta. When compared to the re-evaluated RH_{grs} reconstruction, the 280-year trend in growth season relative humidity in the headwaters is inverse to that in the PAD. However, during the interval AD 1900 to 2000 the h_{GS}- and re-evaluated RH_{grs}-reconstructions are in better agreement, r = 0.77, P < 0.001 (calculated with h_{GS} time-series smooth over 10-years), as apposed to the original RH_{grs}-reconstruction (r = 0.37, P < 0.01).

V.3.3 Temperature and Humidity Reconstruction: Physiographic Setting

The upland (GSL and QFU), lowland (PRC and QFR) and island (BITC) composites were produced by averaging the appropriate sites (Figure V-7). The lowland, upland and island site $T_{SW/GS}$-reconstructions are similar in trend and variability as was observed in Chapter III. This suggests a very strong common $\delta^{18}O$ signal, controlled by the isotopic composition of precipitation. Over the calibration period the lowest reconstructed temperatures were observed at the upland sites followed by the lowland and island sites, respectively.

The h_{GS}-reconstructions for the three settings show similar trends and variability. However, again systematic differences were observed between the three sites. Notable differences between the three reconstructions include the Lowland sites having the highest average humidity over the calibration period. Until the convergence at ~AD 1960, the Island site is the least variable and is consistently drier. The latter relationship was reported in Chapter III where it was proposed that the variation was due to the persistence of ice-cover over Lake Athabasca in the early spring during the initiation of tree growth.

V.3.4 Source-Water Signal

The 280-year source-water ($\delta^{18}O_{SW}$) (Figure V-8) anomaly reconstruction was produced using the ^{18}O-irsa and the h_{GS}-reconstruction (NP) values calculated using the C-irsa. The reconstruction shows an overall ^{18}O enrichment in source water since the turn of the 17th century. Like the h_{GS}-reconstruction, this is inverse to the source

water $\delta^{18}O$ reconstruction developed for the headwaters chronology, Edwards et al. (2008) Figure V-8. The temperature dependent signals in the source-water ^{18}O in the PAD was masked by the circulation-dependent damping, as it was in the headwaters. Notably the 20th century is marked by general covariance of temperature and moisture variability in the headwaters and the PAD under the influence of increasingly intense zonal circulation (HURRELL, 1995a; HURRELL, 1995b).

V.4 Conclusions

The C-irsa model with an NP index-based ΔF proxy was the best method of reconstructing ~AD 1725 to 2005 (280-year) chronologies for winter temperature (*p*December to April, $T_{SW/GS}$) and growth season relative humidity (April to October, h_{GS}) using the composite and site-specific time-series $\delta^{18}O_{Cell}$ and $\delta^{13}C_{Cell}$.

These $T_{SW/GS}$-reconstructions indicate that winter temperatures have been steadily increasing since at least the begining of the 20th century, which is consistent with observed Northern Hemisphere warming (FOLLAND et al., 2001; MANN et al., 1999). The $T_{SW/GS}$-reconstructions are also consistent with the re-evaluated Rockies headwaters reconstructions developed by Edwards et al. (2008) over the instrumental calibration period. Interestingly the range of reconstructed winter temperatures in the PAD during the Little Ice Age is similar to that of the 20th century, although this does depend on the calibration of ΔF.

The humidity reconstruction indicates a pronounced decrease in growth-season humidity in company with rising temperature since the beginning of the 20th century.

Variations in humidity between the different sites in the delta are minimal during flood and drought events but may diverge at other times. During prolonged low-humidity intervals Bustard Island is the driest.

One of the main findings in this chapter is the sensitivity of C-irsa to shifts in the pattern and strength of circulation regime and the resulting non-temperature-dependent variation in the isotopic composition of source water. Another key finding is the variation between alpine climate in the eastern Rocky Mountains and the PAD

(northern Great Plains) climate over the past three centuries. During the Little Ice Age the climate of the Rockies was characterized by cold winters and low growth season relative humidity. In contrast, winter temperatures in the PAD appear to have been similar to the 20th century, whereas growth season relative humidity was probably higher. Climate in both the headwaters and the PAD has been getting warmer and drier over the 20th century, although the PAD is now the driest it has been in the last ~300 years while the headwaters climate is still wetter than during the Little Ice Age.

V.5   *Recommendations and Possible Directions for Future Work*

Based on the findings of this thesis the following recommendations are made:

- An in-depth analysis of the environment around each tree should be recorded at the time of sampling. This information can be of considerable insight during the analysis of $\delta^{18}O_{Cell}$ and $\delta^{13}C_{Cell}$ as microenvironmental factors could be playing a larger role in isotopic labelling than presently thought. Special attention should be given to;

    o   competition with neighbouring trees (irradiance)

    o   canopy thickness

    o   root depth and hydrological setting

- The isotopic sampling of the precipitation should continue so that a better understanding of the local isotope climatology can be gained, especially with regard to $T - \delta^{18}O_{\Pr ec}$ relations under differing circulation regimes.

- Circulation indices should be sought from various proxies and sources to incorporate into the model. More accurate documentation of circulation regimes would help to minimize uncertainty in the source-water labelling season.

- Investigate the potential of incorporating other climatic and environmental parameters, such as reconstructing growth degree days; days in a year that reaches or exceed a particular temperature and humidity that the trees require to grow with minimal stress.

Continue   analysis   of   submerged   logs   at   Greenstar   Lake   to   extend   upland

reconstructions to potentially cover a wider range of Little Ice Age conditions and perhaps the Medieval-Little Ice Age transition.
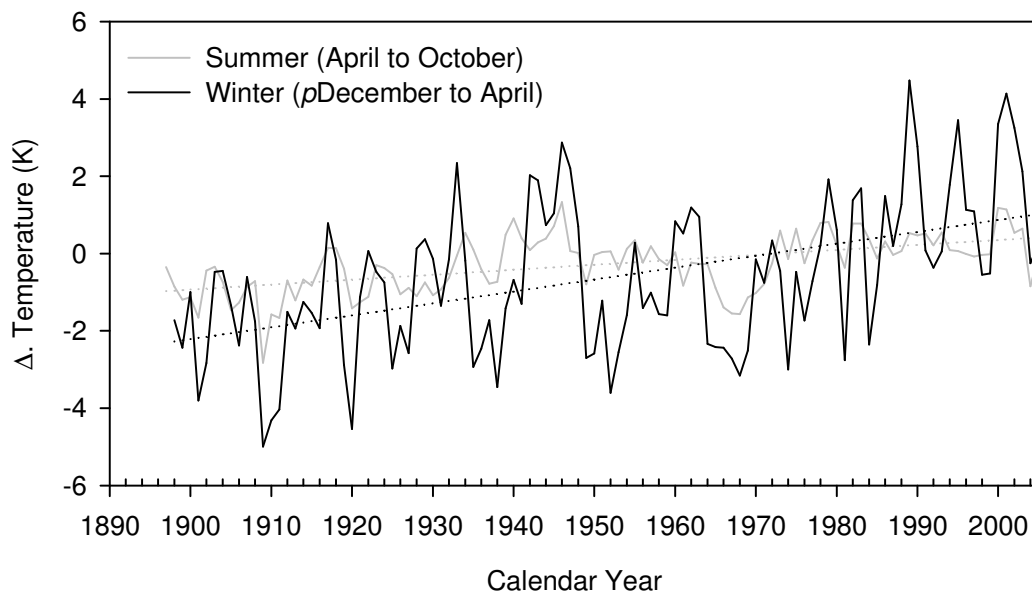
Figure V-1. 108-year (AD 1897 to 2005) comparisons of the growth season temperature (April to October) and winter source-water temperature (*p*December to April) for the Peace-Athabasca Delta, Alberta, Canada (GOODISON and LOUIE, 1986; MEKIS and HOGG, 1997; MEKIS and HOGG, 1999; METCALFE et al., 1997; VINCENT and GULLETT, 1999).
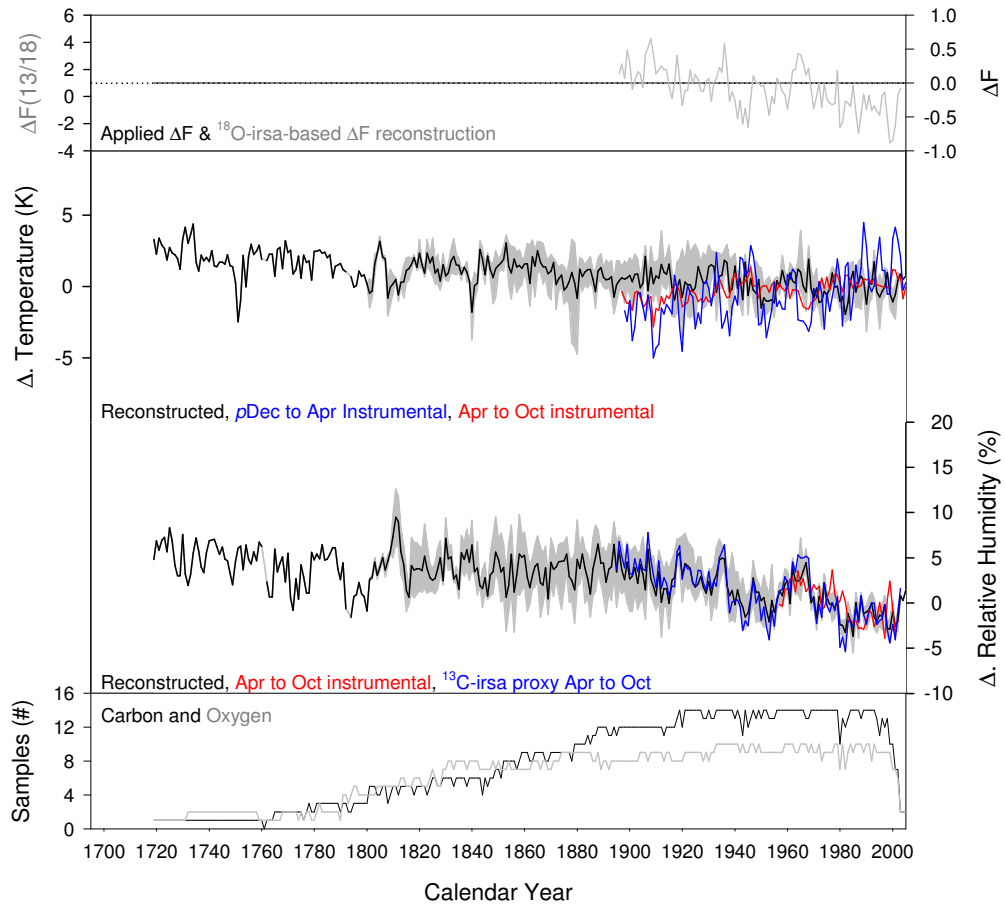
Figure V-2. 280-year reconstruction of temperature and humidity developed using the C-irsa without the aide of circulation indices. To contrast the results, the identified isotopic seasons for carbon and oxygen temperature (red and blue) and humidity (red and blue) are presented. The shading represents the estimated range of uncertainty in the reconstructions.
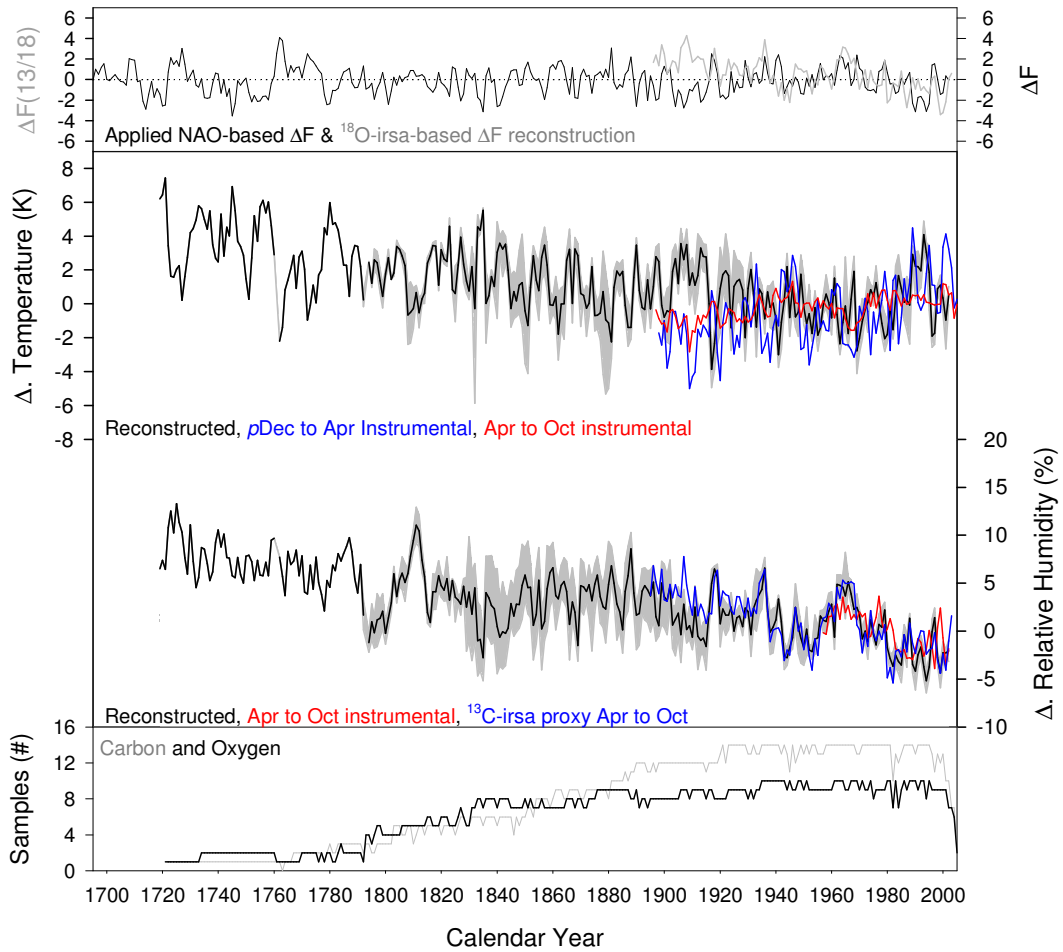
Figure V-3: 280-year reconstruction of temperature and humidity developed using the C-irsa and NAO (North Atlantic Oscillation) index from Hurrell (1995b) (AD 1900-2007) and Hurrell (1995a) (AD 1719-1899). To contrast the results, the identified isotopic seasons for carbon and oxygen temperature (red and blue) and humidity (red and blue) are presented. The shading represents the estimated range of uncertainty in the reconstructions.

144
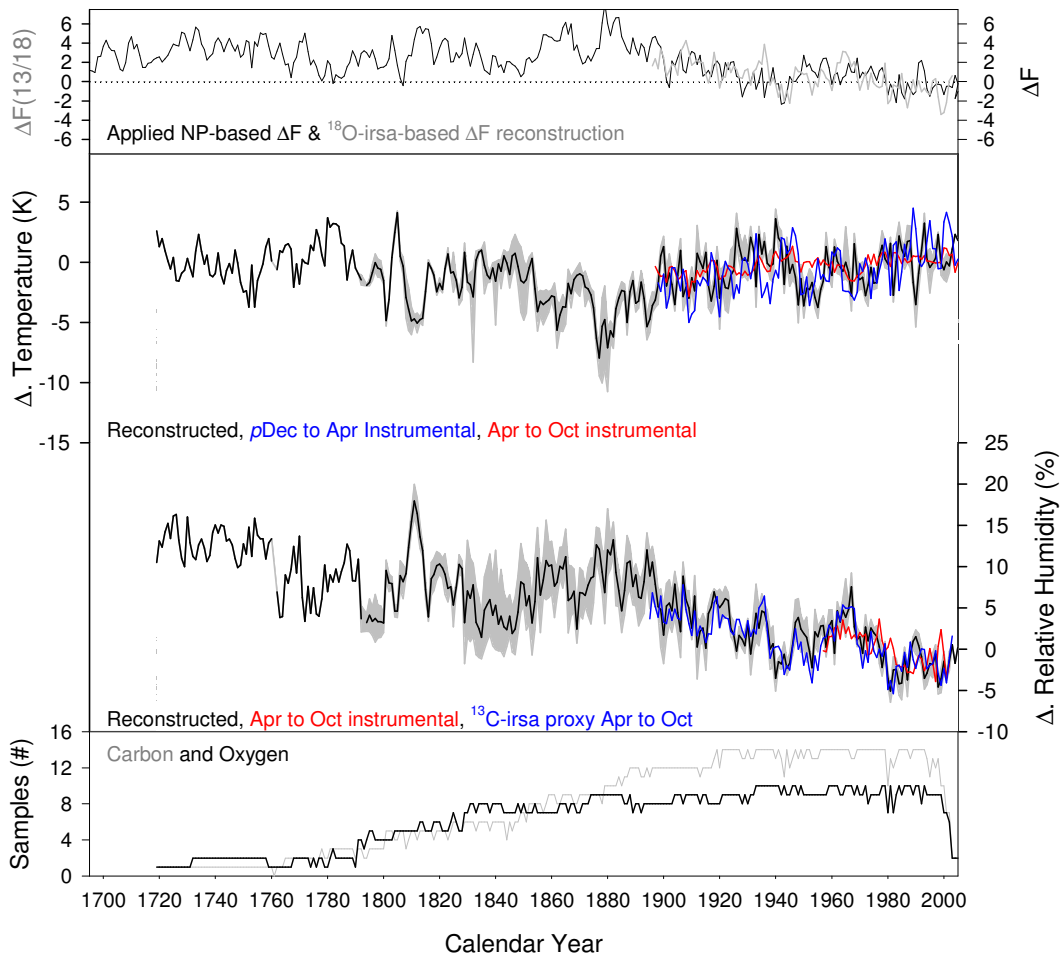
Figure V-4. 280-year reconstruction of temperature and humidity developed using the C-irsa and North Pacific (NP) index from Trenberth and Hurrell (1994) (AD 1900-2007) and D'Arrigo et al. (2005) (AD 1719 - 1899). The identified isotopic labelling seasons for carbon and oxygen temperature (red and blue) and humidity (red and blue) are indicated. The shading represents the estimated range of uncertainty in the reconstructions.
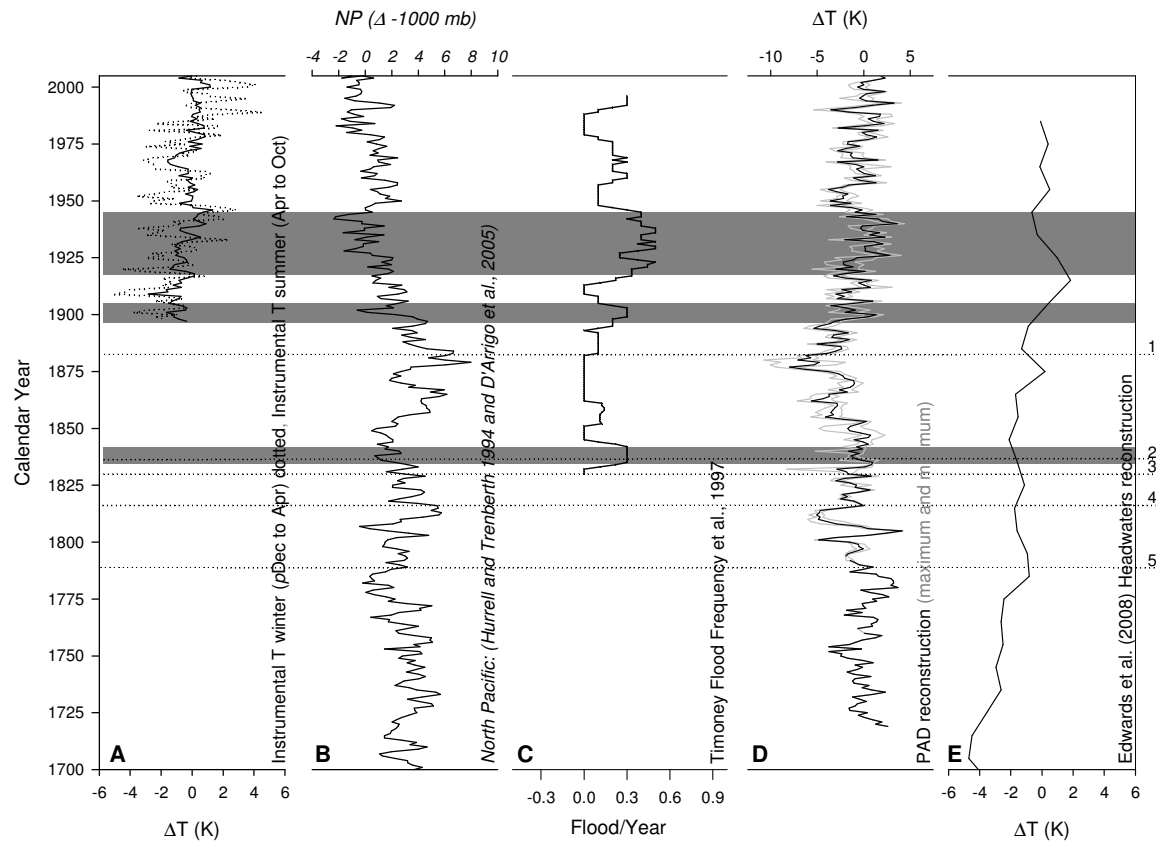
Figure V-5. Measured and reconstructed records. *A*, Measured winter (dotted) and growth season (solid) temperature Ft. Chipewyan. *B*, NP (measured and reconstructed). *C*, Timoney et al. (1997) PAD flood frequency reconstruction, high-flood periods in grey. *D*, PAD C-irsa $T_{SW/GS}$ -reconstruction, the shading represents the estimated range of uncertainty in the reconstructions. *E*, T -reconstruction, Edwards et al. (2008), Volcanic events Krakatau (*1*, 1883), Coseguina (*2*, 1835), Babuyan (*3*, 1831), Tambora (*4*, 1815) and Laki (*5*, 1783).
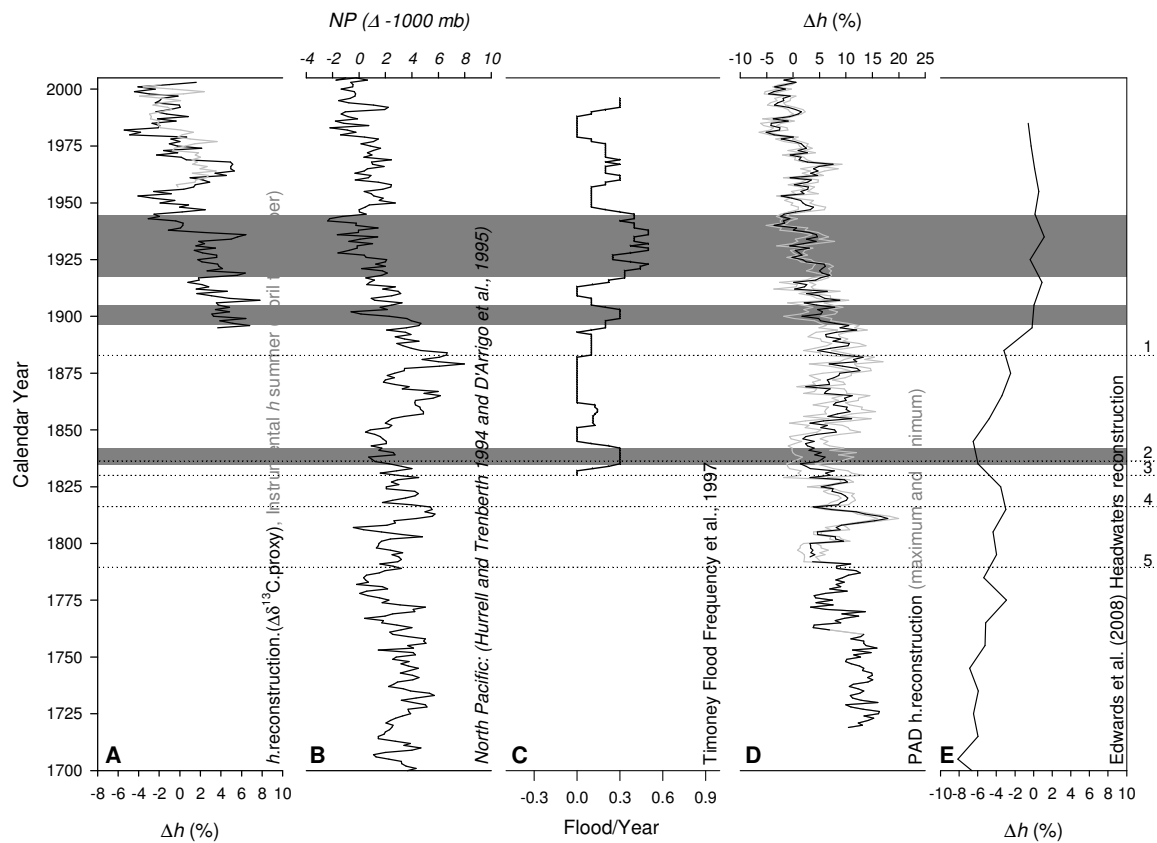
Figure V-6. Measured and reconstructed time-series. *A*, growth season (grey) relative humidity Ft. McMurray, ^{13}C-irsa h_{SW} -reconstruction (black). *B*, NP (measured and reconstructed). *C*, Timoney et al. (1997) PAD flood frequency reconstruction, high-flood periods in grey. *D*, PAD C-irsa h_{SW} -reconstruction, the shading represents the estimated range of uncertainty in the reconstructions. *E*, T -reconstruction, Edwards et al. (2008), volcanic events Krakatau (*1*, 1883), Coseguina (*2*, 1835), Babuyan (*3*, 1831), Tambora (*4*, 1815) and Laki (*5*, 1783).

147
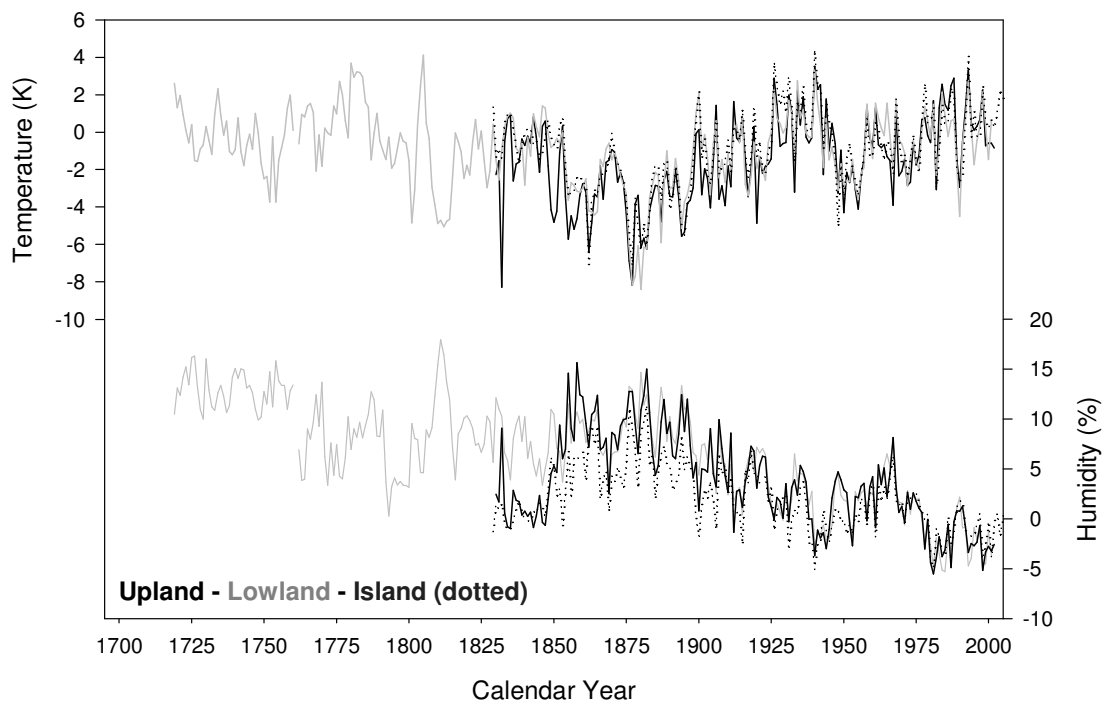
Figure V-7. 280-year reconstruction of temperature and humidity developed using the coupled-isotope response surface approach developed using a composite NP (North Pacific) index from Trenberth and Hurrell (1994) (AD 1900-2007) and D'Arrigo et al. (2005) (AD 1719 – 1899). All chronologies are separated by physiographic setting; Upland (black), Lowland (grey) and Island (dotted).
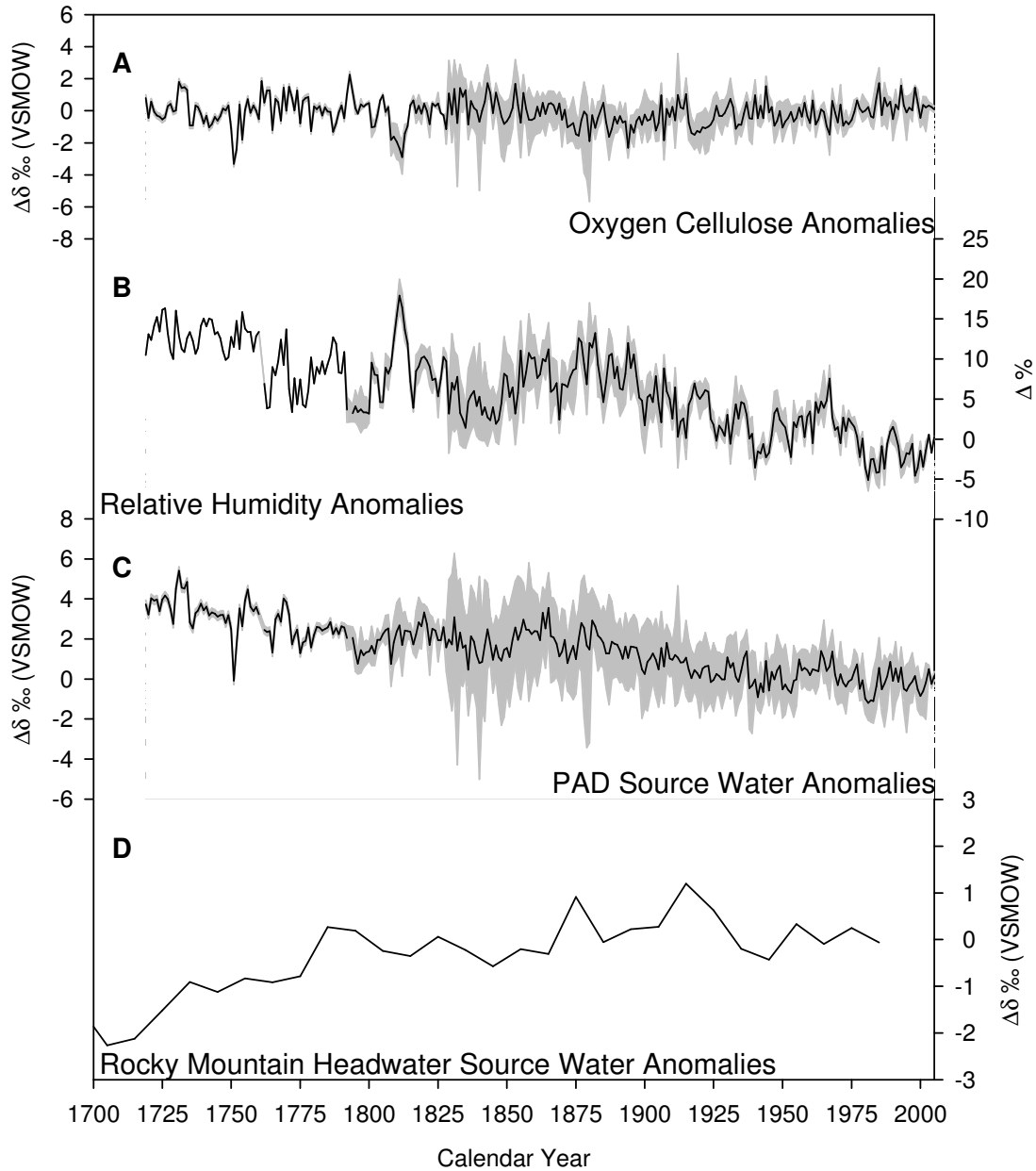
Figure V-8. (*A*) **Cellulose oxygen-18 anomalies for 280 years with max. and min. error.** (*B*) **Relative humidity anomalies reconstruction using the C-irsa and a NP based ΔF with max. and min. error.** (*C*) **Reconstruction of 280 years of winter precipitation source-water anomalies with error.** (*D*) **Equivalent reconstruction of Rocky Mountain headwaters source-waters anomalies Edwards et al. (2008).**
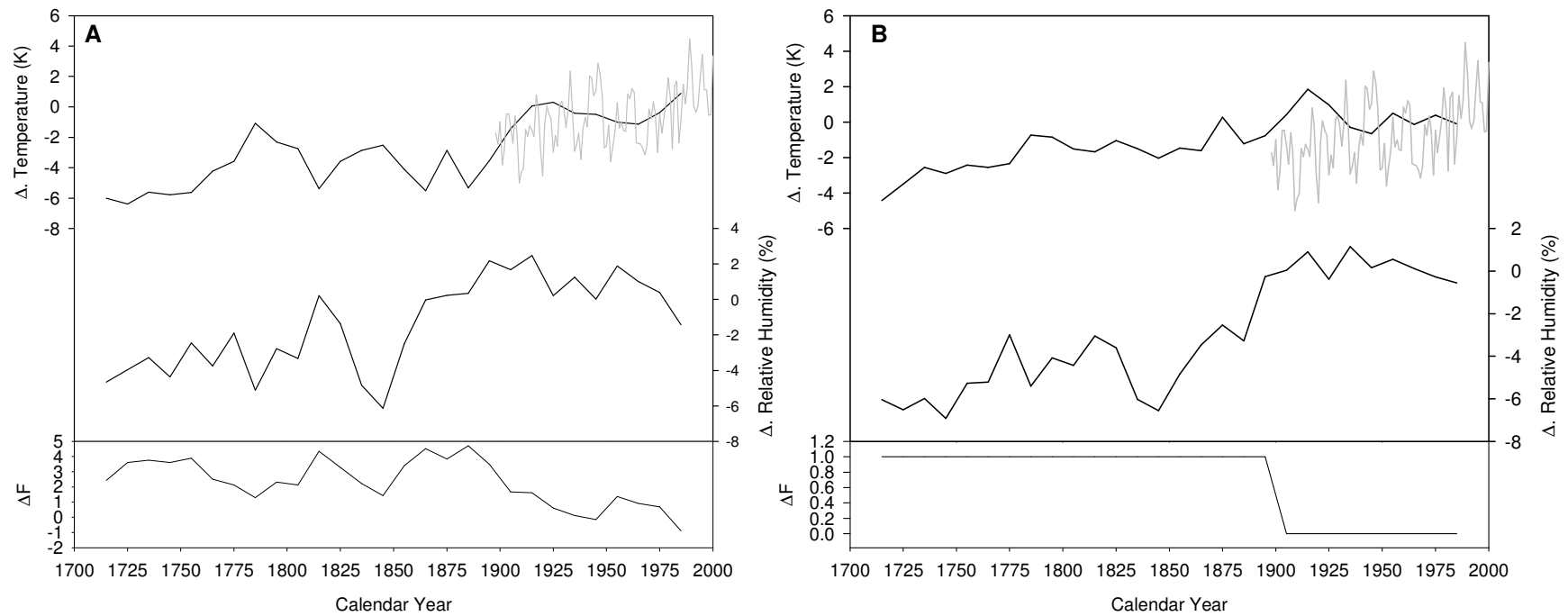
Figure V-9. (*A*) **Re-evaluation of the Edwards et al. (2008) headwater chronologies by applying a variable ΔF based on the NP ΔF (Trenberth and Hurrell (1995b) (AD 1900 - 2007) and D'Arrigo et al. (2005) (AD 1719 - 1899) applied in figure V-4. (*B*) The original Edwards et al. (2008) headwater chronologies generated with a single step-shift. Both sets of reconstructions are generated with the equations and coefficients as follows** $\Delta\delta^{13}C_{Cell} = \left(-0.17‰/\%\right)\cdot\Delta h_{GS} + \left(-0.15‰/K\right)\cdot\Delta T_{WIN}$ **and** $\Delta\delta^{18}O_{Cell} = \left(-0.28‰/\%\right)\cdot\Delta h_{GS} + \left(\left(0.65‰/K\right)\cdot\Delta T_{WIN} + \Delta F\right)$.

Table V-1. Climate Data Comparison (Accompanying statistics for Figure V-2 to V-4): Comparisons of three (NC [No index], NAO [North Atlantic Oscillation (HURRELL, 1995a) and NP [North Pacific (TRENBERTH and HURRELL, 1994) (AD 1900-2007)) climate reconstructions versus summer (April to October) temperature (T) and humidity (h) and winter (*p*December to April) temperature. All values are expressed as r-values, with values being significant at P < 0.01 and P < 0.05 when r reaches or exceeds ±0.36 and ± 0.28 respectively.

	R-value	Temperature (K)						Relative Humidity (%)				Circulation Indices (Δ -1000 mb-‰)			
		Apr-Oct.CO	1950-2000	1900-1949	.pDec-Apr.CO	1950-2000	1900-1949	Apr-Oct(6-20h00).CO	h.CAR(13)	1950-2000	1900-1949	F.18	F.13.18	1950-2000	1900-1949
NC	h	-0.45	-0.47	-0.21	-0.32	-0.28	-0.22	0.45	0.94	0.93	0.90	0.52	0.69	0.68	0.54
NC	T	-0.32	-0.30	-0.17	-0.25	-0.18	-0.21	0.08	0.50	0.54	0.20	0.24	0.44	0.35	0.36
NP	NP.CO											0.52	0.48	0.51	0.41
NP	h	-0.49	-0.44	-0.39	-0.31	-0.25	-0.25	0.48	0.82	0.79	0.77	0.60	0.71	0.71	0.59
NP	T	0.14	0.02	0.25	0.04	0.04	0.04	-0.23	-0.02	0.08	-0.13	-0.28	-0.15	-0.19	-0.15
NAO	NAO.CO											0.51	0.14	0.44	-0.12
NAO	h	-0.33	-0.52	0.03	-0.27	-0.31	-0.09	0.51	0.82	0.86	0.68	0.62	0.62	0.70	0.38
NAO	T	-0.20	0.20	-0.41	-0.09	0.18	-0.27	-0.34	0.14	-0.08	0.19	-0.37	0.10	-0.24	0.29

Table V-2. Climate Data Comparison (Accompanying statistics for Figure V-7): Comparisons of Upland, Lowland and Island climate reconstructions with an NP (North Pacific Hurrell and Trenberth (AD 1900-2007) and D'Arrigo et al. (2005) (~AD 1719-1899) based circulation indices versus summer (April to October) temperature (T) and humidity (h) and winter (pDecember to April) temperature. All values are expressed as r-values, with values being significant at P < 0.01 and P < 0.05 when r reaches or exceed ±0.36 and ± 0.28 respectively.

R-Value	Temperature (K)						Relative Humidity (%)			
	Apr-Oct.CO	1950-2000	1900-1949	.pDec-Apr.CO	1950-2000	1900-1949	.Apr-Oct(6-20h00).CO	h.CAR(13)	1950-2000	1900-1949
h.Upland	-0.46	-0.42	-0.35	-0.31	-0.27	-0.21	0.45	0.82	0.78	0.77
h.Lowland	-0.51	-0.47	-0.40	-0.32	-0.26	-0.26	0.51	0.80	0.77	0.72
h.Island	-0.39	-0.32	-0.35	-0.24	-0.14	-0.25	0.38	0.70	0.74	0.66
T.Upland	0.25	0.13	0.35	0.15	0.15	0.13	-0.38	-0.10	-0.01	-0.18
T.Lowland	0.01	-0.15	0.15	-0.09	-0.12	-0.05	-0.01	0.08	0.22	-0.06
T.Island	0.07	0.06	0.16	-0.01	0.06	-0.02	-0.21	0.01	0.01	-0.12

References

Anderson P. M., Bartlein P. J., Brubaker L. B., Gajewski K., and Ritchie J. C. (1991) Vegetation-Pollen-Climate Relationships for the Arcto-Boreal Region of North America and Greenland. *Journal of Biogeography* **18**, 565-582.

Bailey J. N.-L. (2005) Isotope Dendroclimatology Studies in the Peace-Athabasca Delta, Alberta, University of Waterloo.

Bailey J. N.-L. and Edwards T. W. D. (2008) Reconstruction of Climate from Stable Isotopes in Tree-rings, Peace-Athabasca Delta, Northern Alberta: A Test of the Isotope Response-Surface Approach. *Geological Association of Canada/Association Geologique du Canada: 400 years of Discoveries*, 199.

Barber V. A., Juday G. P., Finney B. P., and Wilmking M. (2004) Reconstruction of summer temperature in interior Alaska from tree-ring proxies: Evidence from changing synoptic climate regimes. *Climate Change* **63**, 91-120.

Barbour M. M. and Farquhar G. D. (2000) Relative humidity- and ABA-induced variation in carbon and oxygen isotope ratios of cotton leaves. *Plant, Cell and Environment* **23**(5), 473–485.

Barbour M. M., Walcroft A. S., and Farquhar G. D. (2002) Seasonal variation in δ^{13}C and δ^{18}O of cellulose from growth rings of pinus radiata. *Plant, Cell and Environment* **26**, 1483-1499.

Bayrock L. A. and Root J. D. (1973) Geology of the Peace-Athabasca Delta region, Alberta. In *Peace-Athabasca Delta Project Group, Technical Report and Appendices: Volume 1, Hydrological Investigations*.

Bednarski J. M. (1999) Quaternary geology of northeastern Alberta. *Geological Survey of Canada Bulletins* **353**.

Birks S. J. (2003) Water isotope partitioning in aquitards and precipitation on the northern Great Plains, Univerity of Waterloo.

Birks S. J., Edwards T. W. D., Gibson J. J., Drimmie R. J., and Michel F. A. (2004) http://www.science.uwaterloo.ca/~twdedwar/cnip/cniphome.html. Canadian Network for Isotopes in Precipitation.

Boyle E. A. (1997) Cool Tropical temperatures shifts the Global δ^{18}O-T relationship: An explanation for the ice core δ^{18}O-borehold thermometry conflict. . *Journal of Geophysical Research* **23**(3), 273-276.

Brooks J. R., Flanagan L. B., and Ehleringer J. R. (1998) Responses of boreal conifers to climate fluctuations: indications from tree-ring widths and carbon isotope analyses. *Candian Journal of Forest Research* **28**(4), 524 - 533.

Buhay W. M., Edwards T. W. D., and Aravena R. (1996) Evaluating kinetic fractionation factors used for ecologic and paleoclimatic reconstructions from oxygen and hydrogen isotope ratios in plant water and cellulose. *Geochimica et Cosmochimica Acta* **60**(12), 2209-2218.

Burk R. L. and Stuiver M. (1981) Oxygen Isotopes Ratios in Trees Reflect Mean Annual Temperature and Humidity. *Science* **211**(4489), 1417-1419.

CANGRID. (2000) Monthly rehabilitated gridded Canadian historical air temperature and precipitation database. *Climate Research Branch, Meteorological Service of Canada, Toronto*, CD-ROM.

Cappa C. D., Hendricks M. D., DePaulo D. J., and Cohen R. C. (2003) Isotopic fractionation of water during evaporation. *Journal of Geophysical Research* **108**, 4525-4535.

Cernusak L. A., Wong S. C., and Farquhar G. D. (2003) Oxygen isotope composition of phloem sap in relation to leaf water in Ricinus communis. *Functional Plant Biology* **30**, 1059-1070.

Couillard G. (2004) δ^{13}C and Ring width analysis: how well do they correlate among themselves and with varying environmental factors, University of Waterloo.

Cowan I. R. (1977) Stomatal behaviour and environment. In *Advances in botanical research* (ed. R. D. Preston and H. W. Woolhouse). Academic Press.

Craig H., Gorden L. I., and Horibe Y. (1963) Isotope exchange effects in the evaporation of water: I. Low temperature experimental results. *Journal of Geophysical Research* **68**, 5079-5089.

Craig H. and Gordon L. I. (1965) Stable Isotopes in Oceanographic Studies and Paleotemperatures. In *Deuterium and Oxygen 18 Variations in the Ocean and the Marine Atmosphere*. Spoleto.

Cuffey K. M., Clow G. D., Alley R. B., Stuiver M., Waddington E. D., and Saltus R. W. (1995) Large Arctic Temperature Changes at the Wisconsin-Holocence Glacial Transition. *Science* **270**, 455-458.

D'Arrigo R., Mashig E., Frank D., Wilson R., and Jacoby G. (2005) Temperature variability over the past millennium inferred from Northwestern Alaska tree rings. *Climate Dynamics* **24**(2-3), 227-236.

Dansgaard W. (1964) Stable Isotopes in Precipitation. *Tellus XVI* **4**, 438-468.

DeNiro M. J. and Cooper L. W. (1989) Post-photosynthetic modification of oxygen isotope ratios of carbohydrates in the potato: Implications for paleoclimate reconstruction based upon isotopic analysis of wood cellulose. *Geochimica et Cosmochimica Acta* **53**, 2573-2580.

Dongmann G. and Nurnberg H. W. (1974) On the Enrichment of $H_2^{18}O$ in the Leaves of Transpiring Plants. *Radiation and Environmental Biophysics* **11**, 41-52.

Dupouey J.-L., Leavitt S., Choisnel E., and Jourdain S. (1993) Modelling carbon isotope fractionation in tree rings based on e!ective evapotranspiration and soil water status. *Plant, Cell and Environment*(16), 939-947.

Edwards T. W. D., Birks S. J., Luckman B. H., and MacDonald G. M. (2008) Climatic and Hydrological variability during the past millennium in the eastern Rocky Mountains and Northern Great Plains of Western Canada. *Quaternary Research*, doi:10.1016/j.yqres.2008.04.013.

Edwards T. W. D. and Fritz P. (1986) Assessing meteoric water composition and relative humidity from ^{18}O and ^{2}H in wood cellulose: Paleoclimatic implications for Southern Ontario, Canada. *Applied Geochemistry* **1**, 715-723.

Edwards T. W. D., Graf W., Trimborn P., Stichler W., Lipp J., and Payer H. D.

(2000) $\delta^{13}C$ response surface resolves humidity and temperature signals in trees. *Geochimica et Cosmochimica Acta* **64**(2), 161-167.

Edwards T. W. D., Hall R. I., and Wolfe B. B. (2004a) High-Resolution of Past Climate, Hydrology, and Ecology, Peace-Athabasca Delta, from Lake Sediment and Tree-Rings. In *Interim Report to BC Hydro*. University of Waterloo.

Edwards T. W. D., Hall R. I., and Wolfe B. B. (2004b) A Multi-Century Flood, Climatic, and Ecological History of the Peace-Athabasca Delta, Northern Alberta, Canada. In *Interim Report to BC Hydro*. University of Waterloo.

Edwards T. W. D., Wolfe B. B., and MacDonald G. M. (1996) Influence of changing atmospheric circulation on precipitation $\delta^{18}O$-temperature relations in Canada during the Holocene. *Quaternary Research* **46**, 211-218.

Elgood R. J., Buhay W. M., Wolfe B. B., and Edwards T. W. D. (1997) $\delta 18O$ in organic matter and water by nickel-tube pyrolysis. In *Technical Procedure 29.0*, Vol. 8 (ed. D. o. E. S. Environmental Isotope Laboratory). University of Waterloo.

Farquhar G. D., Barbour M. M., and Henry B. K. (1998) Interpretation of oxygen isotope composition of leaf material. In *'Stable Isotopes: Integration of Biological, Ecological and Geochemical Processess'* (ed. H. Griffiths), pp. 27-61. BIOS Scientific Publishers: Oxford.

Farquhar G. D., Ehleringer J. R., and Hubick K. T. (1989) Carbon Isotope Discrimination and Photosynthesis. *Annual Review of Plant Physiology and Plant Molecular Biology* **40**, 503-537.

Farquhar G. D. and Lloyd J. (1992) Carbon and Oxygen Isotope Effects in the Exchange of Carbon Dioxide between Terrestrial Plants and the Atmosphere. In *Stable Isotopes and Plant Carbon-Water Relations* (ed. J. R. Ehleringer, A. E. Hall, and G. D. Farquhar). Academic Press, In.

Farquhar G. D., O'Leary M. H., and Berry J. A. (1982) On the Relationship between Carbon Isotope Discrimination and the Intercellular Carbon Dioxide Concentration in Leaves. *Australlian Journal of Plant Physiology* **9**, 121-137.

Farquhar G. D. and Sharkey T. D. (1982) Stomatal Conductance and Photosynthesis. *Annual Review of Plant Physiology* **33**, 317-345.

Feng X. and Epstein S. (1995) Carbon isotopes of trees from arid environments and implications from reconstructing atmospheric CO_2 concentration. *Geochimica et Cosmochimica Acta* **59**, 2599-2608.

Fisher D. A., Wake C. P., Kreutz K. J., Yalcin K., Steig E., Mayewski P. A., Anderson L., Zheng J., Rupper S., Zdanowicz C., Demuth M., Waszkiewicz M., Dahl-Jensen D., Goto-Azuma K., Bourgeois J. B., Koerner R. M., Sekerka J., Osterberg E., Abbot M. B., Finney B. P., and Burns S. J. (2004) Stable isotope records from Mount Logan, Eclipse ice cores and nearby Jellybean Lake. Water cycle of the North Pacific over 2000 years and over five vertical kilometers: sudden shifts and tropical connections. *Geographie Physique et Quaternaire* **58**, 9033-9048.

Folland C. K., Karl T. R., Christy J. R., Clarke R. A., Gruza G. V., Jouzel J., Mann

M. E., Oerlemans J., Salinger M. J., and Wang S.-W. (2001) Observed climate variablity and change. In *Climate Change: The Scientific Basis* (ed. J. T. Houghton, Y. Ding, D. J. Griggs, M. Noguer, P. J. van der Linden, and D. Xiaosu), pp. 99-181. Cambridge University Press.

Francey R. J. and Farquhar G. D. (1982) An explanation of $^{13}C/^{12}C$ variation in tree rings. *Nature* **297**, 28-31.

Friedli H., Lotscher H., Oeschger H., Siegenthaler U., and Stauffer B. (1986) Ice core record of the $^{13}C/^{12}C$ ratio of atmospheric CO_2 in the past two centuries. *Nature* **324**(6094), 237-238.

Fritts H. C. (1976) *Tree Rings and Climate*. Academic Press.

Fritz P. and Fontes J. C. (1986) *The Terrestrial Environment, B*. Elsevier Science Publishers.

Gat J. R. (1996) Oxygen and Hydrogen Isotopes in the Hydrologic Cycle. *Annual Review of Earth Planet Science* **24**, 225-262.

Goodison B. E. and Louie P. Y. T. (1986) Canadian methods for precipitation measurement and correction. *International Workshop on Correction of Precipitation Measurements*, 141-145.

Gray J. (1981) The use of stable-isotope data in climate reconstruction. In *Climate and History* (ed. T. M. L. Wigley, M. J. Ingram, and G. Farmer), pp. 53-81. Cambridge University Press.

Green J. W. (1963) Wood Cellulose. In *Methods of Carbohydrate Chemistry*, Vol. 3 (ed. R. L. Whistler), pp. 9-20. Academic Press.

Grinstead M., J. (1977) A study of the relationships between climate and stable isotope ratios in tree rings., University of Waikato.

Hammarlund D., Barnekow L., Birks H. J. B., Buchardt B., and Edwards T. W. D. (2002) Holocene changes in atmospheric circulation recorded in the oxygen-isotope stratigraphy of lacustrine carbonates from northern Sweden. *The Holocene* **12**, 339- 351.

Heemskerk A. R. and Dieboldt P. (1994) Breakseal organic combustion. In *Technical Procedure 22.0* (ed. D. o. E. S. Environmental Isotope Laboratory), pp. 11. University of Waterloo.

Hoefs J. (1997) *Stable Isotope Geochemistry*. Springer-Verlag Berlin Heidelberg.

Holmes R. L. (2000) COFECHA. Laboratory of Tree-Ring Research.

Horita J. and Wesolowski D. (1994) Liquid-vapour fractionation of oxygen and hydrogen isotopes of water from the freezing to the critical temperature. *Geochimica et Cosmochimica Acta* **58**(16), 3425-3437.

Hosie R. C. (1969) *Native trees of Canada* Canadian Forestry Service, Department of Fisheries and Forestry. .

Hurrell J. W. (1995a) Decadal Trends in the North Atlantic Oscillation: Regional Temperatures and Precipitation. *Science* **269**, 676-679.

Hurrell J. W. (1995b) NAO Index Data provided by the Climate Analysis Section, NCAR, Boulder, USA.

Jouzel J., Alley R. B., Cuffey K. M., Dansgaard W., Grootes P., Hoffmann G.,

Johnsen S. J., Koster R. D., Peel D., Shuman C. A., Stievenard M., Stuiver M., and White J. (1997) Validity of the temperature reconstruction from water isotopes in ice cores. *Journal of Geophysical Research* **102**(C12), 26,471.

Kay W. M. (1966) *Convective heat and mass transfer*. McGraw-Hill.

Kreutz K. J., Mayewski P. A., Meeker L. D., Twickler M. S., Whitlow S. I., and Pittalwala I. I. (1997) Bipolar changes in atmospheric circulation during the Little Ice Age. *Science*, 1294-1296.

Lamb H. H. (1977) *Climatic History and the Future*. Methuen.

Lawrence J. R. and White J. W. C. (1991) The elusive climate signals in the isotopic compositin of precipitation. In *Stable isotope geochemistry: a tribute to Samuel Epstein*, pp. 169-185. Geochemical Soc Spec Publi 3.

Leavitt S. (1993) Environmental information from $^{13}C/^{12}C$ ratios of wood. In *In Climate Change in Continental Isotopic Records*, Vol. Geophysical Monograph 78 (ed. P. K. Swat), pp. 325-331. American Geophysical Union.

Lipp J., Trimborn P., Edwards T. W. D., Waisel Y., and Yakir Y. (1996) Climatic effects on the $\delta^{18}O$ and $\delta^{13}C$ of cellulose in the desert tree *Tamaric jordanis*. *Geochimica et Cosmochimica Acta* **60**(17), 3305-3309.

Lipp J., Trimborn P., Moser H., Becker B., and Frenzel B. (1991) Stable isotopes in tree ring cellulose and climate change. *Tellus B*(43B), 322-330.

MacDonald G. M., Porinchu D., and D. E. T. W. (2005) Preliminary Dendrochronological and Dendroclimatological Assessment of New Tree-Ring Collections From the Peace-Rochers Confluence, Quatre Fourches River, Quatre Fourches Upland, Greenstar Lake, and Bustard Island Sites, Alberta, pp. 20. BC Hydro.

Majoube M. (1971) Fractionnement en oxygene 18 et an deuterium entre l'eau et sa vapeur. *J. Chim. Phys.* **68**, 1423-1436.

Mann M. E., Bradley R. S., and Hughes M. K. (1999) Northern Hemisphere Temperatures During the Past Millennium: Inferences, Uncertainties, and Limitations. *Geophysical Research Letters* **26**(6), 759-762.

McCarroll D. and Loader N. J. (2004) Stable Isotopes in tree rings. *Quaternary Science Reviews* **23**, 771-801.

McKenney D., Papadopol P., Lawrence K., Campbell K., and Hutchinson M. (2007) Customized Spatial Climate Models for Canada. *Frontline Forest Research Applications* **Technical Note No. 108**, 8pp.

Mekis É. and Hogg W. D. (1997) Rehabilitation and analysis of Canadian daily precipitation time series. *10th Conference on Applied Climatology*.

Mekis É. and Hogg W. D. (1999) Rehabilitation And Analysis Of Canadian Daily Precipitation Time Series. *Atmosphere-Ocean* **37**(1), 53-85. .

Melchin J. J. (2007) Comparison of Early- and Latewood $\delta^{13}C$ and $\delta^{18}O$ Signals in White Spruce (*Picea glauca*) from Northern Alberta. B.Sc., University of Waterloo.

Metcalfe J. R., Routledge B., and Devine K. (1997) Rainfall measurement in Canada: changing observational methods and archive adjustment procedures. *Journal*

of Climate **10**, 92-101.

Mollard J. D., Mollard D. G., Penner L. A., Cosford J. I., and Zimmer T. A. M. (2002) Peace-Athabasca Delta Geomorphology: an Assessment of Geomorphic Change Over Time, pp. 131. B.C. Hydro.

Nienstaedt H. and Zasada J. C. (1990) Picea glauca (Moench) Voss white spruce. In *Silvics of North America; Conifers Agricultural Handbook*, Vol. 1 (ed. M. Burns and B. H. Honkala), pp. 204-226. [13385]. U.S. Department of Agriculture, Forest Service.

PADPG P.-A. D. P. G. (1973) A Report on low water levels and their effects on the Peace-Athabasca Delta. (ed. G. o. Canada). Government of Canada.

Pearman G. I., Francey R. J., and Fraser P. J. B. (1976) Climatic implications of stable isotopes in tree rings. . *Nature*(260), 771-772.

Pearson K. (1901) On Lines and planes of closest fit to systems of points in space. *Philosophical Magazine* **2**, 559-572.

Pendall E., Betancourt J. L., and Leavitt S. (1999) Paleoclimatic significance of δ^2H and $\delta^{13}C$ values in pinon pine needles from packrat middens spanning the last 40,000 years. *Palaeogeography, Palaeoclimatology, and Palaeoecology* **147**, 53-72.

Peters D. L. (2003) Controls on the persistence of water within perched basins of the Peace-Athabasca Delta, northern Canada, , Trent University.

Peters D. L., Prowse T. D., Pietroniro A., and Leconte R. (2006) Flood hydrology of the Peace-Athabasca Delta, northern Canada. *Hydrological Processes* **20**, 4073-4096.

Peterson M. (1994) Flood History Study, Task F.1 of Peace-Athabasca Delta Technical Studies,. Wood Buffalo National Park.

Plummer L. N., Michel R. L., Thurman E. M., and Glynn P. D. (1993) *Environmental tracers for age dating young ground water*.

Porinchu D. (2004) Development of Dendrochronologies for Four Sites in the Peace-Athabasca Delta. In *High-Resolution of Past Climate, Hydrology and Ecological, Peace-Athabasca Delta, from Lake Sediment and Tree Rings. Interim Reports to BC Hydro.* (ed. Edwards T.W.D., Hall R.I., and W. B.B.). University of Waterloo.

Porter T. J., Pisaric M. F. J., Kokelj S. V., and Edwards T. W. D. (2007) The use of $\delta^{13}C$ and $\delta^{18}O$ from White Spruce as Paleoclimatic indicators in the Mackenzie Delta region, Canada. *In Prep.*

Ramsar. (1971) Convention on Wetlands of International Importance Especially as Waterfowl Habitat. *International Conference on the Wetlands and Waterfowl*.

Ramsar. (2003) Ramsar Directory of Wetlands of International Importance. (ed. Ramsar). Downloaded at http://wetlands.org/rsbd/.

Roden J. S., Lin G., and Ehleringer J. R. (2000) A mechanistic model for interpretation of hydrogen and oxygen isotope ratios in tree-ring cellulose. *Geochimica et Cosmochimica Acta* **64**(1), 21-35.

Roden J. S., Lin G., and Ehleringer J. R. (2002) Reponse to the comment of V. J.

Terwilliger on "A mechanistic model for interpretation of hydrogen and oxygen isotope ratios in tree-ring cellulose," by J. S. Roden, G. Lin, and J. R. Ehleringer (2000) Geochem. Cosmochim. Acta 64: 21-35. *Geochimica et Cosmochimica Acta* **66**(4), 733-734.

Rozanski K., Araguás-Araguás L., and Gonfiantini R. (1993) Isotopic patterns in modern global precipitation. In *Climate Change in continental isotopic records. Geophys Monogr 78*, pp. 1-36.

Saurer M., Aellen K., and Siegwolf R. (1997) Correlating δ^{13}C and δ^{18}O in cellulose of trees. *Plant, Cell and Environment* **20**, 1543-1550.

Schleser G. H., Bernhardt K.-G., and Hurka H. (1989) Climatic adaptability of populations of Diplotaxis erucoides D. C. (Brassicaceae) from Sicily, based on leaf morphology, leaf anatomy and δ^{13}C studies. *International Journal of Biometeorology*(33), 109-118.

Schleser G. H., Helle G., Lucke A., and Vos H. (1999) Isotope signals as climate proxies: the role of transfer functions in the study of terrestrial archives. *Quaternary Science Reviews* **18**, 927-943.

Schweingruber F. H. (1988) *Tree Rings*. D. Reidel Publishing Company.

Sinnatamby R. N. (2006) An Assessment of Hydro-ecological Changes at Two Closed-drainage Basins in the Peace-Athabasca Delta, Alberta, Canada, University of Waterloo.

Sternberg L. S. L. (1989) Oxygen and Hydrogen isotope measurements in plant cellulose analysis. In *Modern Methods of Plant Analysis: Plant Fibers*, Vol. 10 (ed. H. F. Linskens and J. F. Jackson), pp. 89-99. Springer-Verlag.

Sternberg L. S. L., DeNiro M. J., and Savidge R. (1986) Oxygen isotope exchange between metabolites and water during biochemical reactions leading to cellulose synthesis. *Plant Physiology* **82**(423-427).

Stokes M. A. and Smiley T. L. (1968) *An Introduction to Tree-Ring Dating*. University. of Chicago.

Suess H. E. (1970) Bristlecone-pine calibration of the radiocarbon time-scale 5,000 BC to present. In *Radiocarbon Variations and Absolute Chronology* (ed. I. U. Olsson), pp. 303–311. Wiley.

Thompson D. W. J. and Wallace J. M. (2001) Regional Climate Impact of the Northern Hemisphere Annular Mode. *Science* **293**(5527), 85-89.

Thompson R. S., Anderson K. H., and Bartlein P. J. (2000) Atlas of Relation between Climatic Parameters and Distribution of Important Trees and Shrubs in North America - Introduction and Conifers. In *U.S. Geographical Survey Professional Papers 1650-A*. U.S. Geographical Survey.

Thomson S. (1993) Peace-Athabasca Delta Flood History, Parks Canada, Historical Services, Prairie and Northern Region. Wood Buffalo National Park.

Timoney K. (2002) A dying delta? A case study of a wetland paradigm. *Wetlands* **22**, 282–300.

Timoney K., Peterson G., Fargey P., Peterson M., McCanny S., and Wein R. (1997) Spring Ice-Jam Flooding of the Peace-Athabasca Delta: Evidence of Climate

Oscillation. *Climate Change* **35**, 463-483.

Trenberth K. E. and Hurrell J. W. (1994) Decadal Atmosphere-Ocean Variations in the Pacifc. *Climate Dynamics* **9**, 303-319.

Vincent L. A. and Gullett D. W. (1999) Canadian historical and homogeneous temperature datasets for climate change analyses. *International Journal of Climatology* **19**, 1375-1388. .

Visbeck M. H., Hurrell J. W., Polvani L., and Cullen H. M. (2001) The North Atlantic Oscillation: Past, present, and future. *Science* **98**(23), 12876-12877.

Wallace J. M. and Gutzler D. S. (1981) Teleconnections in the geopotential height field during the Northern Hemisphere Winter. *Monthly Weather Review* **109**, 784-812.

Wang X.-F., Yakir D., and Avishai M. (1998) Non-climatic variations in the oxygen isotopic composition of plants. *Global Change Biology* **4**, 835-849.

Wershaw R. L., Friedman I., and Heller S. J. (1966) Hydrogen isotope fractionation in water passing through trees. In *Advances in Organic Geochemisty* (ed. F. Hobson and M. Speers), pp. 55-67. Pergamon.

Wolfe B. B., Karst-Riddoch T. L., Vardy S. R., Falcone M. D., Hall R. I., and Edwards T. W. D. (2005) Impacts of climate and river flooding on the hydro-ecology of a floodplain basin, Peace-Athabasca Delta, Canada since A.D. 1700. *Quaternary Research* **64**, 147 – 162.

Wolfe B. B., Karst-Riddoch T. M., Hall R. I., Edwards T. W. D., English M. C., Palmini R., McGowan S., and Vardy S. R. (2007) Classification of hydrologic regimes of northern floodplain basins (Peace-Athabasca Delta, Canada) from analysis of stable isotopes (δ^{18}O, δ^2H) and water chemistry. *Hydrological Processes* **21**, 151-168.

Yakir Y. and DeNiro M. J. (1990) Oxygen and hydrogen isotope fractionation during cellulose metabolism in *Lemna gibba*. *Plant Physiology* **93**, 325-332.

Yakir Y., Gat J., Issar A., Adar E., Trimborn P., and Lipp J. (1994) ^{13}C and ^{18}O of wood from the Roman seige rampart in Masada (AD 70-73): evidence for a less arid climate for the region. *Geochimica et Cosmochimica Acta* **58**, 3535-3539.

Yapp C. and Epstein S. (1982) A re-examination of cellulose carbon-bond hydrogen dD measurements and mose factors affecting plant-water D/H relationships. *Geochimica et Cosmochimica Acta* **46**, 955-965.

Yi Y., Brock B. E., Falcone M. D., Wolfe B. B., and Edwards T. W. D. (2008) A coupled isotope tracer method to characterize input water to lakes, pp. 25.

Zerefos C. S., Gerogiannis V. T., Balis D., Zerefos S. C., and Kazantzidis A. (2007) Atmospheric effects of volcanic eruptions as seen by famous artists and depicted in their paintings. *Atmospheric Chemistry and Physics* **7**, 4027–4042.

Appendix

Application of the Dongmann Model

Supplementary Calculation showing that Atmospheric Vapour and Source-water are

not in equilibrium;

If modern trees in the PAD use winter precipitation as $\delta^{18}O_{sw}$ (average -23.9 ‰ CNIP 2004) during the growth season (supported by statistical analysis above) and reasonable estimates for $\delta^{18}O_{vap}$ (average -26.6‰) (YI et al., 2008), $\delta^{18}O_{Cell}$ (average measured -21.6‰) and daytime relative humidity ~50% (EC 1951-1980) are available we can calculate the expected enrichment of $\delta^{18}O_{lw}$ (-3.7 ‰) and the effective damping (0.126).

$$
\begin{aligned}
\delta^{18}O_{lw} &= \alpha_{k/kb} \cdot \alpha_e (1-h)(10^3 + \delta^{18}O_{sw}) + \alpha_e (h)(10^3 + \delta^{18}O_{vap}) - 10^3 \\
&= (1.024) \cdot (1.010)(1-0.50)(10^3 + (-23.9‰)) \\
&\quad + (1.010)(0.5)(10^3 + (-26.6‰)) - 10^3 \\
&= -3.7‰
\end{aligned}
$$
<div align="right">Calc. 1</div>

$$
\begin{aligned}
\delta^{18}O_{Cell} &= f_o \cdot (\alpha_b \cdot \delta^{18}O_{sw} + \varepsilon_b) + (1-f_o) \cdot (\alpha_b \cdot \delta^{18}O_{lw} + \varepsilon_b) \\
&= f_o \cdot (1.028 + (-23.9‰) + 28.0‰) \\
&\quad + (1-f_o) \cdot (1.028 + (-3.7‰) + 28.0‰) \\
&= (1.024) \cdot (1.010)(1-0.50)(10^3 + (-23.9‰)) \\
&\quad + (1.010)(0.5)(10^3 + (-26.6‰)) - 10^3
\end{aligned}
$$
<div align="right">Calc. 2</div>

$$
\delta^{18}O_{sw} = 21.6‰ \text{ (measured)} \therefore f_o = 0.126
$$

Assuming equilibrium, kinetic and biological fractionations factors of 1.010 (at ~285K), 1.024 ($\alpha_k = 1.0285$ and $\alpha_{kb} = 1.0189$) and 1.028 (Edwards 1993), respectively.

This damping factor suggests that 86% of leaf water evaporative enrichment is

conserved. A similar calculation can be conducted to test the simplifying assumption (BUHAY et al., 1996; BURK and STUIVER, 1981; EDWARDS and FRITZ, 1986) that atmospheric vapour and source-water are in isotopic equilibrium. This results in a physically unreasonable damping factor of -0.31 for $\delta^{18}O_{sw} = -23.9\%o$ and the resulting $\delta^{18}O_{vap} = -33.9\%o$. This calculation shows that source water and the vapour around the tree during humidity-dependent labelling are not in equilibrium